REVIEW ARTICLE | MARCH 24 2026

Advances in sensor integration for real-time monitoring of joint-on-chips

A. Mantegazza ; S. Materne ; M. Rasponi ; P. Occhetta

Biophysics Rev. 7, 011308 (2026)
https://doi.org/10.1063/5.0287852

Biophysics Reviews REVIEW pubs.aip.org/aip/bpr

Advances in sensor integration for real-time monitoring of joint-on-chips

Cite as: Biophysics Rev. **7**, 011308 (2026); doi: 10.1063/5.0287852
Submitted: 4 November 2025 · Accepted: 25 February 2026 ·
Published Online: 24 March 2026

A. Mantegazza, S. Materne, M. Rasponi, and P. Occhetta[a)]

AFFILIATIONS

Department of Electronics, Information and Bioengineering, Politecnico di Milano, Piazza Leonardo da Vinci, 32, Milano 20133, Italy

[a)]Author to whom correspondence should be addressed: paola.occhetta@polimi.it

ABSTRACT

Joint-on-chip (JoC) platforms represent a transformative approach to modeling the complex functional units of joints, offering valuable tools for disease modeling, drug discovery, and biomarker identification. However, the field faces two key challenges: the accurate recapitulation of the multifaceted joint environment and the lack of integrated online readouts to monitor cellular and tissue responses in real-time. This review underscores the importance of capturing the interplay of joint tissues and highlights the potential of diverse monitoring strategies—including optical, electrical, mechanical, and biochemical modalities—for real-time assessment. Drawing on examples from musculoskeletal and other organ-on-chip systems, we discuss current advancements and gaps in the field. Finally, we provide a forward-looking perspective on how addressing these limitations can accelerate the development of robust JoC platforms for translational musculoskeletal research.

TABLE OF CONTENTS

I. INTRODUCTION

Joint pathologies, such as osteoarthritis (OA) and rheumatoid arthritis (RA), are among the most prevalent degenerative musculoskeletal disorders. They significantly impact global health and the quality of life for 7% of the worldwide population. These conditions are projected to affect 1×10^9 people by 2050.[99,160]

OA, the most common form of arthritis, typically affects one or few synovial joints and is characterized by chronic pain and loss of mobility.[366] Once considered only a cartilage disease, OA is now recognized as a whole organ disease involving inflammation and

degeneration of all joint tissues. Risk factors of OA include mechanical overload, trauma, genetic predisposition, co-existing metabolic syndromes, age, and sex. In contrast, RA is a systemic autoimmune disease that leads to an elevated inflammatory response progressively affecting all joints in the body. RA is influenced by a combination of genetic, environmental, and lifestyle factors, including obesity and smoke.[99]

Current treatment strategies for OA are mainly palliative, aimed at managing the symptoms rather than halting the disease degenerative progression. Instead, some disease-modifying anti-rheumatic drugs are available for RA, but their efficacy is significantly limited by the genetic heterogeneity of this pathology. Overall, despite the extensive research, no fully effective disease-modifying drugs have been found for either disease. One of the major obstacles toward the development of actual OA/RA reversing therapies is the gap of knowledge on initial disease mechanisms, linked to the unavailability of reliable preclinical joint models suitable to identify them. Such models would be crucial for providing insights into OA/RA onset, etiology, and pathophysiological mechanisms, thus facilitating biomarkers identification for distinct disease phenotypes and advancing drug discovery and testing before clinical trials in humans.

Historically, animal models have often been used to study joint disorders. While they have been helpful in following disease onset and its progression, inter-species differences have led to moderate predictive power for drug efficacy in patients.[202] It is indeed currently accepted that no animal model fully captures the complexity and heterogeneity of OA/RA observed in humans.[283] In terms of *in vitro* models, traditional two-dimensional (2D) cell cultures have been the most commonly used preclinical models due to their experimental reproducibility, ease of use, low cost, and compatibility with high-throughput testing. Unfortunately, these models lack physiological relevance because they fail to reproduce the complexity of the 3D joint microenvironment observed *in vivo*. To increase the translational power, 2D models have been replaced by 3D cell culture setups (e.g., pellet culture), which can provide a more biologically faithful recapitulation of the joint extracellular matrix (ECM), potentially building a microenvironment responsive to physicochemical stimuli.[202] However, most 3D cell-based culture systems typically integrate only one cell type, with chondrocytes being the most studied one, preventing them from replicating the inter-tissue crosstalk found *in vivo*.[283] Lately, 3D macroscale systems integrating different cell types, biochemical and/or biophysical cues and ECM-like matrices have been introduced, aiming to recapitulate both cellular-specific contributions and ECM architecture. While holding huge promise as grafts to promote the repair of joint injuries, they require bioreactor systems that may be bulky and difficult to use, thus preventing their widespread use as preclinical *in vitro* models. For a more detailed comparison of conventional preclinical models, the reader is referred to previous reviews.[84,229,322]

Despite the clinical advancements obtained with traditional *in vitro* preclinical models, more representative high-fidelity models are required to recapitulate the native human joint microenvironment. In this context, organs-on-chip (OoC), a subset of microphysiological systems (MPS) that replicate aspects of an organ's *in vivo* structure or function within a non-biological microfluidic platform, have high potential as models for OA/RA preclinical studies. In fact, OoC can integrate both cellular and extracellular components of the native tissue to be modeled and allow to reproduce tissue-specific microarchitecture with a high spatial fidelity, enabling the study of inter-tissue crosstalk.[202] Additionally, a main OoC advantage is their ability to control the 3D dynamic tissue microenvironment by applying external biochemical and biophysical cues (e.g., chemical gradients, flow rate, mechanical and electrical stimulation).[229,322] From a technological perspective, OoC can be parallelized and automated to increase their throughput, thus allowing to reduce cost and time during the drug development process while keeping a high translational power.

Specifically limited to the topic of the present review, the concept of joint-on-chip (JoC) has been proposed in the past few years as a promising tool enabling a faithful *in vitro* recapitulation of the native multi-tissue joint-like microenvironment. This motivation is directly rooted in joint biology: the joint is a multi-tissue organ in which each compartment hosts distinct cell populations, including the synovial membrane (synoviocytes, macrophages, and nerve cells), articular cartilage (chondrocytes), and the vascularized and innervated subchondral bone (osteoblasts, osteoclasts, and nerve cells).[283] Articular cartilage is an avascular and aneural tissue hierarchically organized (i.e., superficial, middle, and deep zone), where chondrocytes are embedded in an ECM rich in collagen types I and II and negatively charged proteoglycans (Fig. 1). This composition, together with water and electrolytes, enables cartilage to withstand high cyclic loading and transmit loads.[271,283] As a consequence, the joint microenvironment is intrinsically mechano-chemical: compressive loading, shear stresses, and hydrostatic pressure shape cell behavior and tissue homeostasis, while biochemical and metabolic factors control inflammation and matrix turnover.[89,271]

From this point of view, JoC aims to capture not only individual tissues but also the *interconnected* nature of joint compartments and their crosstalk. This communication, potentially conducted through joint fluid, blood vessels, and lymphatic vessels, is often challenging to replicate *in vitro*. Toward the overcoming of this challenge, different studies have been lately proposed on combining 3D miniaturized models of cartilage, synovium, and bone-like tissues within single OoC platforms,[204,207,230,255,286,293,321,327] potentially enabling to control fluidic communication reflecting the dynamic crosstalk that characterizes a functioning joint.[296] Efforts have also been focused on the integration of biophysical cues within such JoC models, given the recognized key role of mechanical signaling in joint development, homeostasis, and OA/RA progression. Techniques such as cyclic compression,[271,285] hydrostatic pressure,[188] and fluid shear stress[319] or their combination[282] have been recently applied to stimulate tissue-specific physical responses in JoC, enabling researchers to investigate mechano-transduction pathways underlying both joint maintenance and pathogenesis. For an in-depth review of existing dynamics multi-tissue JoC systems, readers are referred to recent comprehensive reviews.[81,283,427]

Importantly, OA and RA can be interpreted as diseases of a disrupted joint microenvironment (Fig. 1). A healthy joint environment is characterized by a balance between cellular metabolism, cytokine signaling, protease activity, and ECM/pericellular matrix (PCM) organization.[336] In a damaged joint, this balance is perturbed, resulting in increased catabolic activity [e.g., decreased adenosine triphosphate

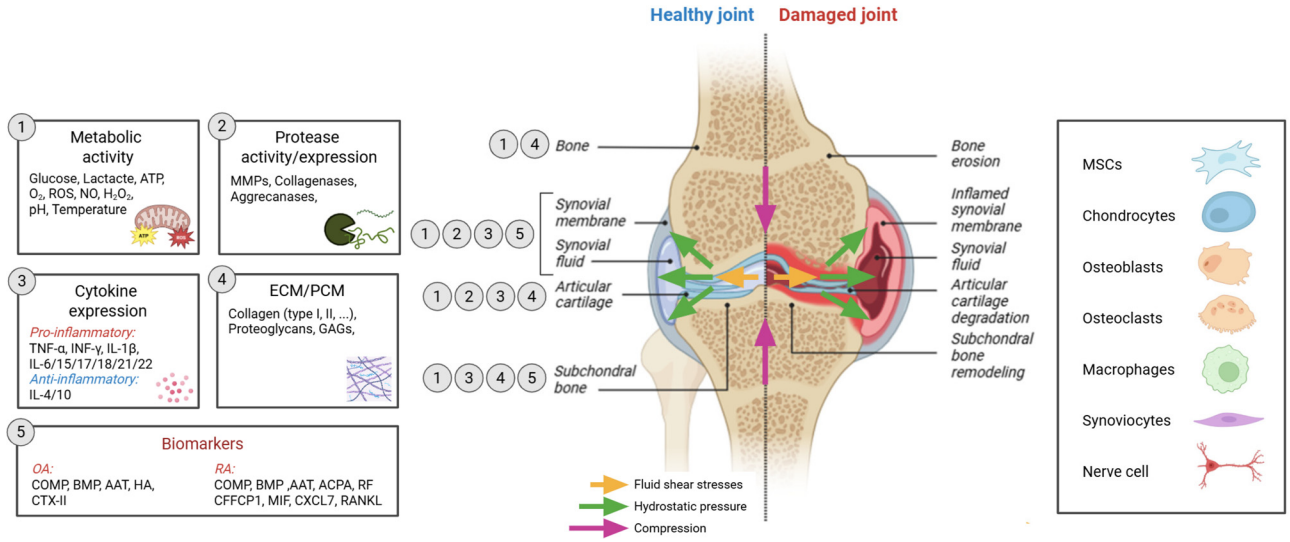

FIG. 1. Joint structure and disease-associated microenvironmental signatures motivating multi-sensing. Schematic comparison of a healthy vs damaged (OA/RA) synovial joint, highlighting the main anatomical compartments and cell types. Mechanical cues relevant to joint homeostasis and pathology—fluid shear stresses, hydrostatic pressure, and compression—are indicated with arrows. The key classes of measurable targets for integrated sensing are shown: (1) metabolic activity, (2) protease activity/expression, (3) cytokine expression, (4) ECM/PCM composition, and (5) disease-associated biomarkers. Circled numbers placed next to each joint compartment denote which classes of analytes are present, produced, or measurable in that specific compartment to emphasize how tissue- and fluid-specific analytes can guide selection of complementary real-time and on-chip readouts in next-generation platforms. This figure was partially created with elements from BioRender (Biorender.com).

(ATP) generation, hypoxia, lactate accumulation, increased nitric oxide (NO) and hydrogen peroxide (H_2O_2),[218] low pH[1,129]] up-regulation of matrix-degrading enzymes [e.g., matrix metalloproteinases (MMPs)], altered ECM/PCM architecture,[125] and downstream structural changes such as chondrocyte clustering, vascularization,[160] calcification, and bone remodeling, ultimately leading to joint dysfunction.[187,322,336,410] These processes are accompanied by increased pro-inflammatory cytokines [e.g., interleukin 6 (IL-6), interleukin 1β (IL-1β), and tumor necrosis factor α (TNF-α)][35,254] and disease-associated biomarkers, such as cartilage oligomeric matrix protein (COMP),[348,359,392] bone morphogenetic protein (BMP),[68] and α1-antitrypsin (AAT).[146,162,348] Such disease-associated dynamic changes in joint microenvironmental signatures motivate the need for integration of real-time sensing strategies in JoC platforms to capture the coupled evolution of tissue mechanics and inflammation during disease progression or drug response.

Although significant advancements have been obtained in the JoC field, most of the recently proposed JoC solutions still rely on off-chip or end point assays, which limits the possibility to capture the temporal evolution of the system that is crucial, for example, to monitor disease progression or acute/chronic response to a therapy. Toward this vision, as already demonstrated for different OoC applications like heart-on-chip[240] or brain-on-chip,[431] the integration of multiple biosensors for noninvasive, continuous, and real-time monitoring would represent a breakthrough in the field of JoC and OA/RA modifying drug discovery. These biosensors could be used to monitor real-time extra-cellular environment remodeling as well as cell behavior in response to spatiotemporal pattern of external stimuli (e.g., biophysical stimuli intended to drive the tissue maturation or the administration of drugs). Such technological advancement may allow to obtain a seamless amount of data from fully functional representations of the joint microenvironment, thus establishing a new gold standard in joint preclinical models.[98]

In this review, technological advancements in OoC field for real-time monitoring of cell culture are analyzed, which could overcome the limitations of the majority of current JoC models that currently rely on off-chip analysis or end point assays. Optical, electrical, mechanical, and biochemical sensing modalities derived from musculoskeletal and other OoC systems are presented, demonstrating their potential application to develop a more integrated JoC platform (Sec. II). Finally, a forward-looking perspective is provided on integrating biomechanical stimulation, multi-sensing capabilities, and multi-tissue interactions to achieve a robust JoC platform, which would represent a transformative approach for musculoskeletal research and drug discovery (Sec. III).

II. BIOSENSORS FOR REAL-TIME JOINT-ON-CHIP MONITORING

In Sec. I, we highlighted the importance of developing JoC able to recapitulate the multifaceted dynamic native-like joint microenvironment. In this section, we underscore the need of integrating online readouts within such JoC to amplify the quantity and quality of data that can be inferred from these models. In fact, traditional characterization methods for the cell viability and morphology (e.g., by offline imaging), gene expression [e.g., based on quantitative polymerase chain reaction (qPCR) analysis], or biomarker assessment [e.g., via enzyme-linked immunosorbent assay (ELISA)] rely on time-consuming off-chip analysis and end point imaging modalities, which do not allow to evaluate the cell behavior/microenvironment over time and lead to the termination of experiments.

As an alternative approach, the integration of biosensors for continuous, real-time, and noninvasive monitoring on-chip would

enable the temporally and spatially resolved measurements of physicochemical parameters related to phenomena such as (i) cell signaling, (ii) metabolic activity, (iii) ECM composition and remodeling, and (iv) inflammatory states in pathological and physiological conditions. These biosensors can also be used to monitor transient events that would not be detected with traditional offline sensing techniques.[333]

To date, multiple types of integrated biosensing modalities have been developed for OoC applications. In the following, we will discuss optical (Sec. II A), electrical (Sec. II B), mechanical (Sec. II C), and biochemical sensing techniques (Sec. II D), classifying them according to the related main sensing principle. Table I presents a concise overview correlating each class of sensing techniques with the joint-related target parameters that they can measure, together with an analysis of related advantages and limitations. For each category, we review examples already implemented in JoC platforms (when available) and report on emerging biosensors—although not yet incorporated into OoC devices—being specifically developed to detect biomarkers associated with joint pathophysiology. Additionally, we examine the potential translation from other OoC applications, from which technical feasibility and maturity of sensor integration may be demonstrated. By highlighting successful implementations in other OoC systems, we aim to inspire and provide concrete technological reference points for researchers working on next-generation JoC models, facilitating the transfer of already validated sensing solutions into joint-specific applications and ultimately accelerating progress in this emerging area.

A. Optical sensing techniques

Optical sensing techniques exploit light-based techniques to analyze the cell behavior or the biochemical composition of the extracellular microenvironment by monitoring optical properties such as absorption, illumination, refractive index, or scattering. The integration of this sensing technique is particularly convenient for OoC applications because it exploits the optical transparency typical of OoC systems, preventing a physical contact between the sensing element and the sample, thus enabling a noninvasive continuous monitoring for the whole duration of the cell culture. With the exception of absorbance measurements that are limited by the short optical path in microfluidic devices, optical sensing techniques generally feature a good sensitivity at low analyte concentration. This constitutes a peculiar advantage for OoC technologies operating in microfluidic environments with low sample volumes. Nevertheless, optical sensing may face physical challenges at extremely low sample volumes when the single-molecule detection limit is approached due to instrumental limitations and background noise biasing the measurements. At very low analyte concentrations, measurements can be limited by background noise. Several strategies can boost signal strength, including sample preconcentration, surface functionalization, multi-pass optical paths,[172] and nanophotonic sensor designs.[245]

Optical measurements in OoC can be additionally challenging for two reasons: multilayer chip designs and thick 3D microtissues. These tissues (e.g., cell-laden hydrogels) can scatter and absorb light, which lowers the signal-to-noise ratio (SNR) and limits spatial resolution. Mitigation strategies may be applied to reduce these effects by using

TABLE I. Classification of the four classes of sensing techniques identified as relevant in applications in terms of target parameters (as defined in Fig. 1), advantages, and limitations.

Sensing technique	Target parameter	Advantages	Limitations
Optical	Metabolic activity; protease activity/expression; cytokine expression	Sensitivity at low analyte concentration; analyte specificity; contactless sensing	Usually not label-free; background noise; single-molecule detection limit; OoC thickness-induced low SNR and limited spatial resolution; material transparency
Electrical	Metabolic activity; protease activity/expression; cytokine expression; ECM/PCM; OA/RA biomarkers	High sensitivity and temporal resolution; versatility; usually label-free; ease of fabrication and OoC integration	Sensitivity to environmental conditions; interference for multiplexed measurements; liability to electrode material/position
Mechanical	Protease activity/expression; ECM/PCM; OA/RA biomarkers	Multiplexed measurements (applied forces and resulting strain, stress, mechanical properties); usually label-free	Sensitivity to environmental conditions; miniaturization challenges and integration with actuation systems; calibration drift; signal interpretation
Biochemical	Metabolic activity; cytokine expression; OA/RA biomarkers	Analyte specificity; multiplexed measurements; high throughput; cost-efficiency	Sensitivity to environmental conditions; surface functionalization; bio-recognition element immobilization; stability; often conjugated with other sensing techniques

optically clear materials, integrating light delivery/collection hardware (e.g., optical fibers) close to the sensing area as well as favoring longer-wavelength or label-free modalities.

In Secs. II A 1–II A 6, different optical sensing techniques are described and discussed, focusing on examples of their application in OoC (prioritizing JoC where available), performance, and specific integration challenges.

1. Absorbance

Absorbance measurements are used to quantify the concentration of biological molecules or biochemical solutes dispersed in a solution by correlating it to the amount of light absorbed by the sample at a specific wavelength. In the context of OoC technologies, absorptiometry involves measuring the light absorbed by the cells cultured on the chip as well as by the biomolecules that may be present in the culture medium. A light source (e.g., photodiode) emits radiation at a specific wavelength to illuminate an indicator dye dissolved in the OoC. The indicator dye changes its absorption spectrum upon the interaction with an analyte. The incident light is partially absorbed by biomolecules or cells, and partially by the indicator dye, while the remaining light passes through the system and is captured by a downstream detector. The ratio of the transmitted to the incident light across the OoC system gives a measure of the sample absorbance, which can be used to compute the analyte concentration using the Beer–Lambert law.

In addition to the concentration of the analyte, absorption measurements depend also on the molar absorption of the indicator dye and on the optical path along the microfluidic channels. The latter is the main constraint for the fabrication of miniaturized absorption sensors in OoC devices due to their intrinsically small length scale. At the same time, attention should be paid to the choice of the chip substrate to prevent a blocking-out effect, which would prevent the incident light to pass through the sample to be analyzed. From an analytical perspective, other limitations of this sensing method are light scattering and potential interference from other soluble contaminants that would bias the absorbance measurement. Therefore, background noise corrections are needed to attribute absorbance changes specifically to the analyte of interest. Strategies to cope with background noise typically involve optical path calibration and blank subtraction, where absorbance measurements performed in cell-free OoCs are subtracted from the measurements in the presence of cells.

Absorbance sensing techniques have been used to quantify several biomarkers for joint function and disease modeling in standard cell culture setups: ECM composition, inflammatory, and immune response mediators such as interleukins (e.g., IL-1β, IL-6, and IL-8), MMP-3, TNF-α,[182,329] and interferon-γ (IFN-γ).[286] Within JoC, absorbance-based optical sensors may also be used to monitor in real-time the concentration of reactive oxygen species in the extracellular environment, which correlates with the progression of an inflammatory state. In fact, NO and H_2O_2 are biomarkers for cell metabolism produced due to oxidative stresses that have been found to increase in the case of OA and RA.[218] While not yet integrated in JoC devices, Koman *et al.*[176] demonstrated the feasibility of using absorbance sensing techniques for the multiplexed continuous monitoring of cell metabolism byproducts such as hydrogen peroxide at the microscale. The strategy exploits the link between cytochrome c (Cyt c) absorbance and oxidation state: when Cyt c is oxidized by hydrogen peroxide (produced during enzymatic conversion of glucose or lactate), its absorbance spectrum shifts. Drops containing Cyt c and glucose or lactate oxidase (GOx/LOx) were deposited on a polydimethylsiloxane (PDMS) porous membrane in the bottom microfluidic layer. The sensors showed a linear response in the range 0.01–100 μM for glucose and 0.1–1000 μM for lactate concentration, with a respective limit of detection (LOD) of 240 and 110 nM (cf. Table II). Sensor sensitivity scaled with GOx/LOx concentration, indicating that translation to OoC would require careful enzyme-loading control to avoid excess hydrogen peroxide generation and crosstalk between adjacent sensing spots. Increasing the distance between sensing spots may help mitigate such undesired interactions.

Additionally, joint inflammation is associated with a noticeable decrease in the pH of the synovial fluid resulting from the increased activity of inflammatory cells, which often shift to anaerobic glycolysis producing lactic acid. As a consequence, the pH in the synovial fluid of OA patients can drop from physiological values to 6.6–7.2, with studies reporting pH as low as 6.0 in severe OA cases.[129] This acidic environment contributes to cartilage degradation and promotes the activity of metalloproteinases that further breaks down ECM components. Although not directly applied to JoC, Shaegh *et al.*[258] showed that it is possible to integrate an absorbance-based optical sensor in an OoC containing human fibroblasts to continuously monitor such changes in the pH level for up to 3 days. The incident light was generated by a laser emitting diode (LED), and real-time measurements of optical absorption by flowing culture medium containing phenol red were performed to measure the pH level, exploiting silicon photodiodes as detectors for the transmitted light. The sensors allowed to measure the pH in the range 6.5–8 with a resolution of 0.03 pH unit and a sensitivity one order of magnitude higher than electrochemical pH sensors based on iridium oxide thin films (cf. Table II). The system was also complemented with a luminescence sensor to measure the oxygen (O_2) level in the range 0%–21% using an oxygen-sensitive ruthenium dye immobilized within a thin-film inside the OoC (Sec. II A 2). A differential photodiode setup was implemented to remove the effect of background light achieving a high SNR (39.2 and 36.3 dB for pH and oxygen measurements, respectively). Zhang *et al.*[429] further optimized the optical multi-sensing strategy by developing a fully integrated OoC platform combining optical and electrochemical sensors to monitor extracellular parameters (pH, oxygen, temperature) and soluble proteins, respectively. The platform was applied to drug-toxicity testing in a dual-organ human liver–heart-on-a-chip exposed to acetaminophen (up to 5 days) and a dual-organ liver-cancer–heart-on-a-chip challenged with doxorubicin (up to 24 h). pH was quantified by phenol red absorbance in culture medium, while oxygen relied on luminescence quenching of a ruthenium dye. A sensitivity of 0.159 $V/unit_{pH}$ and 7 $mV/\%O_2$ was obtained for the two sensor types. Despite enabling a continuous and automated monitoring of environmental and biochemical parameters simultaneously, the platform still faces technological/analytical challenges. The platform size and fabrication complexity call for miniaturization and compatibility improvements to favor scalability. The OoC prototype was manufactured in PDMS, which biased the evaluation of the drug toxicity due to the partial absorption of doxorubicin, motivating future adoption of thermoplastics for microfluidic channels.

2. Luminescence

Luminescence sensors are another important category of optical sensors whose working principle is based on the emission of light by

TABLE II. List of optical sensing techniques relevant for applications. Lactate oxydase (LOx); glucose oxydase (GOx); limit of detection (LOD); polydimethylsiloxane (PDMS); hydrogen peroxide (H_2O_2); tris(4,7-diphenyl-1,10-phenanthroline)ruthenium(II) chloride ($[Ru(dpp)_3]^{2+}Cl_2$); signal-to-noise ratio (SNR); organic photodiode (OPD); platinum(II) meso-tetra(4-fluorophenyl) tetrabenzoporphyrin (Pt-TPTBPF); antibody (Ab); localized surface plasmon resonance (LSPR); bovine serum albumin (BSA); phosphate buffer saline (PBS); runt-related transcription factor 2 (Runx2); transcription factor SOX-9 (Sox9); IL-6; tumor necrosis factor α (TNF-α); neurotrophic growth factors (NGF); enzyme-linked immunosorbent assay (ELISA).

Sensing technique	Target analyte	Sensing element	OoC integrated?	Sensing performance	References
Absorbance	Lactate and glucose	Metalloprotein Cyt c oxidation state in the presence of LOx and GOx	No, but applied to joint	Lactate: range = 0.1–1000 μM, LOD = 240 nM; glucose: range = 0.01–100 μM, LOD = 110 nM	176
	Challenges	PDMS and glass transparency needed to have optical access to the sensor spots; sensor sensitivity proportional to LOx/GOx. This increases the enzymatically produced H_2O_2, which may lead to crosstalk and interference between neighboring sensors.			
Absorbance and luminescence	pH and O_2	Phenol red for pH and luminescent ruthenium dye ($[Ru(dpp)_3]^{2+}Cl_2$) for O_2	Yes, fibroblasts cultured on chip	pH: range = 6.5–8, LOD = 0.03 pH, sensitivity = 160 mV/pH, SNR = 39.2 dB; O_2: range = 0–21%, LOD = 0.8%, sensitivity = 6 mV/%O_2, SNR = 36.3 dB; time stability = 3 days	258
	Challenges	Biofouling minimization with a PDMS coating over the oxygen dye; differential photodiode setup to remove background light noise; fabrication challenge to integrate the sensing module into a microfluidic bioreactor.			
Luminescence and optical fibers	O_2	SP-PSt7-NAU-D3-YOP oxygen sensor spots (Precision Sensing GmbH)	Yes, multiple cell types cultured on chip	Range: 0%–20%; time stability = 4 days	32
	Challenges	Material transparency needed to have optical access; sensor integrated within the microfluidic device to have direct contact with O_2; signal interference: influence on O_2 measurement due to diffusion of atmospheric O_2 and CO_2 through PDMS.			
Light scattering and optical fibers	Change in tissue architecture	Light scattering detection using OPD arrays	Yes, synovium-on-chip	Range = 0–5000 cell/μl, LOD = 500 cell/μl, sensitivity = 1.9 mV (cell/μl), SNR = 3× LOD, time stability = 8 days	320
	Challenges	Background noise compensated using acellular Matrigel controls; biofouling minimized by S-layer protein coating (SbpA from Lysinibacillus sphaericus); fabrication challenge: OPD embedded beneath each microchamber, one glass layer interfering between sensor and analyte; organoid positioning within ring-shaped PDMS waveguides is required.			
Luminescence and optical fibers	O_2 and glucose	Polystyrene beads stained with oxygen sensitive dye (Pt-	Yes, epithlial cells cultured on chip	Glucose: range 0–30 mM, LOD = 0.7±0.5 mM, sensitivity = 3.0±0.7 hPa mM^{-1},	104

TABLE II. (*Continued.*)

Sensing technique	Target analyte	Sensing element	OoC integrated?	Sensing performance	References
		TPTBPF); GOx cross-linked enzyme aggregates (GOx-CLEAs)		T95 response time = 188 ± 53 s; time stability = 5 days	
	Challenges	O_2 consumption by GOx requires a O_2 reference sensor; H_2O_2 is obtained as a by-product, which deactivates enzymes and influences cells, catalysts added to remove it; GOx stability is affected by temperature and pH; porous PET membranes act as diffusion barriers between the analytes and the sensors; fabrication challenge: integration of optical fibers underneath the sensing spots; throughput limited by complex multi-step fabrication.			
Surface plasmon resonance	IL-4, IL-6, IL-10, and TNF-α	Ab-conjugated Au nanorod LSPR microarrays	Yes, adipose tissue-on-chip	Range = 10–10 000 pg/ml, LOD = 20 pg/ml, sampling volume = 1 μl, assay time = 30 min	433
	Challenges	Need for sampling without affecting cytokine concentration and compromising continuous monitoring; biofouling minimized by BSA passivation coating and PBS washing; Au nanorods distributed with distance >100 nm to avoid plasmonic coupling.			
Fluorescent nanoprobes	Runx2 and Sox9 mRNA	Au particles labeled with oligonucleotides specific for Runx2 or Sox9 genes, and a fluorescent peptide	No, but applied to joint	Incubation ∼16 h; probes uptake = 81%–87% (Runx2), 95%–97% (Sox9), >80% (Runx2 and Sox9)	193
	Challenges	Relatively long incubation time. Uptake efficiency and variability. Intracellular localization and probe release. Semi-quantitative mRNA expression data.			

an analyte that has absorbed energy. Luminescence sensors can be classified into three main subcategories: photoluminescence, chemiluminescence, and bioluminescence. In the following, we will focus on photoluminescence sensors (fluorescence- or phosphorescence-based) since they are more commonly applied to OoC. Photoluminescence occurs when a molecule absorbs light and then returns to its ground state by emitting light of a longer wavelength. During this process, sensors can measure two different optical properties: luminescence lifetime and intensity. Amplification or quenching of the luminescence signal can both occur if other excitable molecules are present together with the luminescent indicator dye. Luminescence lifetime, an intrinsic property of the indicator dye, offers a robust readout with minimal susceptibility to measurement bias. Unlike intensity-based approaches, lifetime measurements remain largely unaffected by fluctuations in dye concentration or illumination. In contrast, luminescence intensity is prone to multiple sources of error, including dye bleaching, autofluorescence, spectral overlap from different biomolecules, and spatial inhomogeneities in the excitation field, all of which compromise the measurement. The primary limitation—photobleaching—can be effectively mitigated through lifetime-based strategies.[20,277]

From the setup point of view, a typical photoluminescence sensor comprises a sensing element (eventually to be integrated in the OoC) and an external optical system including a light source, filters, and an externally mounted detector. The sensing element is usually made by a matrix hosting a luminescence indicator dye sensitive to a target analyte. In microfluidic cell culture systems, the sensing element can be embedded using a variety of formats, each offering distinct capabilities for OoC integration. The simplest strategy is to integrate thin films, patterned films, or beads directly into the device substrate. More sophisticated approaches include optical fiber-based probes, micro- or nanoparticle sensors, or the direct staining of cells or culture media with soluble oxygen-sensitive dyes. Sensor performance is dictated by the choice of matrix and dye, which also influences fabrication complexity and compatibility with the OoC environment. Thin films enable 2D spatial mapping but must be embedded on the device surface. Patterned films (still to be integrated on the device surface) help minimize signal interference by confining sensing regions, while preserving spatial resolution. Their performance scales with the sensing area, which may demand advanced optical readout systems when signal intensity is low. Bead-based sensors, in contrast, can be embedded within hydrogels to capture 3D gradients (e.g., oxygen gradients), offering greater placement flexibility, but at the cost of low positional control and potential cell interaction. Dispersing nanoparticles or soluble dyes directly into the culture medium simplifies the device fabrication, yet the unstable location of these sensing elements can compromise both signal stability and measurement precision. For more information on the format and integration of these sensors in microfluidic devices, the reader is referred to the review by Grist *et al.*[122]

Luminescence has been mostly used in microfluidic applications for the measurement of oxygen concentration,[9,261] pH,[258] and some soluble biomolecules (e.g., IL-6, TNF-α[380]) or vascular endothelial growth factor (VEGF[193]) due to the availability of indicator dyes for only selected analytes. To circumvent this limitation, a biological recognition element is typically immobilized on the surface of the sensor to catalyze the conversion of the target analyte. The byproduct of the catalytic reaction is then detected by the luminescent indicator dye. This method has been applied to measure glucose,[347] glutamate,[141] ATP,[330] lactate,[361] H_2O_2,[215,375] and other metabolic biomolecules.[24] Exploiting this principle, luminescence sensors can be employed to study the pathological progression of OA and RA in a JoC by tracking the concentration of deposited collagen[432] and also pathological biomarkers, such as cytokines,[380] MMP,[196] or NO.[19]

Song *et al.*[359] implemented an immunoassay on-chip based on fluoro-microbeads for the rapid and sensitive detection of COMP, an important OA biomarker, in human serum and synovial fluid. COMP-specific monoclonal antibodies were immobilized on gold-patterned surfaces via self-assembled monolayers (SAMs), and COMP was detected using fluorescence-labeled antibody-conjugated microbeads. The chip used PDMS microchannels over four immunoreactive regions, each with five patterned sensing areas, enabling multiplexed, simultaneous assays. The reported LOD was 0.8 ng/ml within a linear range of 4–128 ng/ml, with excellent correlation to commercial ELISA results but with a shorter assay time (~20 min). Integration into JoC would still require robustness under dynamic culture (flow, long exposure to media), and the study already included an initial mitigation step via ethanolamine/L-lysine passivation and background correction to reduce nonspecific contributions from culture-medium components.

A translatable study with relevance for joint research was reported by Bussooa *et al.*,[32] who integrated oxygen sensor spots in a OoC using mesenchymal spheroids composed of co-cultured primary human fibroblasts and human umbilical vein endothelial cells (HUVEC). The study demonstrated the better performance of optical oxygen sensors embedded within thermoplastic platforms compared to conventional PDMS-based OoCs to achieve physiologically relevant oxygen control for cell culture. Commercially available optical sensors (SP-PSt7-NAU-D3-YOP, PreSens Precision Sensing GmbH) were integrated into cyclic olefin copolymer (COCoxy) devices, enabling contactless and real-time oxygen measurements at 1-s intervals with non-consumptive detection capabilities. The thermoplastic system achieved greater oxygen control, shorter response time (~1 s vs >30 min in PDMS devices), successfully maintaining oxygen levels as low as 4% at physiologically relevant flow rates and detecting oxygen consumption by spheroids (decreasing from 17.1% to 11.1% over 96 h) while maintaining >90% cell viability (cf. Table II). Although the system faced integration challenges, such as 3.6%–5.0% oxygen leakage through fluidic connections and delayed responses at very low flow rates, the platform successfully validated long-term spheroid cultures under controlled hypoxic conditions (~11% of oxygen), establishing thermoplastic OoCs with integrated optical sensors as functional platforms for oxygen control in cell culture systems.

Luminescence-based sensing has been successfully used for oxygen monitoring also in other OoC platforms. For instance, Shah *et al.*[345] integrated a luminescence sensor (i.e., O_2 optodes) to monitor the oxygen level in the perfusion and microbial microchambers of a gastrointestinal human–microbe interface OoC. Similarly, Rennert *et al.*[313] performed continuous and contactless oxygen measurements under flow conditions by luminescence-emitting sensor spots in a liver-on-chip to monitor the hepatocytes metabolic activity. These examples further underscore the versatility of luminescence as a continuous and noninvasive optical sensing technique for applications targeting multiple OoCs.

3. Optical fibers

Another promising alternative to time-consuming microscopy and off-chip viability assays is the integration of optical fibers into OoC systems. Optical fibers are made of a plastic or glass core and a surrounding cladding with a lower refractive index. Light generated by laser or LED is transmitted through the core and delivered to a sample. The light reflected by the sample is collected by a photodetector at the receiving end of the optical fiber.[315] In terms of mode of operation, optical fibers function as both standalone transducers and in combination with complementary optical sensors such as luminescence-based probes. As standalone transducers, optical fibers detect changes in light transmission or reflection. These changes reflect physicochemical properties such as refractive index, absorbance, or scattering, enabling label-free and real-time measurements.[10,413] Instead, when optical fibers are used in combination with other optical sensing techniques, they can be used to monitor temperature, pH, oxygen, ECM components, and glucose.[142,194]

Rothbauer *et al.*[320] developed a 3D synovium-on-chip model to monitor the onset and progression of inflammatory synovial tissue response to TNF-α using noninvasive light scattering. The setup comprised laser beam splitters, fiber couplers, and collimators that directed a 1.2-mm diameter beam through the synovial organoids. The system collected light scattered at angles greater than 20° from the incident beam. A notch filter removed unwanted components, and organic photodiodes converted the remaining signal into electrical outputs [Fig. 2(a)]. This fiber-optic system allowed for multiplexed measurements across multiple chip chambers simultaneously, making the platform suitable for high-throughput screening applications. The primary target analytes were 3D tissue-level architectural changes within synovial organoids, specifically monitoring structural events such as motility, proliferation, and invasion. The optical sensor demonstrated excellent analytical performance with a detection limit of approximately 500 cells/μl and a sensitivity of 1.9 mV/(cells/μl), demonstrating sustained operational stability for over 8 continuous days (cf. Table II). However, the approach has key analytical challenges. Some hydrogels (e.g., fibrin) introduce optical interference that biases scatter measurements. In addition, the signal can be nonspecific, making it hard to separate cellular changes from ECM changes. No phototoxic effects were observed at the highest power output (85 μW) over 8 days. However, longer experiments with repeated laser exposure—common in cartilage-on-chip[230] studies—may still introduce phototoxicity. In terms of fabrication challenges, the fabrication process requires precise alignment of the multi-layer device to limit the manufacturing variability that could affect optical measurements. Despite these challenges, the synovium-on-chip distinguished diseased tissue within 2–3 days after seeding. By comparison, conventional proliferation and cytokine assays are typically performed 14–21 days post-seeding.

Glucose is fundamental for joint homeostasis. It is the main energy source for chondrocytes via anaerobic glycolysis. It also serves as a precursor for ECM macromolecules such as glycosaminoglycans (GAGs) and hyaluronic acid. Physiological glucose levels promote ECM synthesis and anti-inflammatory activity in chondrocytes, whereas hyperglycemia can lead to the accumulation of advanced glycation end products (AGEs), triggering inflammation and cartilage degradation.[295] In this context, a cartilage-on-chip platform integrated with a glucose sensor would be helpful to assess metabolic shifts in chondrocyte activity upon triggering of pathological conditions. For example, the model could be exposed to hyperglycemia, over-physiological mechanical loading, or pro-inflammatory cytokines. The feasibility of using optical fibers to monitor glucose concentration was demonstrated by Fuchs *et al.*,[104] who developed a plug-and-play optical glucose sensor designed for integration in microfluidic cell culture systems [Fig. 2(b)]. The sensor-targeted glucose using GOx cross-linked enzyme aggregates embedded in a biocompatible hydrogel with oxygen-sensitive phosphorescent particles and hydrogen peroxide-degrading catalysts. Fabrication involved microdispensing the sensor formulation onto biocompatible adhesive tape, covered with porous polyethylene terephthalate (PET) membranes as diffusion barriers to tune sensitivity and range. Optical fibers are directly fixed onto the adhesive substrate beneath the sensing spots to enable precise, stable optical readouts of phosphorescence signals. The sensor demonstrated stable performance over 5 days at 37 °C with minimal drift, tolerated sterilization and operated effectively across relevant pH (6.5–8) and flow conditions, matching commercial sensor accuracy with cell culture samples. Extensive data on the sensor performance are reported in Table II. The sensor, which is only 1 mm in size, fits efficiently into OoC platforms, presenting minimal fabrication challenges. Several analytical challenges must be addressed before using this sensor in a JoC. First, oxygen cross-sensitivity requires compensation (e.g., with reference sensors). Second, GOx stability must be protected against hydrogen peroxide, potentially via lifetime-based strategies and non-cytotoxic catalysts. Third, diffusion-barrier porosity should be tuned to the glucose range of the specific culture system. Finally, performance should be tested below pH 6.5 if modeling pathological conditions. Attention should be paid to the integration of multiple components (enzyme, catalyst, oxygen-sensitive particles, hydrogel matrix) while maintaining their individual functionalities.

The potential of using optical fiber-based sensors was also demonstrated for other applications as the real-time oxygen concentration in OoCs seeded with epithelial cells[360] or spheroids made of primary fibroblasts and HUVECs, as previously discussed.[32] Interestingly, Zirath *et al.*[436] developed an optical system to noninvasively monitor dissolved oxygen levels in both 2D and 3D platforms targeting multiple cell types, including lung epithelial cells (A549), HUVEC, normal human dermal fibroblasts (NHDFs), adipose-derived stem cells (ASCs). The sensing element was prepared by dispersing amine-functionalized polystyrene beads into a solution containing platinum(II) meso-tetra(4-fluorophenyl)tetrabenzoporphyrin (PtTPTBPF), which exhibits luminescence quenching properties in response to oxygen concentration changes, allowing the oxygen-sensitive dye to stain the bead surfaces. Fabrication involved dispersing the dye into bead suspensions followed by purification and immobilization of sensor spots onto glass substrates within the microfluidic chips. The sensor spots are integrated in PDMS devices by pipetting onto the glass substrate before sealing with adhesive film or plasma bonding, with optical fibers embedded around the chip to couple excitation and emission light to an optical meter for real-time readout. The sensor demonstrated excellent reproducibility with low sensor-to-sensor variation, sensitive detection across 0.5%–20% oxygen, and capability for dynamic oxygen monitoring in cell cultures, which allowed to distinguish between cell types based on their oxygen consumption. The same group later proposed a dual-sensor integrated microfluidic cell analysis platform for the noninvasive and time-resolved monitoring of cellular oxygen uptake and metabolic activity (i.e., pH) based on

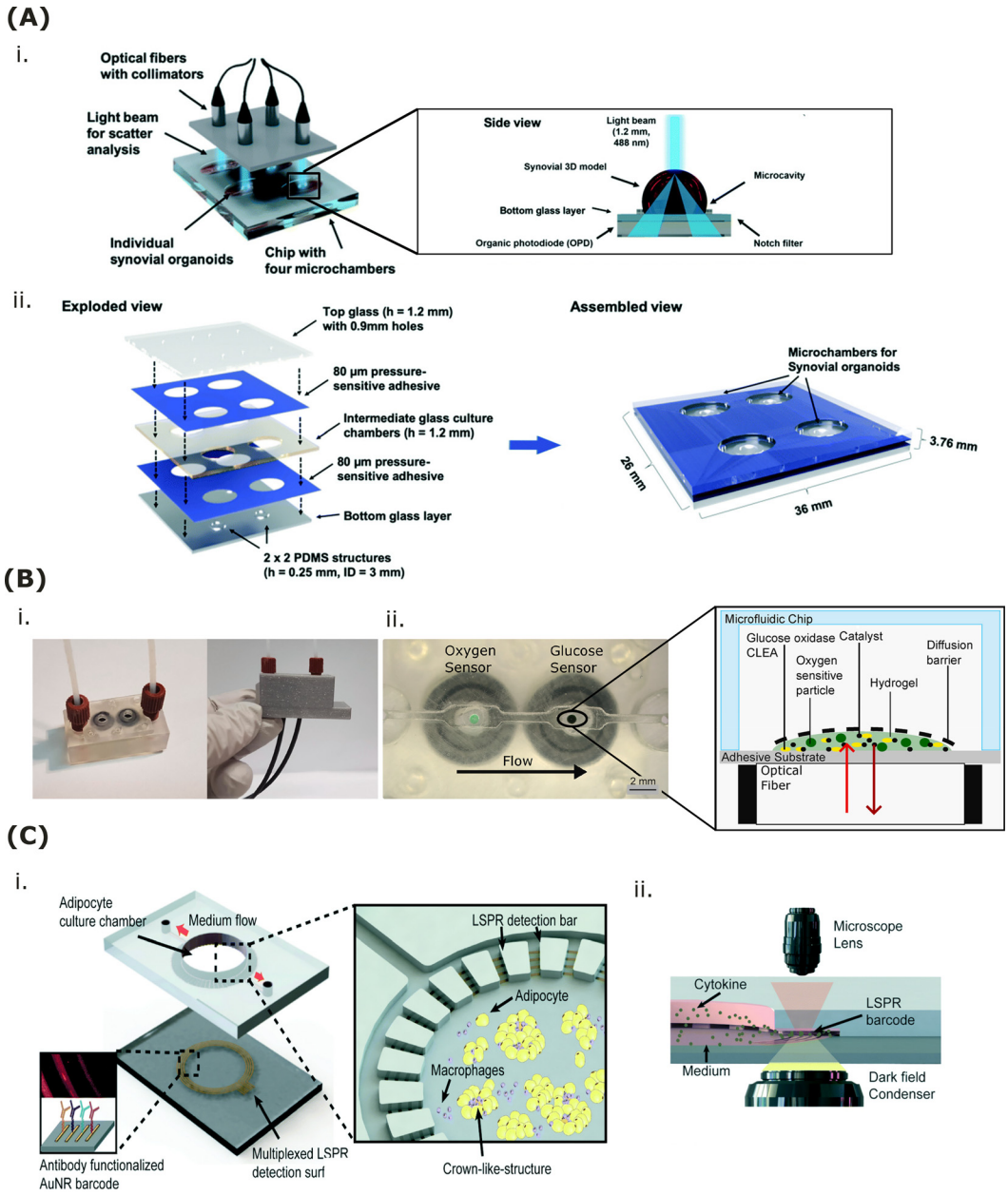

FIG. 2. Examples of optical sensors. (a) Synovium-on-a-chip system with integrated time-resolved light scatter biosensing for monitoring tissue-level remodeling during early inflammatory arthritis. (i) Schematic of the device with four microchambers containing 3D human synovium organoids; light scatter through the organoids is detected by organic photodiodes beneath the chip. (ii) Simplified device layout showing the layered glass/adhesive structure and PDMS ring-shaped waveguide microstructures that guide scattered light to the photodiodes. Reproduced with permission from Rothbauer *et al.*, Lab Chip **20**, 8 (2020). Copyright 2020 Authors, licensed under a Creative Commons Attribution (CC BY) license. (b) (i) Oxygen and glucose sensors integrated into a microfluidic flow cell. (ii) Microfluidic device featuring both sensors, with a schematic of the structure of the glucose sensor. The sensing layer consists of GOx-CLEAs, particles stained with an oxygen-sensitive dye, and an additional catalyst for hydrogen peroxide degradation. These components were embedded in a hydrogel and covered by a porous membrane serving as a diffusion barrier. The sensor can be mounted in a microfluidic device using the adhesive sensor substrate, with optical fibers directly fixed onto the substrate for optical readout. Reproduced with permission from Fuchs *et al.*, Biosens. Bioelectron. **237**, 115491 (2023). Copyright 2023 Authors, licensed under a Creative Commons Attribution (CC BY) license. (c) Adipose-tissue-on-chip sensing platform for *in situ* analysis of adipose tissue inflammation. (i) Optofluidic device combining a bottom AuNR-patterned LSPR barcode for multiplexed cytokine sensing with a PDMS culture chamber supporting adipocytes and macrophage-induced CLS formation. The inset shows a schematic of the adipocyte culture chamber surrounded by multiple microchannels connected to LSPR cytokine detection barcode arrays. Circular LSPR sensing arrays are aligned beneath the microchannel patterns, allowing diffusion of adipocyte–macrophage culture supernatant into the microchannels where it interacts with the AuNR LSPR sensors. (ii) Schematic of LSPR signal detection performed on a dark-field microscopy stage. Reproduced with permission from Zhu *et al.*, Lab Chip **18**, 23 (2018). Copyright 2018 Royal Society of Chemistry.

optical fiber measurements.[437] Results showed that the measured decrease in oxygen consumption and pH increase could be correlated with the loss of viability for intestinal Caco-2 cells and HUVECs after exposure to cytotoxic silica nanoparticles.

As a last example, it is worth reporting an optical sensor developed for skeletal muscle tissue engineering applications. Iuliano *et al.*[150] recently proposed a multi-channel sensor based on optical fibers that use the principle of light interferometry to detect the contraction of 3D tissue-engineered muscles. Thanks to the integration of electrodes for electrical pulse stimulation, 3D cell constructs obtained from human induced pluripotent stem cell (hiPSC)-derived myogenic progenitors lines were stimulated for up to 7 days, and continuous noninvasive optical measurements were performed, providing an indirect estimation of contraction forces down to a nano-Newton resolution. This technology was also used to investigate the effect of caffeine, verapamil, and the β-agonist clenbuterol on 3D tissue-engineered muscles. Despite representing an indirect way to measure forces, this optical fiber sensor may hold great potential for JoC applications, where mechanical stresses within different joint tissues have been correlated with the development of pathological phenotypes in OA/RA models.

4. Surface plasmon resonance

Surface plasmon resonance (SPR) is a label-free optical technique that detects when biomolecules (e.g., proteins and nucleic acids) bind to a metal surface by measuring changes in how light behaves at that surface. The SPR working principle is based on the excitation of surface plasmons, which are coherent electron oscillations at the interface between a metal (i.e., gold or silver) and a dielectric material.[140] If a biomolecule binds to the metal surface, the refractive index at the metal/dielectric interface changes. In turn, a shift in plasmon excitation is determined by the resonance angle variation, which is induced by the change in the refractive index proportionally to the biomolecule attached to the metal surface.

SPR is a complex sensing technique involving several steps ranging from substrate preparation to analyte measurements. First, the metallic sensor surface is cleaned and activated to remove any contaminants and prepare it for further chemical modifications. After activation, linker molecules (e.g., thiol-containing compounds) are deposited onto the metallic substrate to enable covalent immobilization of ligands. Subsequently, the target ligand—such as a protein or receptor—is immobilized on the sensor surface under controlled conditions to ensure optimal binding density and activity. Any remaining active sites on the surface are then blocked using agents like ethanolamine to reduce non-specific binding during sensing. In the sensing phase, the analyte solution is flowed over such prepared substrate, and binding interactions between the analyte and immobilized ligand are monitored in real-time by detecting changes in the local refractive index near the sensor surface. After the measurement, the surface can be regenerated by removing bound analytes while preserving ligand functionality, allowing repeated use of the sensors. For more information on standard SPR methodologies, the reader is referred to dedicated comprehensive reviews.[139,147]

SPR-based sensors have been widely applied in biological research, ranging from the measurement of small biomolecule concentration (e.g., ATP[403]) and biomarker identification (e.g., IL-6[43] or IL-1β[44]) to detecting cancer cells[165,288] and monitoring of cellular response to external stimulation (e.g., osmotic stress[378]). For pathological models of JoC, SPR sensors offer the possibility to measure inflammatory cytokines (e.g., IL-6 or IL-1β[43,44]) production by specific joint cells/tissues during inflammatory states (e.g., induced by biochemical stress such as TNF-α administration). Toward this direction, Zhu *et al.*[433] proposed an antibody-conjugated gold nanorod (AuNR) SPR nanobiosensor to be integrated in an adipose tissue-on-chip to monitor the adipose tissue inflammation [Fig. 2(c)]. The platform enabled simultaneous multiplexed measurements of pro-inflammatory (IL-6 and TNF-α) and anti-inflammatory (IL-10 and IL-4) cytokines secreted by adipocytes and macrophages. This on-chip sensing technology offers a wide dynamic cytokine detection range (10–10 000 pg/ml), requires a low operating sample volume (down to $\sim$1 μl), has a short assay time ($\sim$30 min), and shows a strong correlation with gold standard ELISA experiments (cf. Table II). Results demonstrated the feasibility of detecting pro-inflammatory cytokines in OoC, which indicates that it is possible to translate this optical sensor to joint specific tissues.

The functionalization of the substrate metallic surface, as well as the resolution enhancements with nanomaterials, makes SPR a versatile sensing strategy to be implemented in different OoC platforms. Ortega *et al.*[278] developed a SPR sensor made of gold nanoantennas functionalized with an insulin monoclonal antibody. The sensor was integrated into a pancreatic islet-on-chip realized by culturing primary mouse pancreatic islets embedded in a non-biodegradable cellulose-based scaffold. Continuous *in situ* measurement of insulin secretion by pancreatic islets upon chemical stimulation with glucose was performed up to 3 h, and a detection limit of 0.85 μg/ml was reported. Interestingly, Shevchenko *et al.*[350] reported an optical sensor for real-time and label-free monitoring of cellular response after chemical stimulation. The sensor was made of optical fibers and exploited the SPR on the surface of the optical fibers as a sensing mechanism. The authors showed that the sensor was able to measure the effects of trypsin, serum, and sodium azide on NIH-3T3 fibroblasts, such as cell detachment from the sensor surface, serum uptake, and inhibition of cell metabolism. Finally, a nanoplasmonic biosensor was reported by Li *et al.* for the real-time monitoring of cellular secretion in the culture medium.[199] The performance of the sensor was demonstrated by analyzing the real-time secretion of VEGF from HeLa cancer cells for 10 h. The sensor showed an impressive sensitivity of 145 pg/ml for VEGF detection.

Despite these success stories, implementing SPR-based sensors in OoC platforms still presents several significant challenges. Technically, integrating stable SPR sensor surfaces within microfluidic chip architectures is complex due to miniaturization requirements and the need of maintaining optical access without disrupting the biological environment. The sensor materials must be compatible with chip substrates, potentially affecting sensor performance and biological relevance. The OoC complexity, which includes heterogeneous cell populations and target analytes at low concentration, complicates data interpretation. Analytically, avoiding non-specific binding and maintaining a high SNR are persistent issues that require sophisticated surface chemistry and assay optimization. From a fabrication perspective, achieving reproducible, uniform functionalization of sensor surfaces within confined chip geometries is challenging. Ensuring robust ligand immobilization and sensor regeneration in these small-scale environments while preserving biological functionality is critical for reliable

measurements. Finally, SPR sensors might have limited use in current commercially available OoC systems because of low throughput and the complex instrumentation, which may hamper multiplexed analyses. Nonetheless, the SPR high sensitivity and its non-destructive nature support dynamic monitoring over time without compromising cell viability or function, making it appealing for OoC integration.

5. Raman spectroscopy

Raman spectroscopy (RS) is an optical technique to detect molecules and determine their composition by analyzing their vibration when light interacts with them without needing to add any fluorescent labels to the target analyte. Monochromatic light is used to probe molecular vibrations by measuring the inelastic scattering of light. The use of RS for biological applications is constrained by minimum concentration requirements for the target analyte (at least >1–10 mM).[174] Signal enhancement mechanisms are necessary to detect analytes at lower concentrations (i.e., nanometer to micrometer) typical of physiologically relevant liquid samples. This is achieved by the surface-enhanced Raman spectroscopy (SERS) that allows to significantly enhancing the Raman signal through contact of analytes with the surface plasmon of a metallic substrate. Electromagnetic and chemical interactions between the metal surface and the adsorbed target molecules enable to increase sensitivity, making the detection and analysis of the Raman signal more effective, even down to a single-molecule level.[394] The possibility to functionalize defined substrate regions with metals allows to design hotspots where the Raman signal amplification is most pronounced, achieving localized ultrasensitive molecule detection.[290] Because of its high efficiency, SERS is suitable for multiple biological applications. Examples include biomolecule identification,[174] classification of healthy and cancer cells,[95] monitoring of spheroids and organoids differentiation,[170,294] and ultrasensitive and rapid genotype analysis of gene mutations.[93] In the field of microfluidics, SERS is an interesting sensing technique because it offers non-destructive, rapid, and *in situ* measurements of biomarkers, whose spectroscopic fingerprints can be retrieved from databases of known biological substances.

Limited to the context of joint applications, an example of how RS can be used to characterize chondrocyte-derived engineered cartilage grafts was reported by Power *et al.*[303] The study showed that hyaline cartilage and perichondrium could be identified with a sensitivity of 89% and specificity of 77% by RS measurements. Also, the maturity of engineered grafts could be accurately estimated based on the ratio of GAGs to DNA and histological score. In the OoC field, RS was recently applied to an intestinal epithelium on-chip to noninvasively evaluate permeability alterations.[34] Caco-2 cells derived from human colorectal adenocarcinoma were treated with a chelating agent that disrupts tight junctions and increases epithelial permeability. Cells were cultured on PET membranes with a pore size of 0.4 μm placed into a modified commercial biochip (Fluidic 653 microfluidic ChipShop, Jena, Germany) previously modified to have a chamber opening on top for optical access. Single-point measurements on Caco-2 cells monolayers were performed using a Raman microspectroscopy apparatus and proved to be stable for up to 4 h. To account for the substrate background signals, Raman analyses were performed first on the cell-free transwell membrane, then on confluent cells onto the same membrane before and after the chelating agent exposure. Results indicated that RS, combined with machine learning techniques for spectra classification, enabled a real-time classification between intact and different levels of damaged epithelium without performing preliminary procedures (e.g., for immunofluorescent staining). From a fabrication perspective, the use of commercially available microfluidic chips and standard RS apparatus made the implementation seamless. Analytically, the OoC platform resulted in efficient in quantifying changes in Caco-2 cell tight junctions noninvasively and in real-time. The inherently weak RS signal was the source of analytical challenges in discriminating heavily damaged epithelium from cell-free membranes due to physical similarity and signal from underlying substrate. Signal enhancement strategies may be useful to reduce the acquisition time and increase the sensitivity and throughput of this platform. Zbinden *et al.*[419] demonstrated potential of RS to characterize the endocrine functionality of EndoC-βH3 cells in a model of pancreas-on-chip. Kinetics of insulin secretion in response to glucose stimulation was locally monitored in real-time and in a contactless fashion. RS also allowed to detect lipids, mitochondria, and nuclei. Raman spectral analysis also showed a glucose stimulation-dependent increase in mitochondrial activity as well as changes in the lipid composition of insulin-secreting vesicles. These findings demonstrate the potential of the pancreas-on-chip model, combined with RS, as a tool for studying pancreatic function and related metabolic processes.

In general, apart from the equipment cost and complexity, the direct integration of RS in OoC poses some challenges. From a sensing perspective, the Raman signal is often weak. If electromagnetic or chemical enhancement strategies are not implemented, a trade-off must be accepted between real-time monitoring and maximum sampling frequency, which may increase the acquisition time. Achieving high spectral resolution and sensitivity may be challenging in a miniaturized OoC setup, especially when subtle biochemical changes have to be distinguished or overlapping peaks from various biomolecules and the substrate are present. Additionally, the RS spatial resolution may also be decreased by light scattering and tissue fluorescence that can mask the spectra.[34] As for other optical sensing techniques, microfabrication must ensure optical accessibility and minimize the number of layers along the optical path to avoid signal interference. Calcium fluoride (CaF_2) is the favorite material as Raman substrate because it introduces almost no spectral clutter, it is non-fluorescent and exhibits a single narrow Raman band. This makes it ideal for minimizing substrate background compared to glass or quartz, which often add photoluminescence or multiple bands that overlap with spectral regions relevant for biomolecules.[167] However, while the advantages of CaF_2 for Raman are clear, its integration into microfluidic tissue models is not straightforward. From a fabrication perspective, CaF_2 is mechanically brittle, making precision machining and thickness control challenging. Bonding CaF_2 to common OoC materials such as PDMS can also problematic due to mismatched thermal expansion coefficients and the use of adhesives that can lead to delamination. Practical implementation strategies therefore favor the use of CaF_2 as an optical window rather than a structural material for the microfluidic channel manufacturing.[210] Technologically, the integration of RS into OoCs must also contend with the bulkiness of conventional spectrometers. For future applications, portable Raman systems may overcome this problem, providing good sensing performances combining high-quality optics and compact design for miniaturized lasers and detectors.[280]

6. Fluorescent nanoprobes

Nanoprobes are advanced nanomaterials engineered for sensitive bioimaging, biosensing and diagnostics. They can be broadly classified into non-fluorescent nanoprobes (such as gold[23] and magnetic[48,414] nanoparticles) and fluorescent nanoprobes (e.g., organic dyes[388] and inorganic nanocrystals such as quantum dots[110]). Gold nanoprobes act as colorimetric indicators through light absorption changes, enabling rapid, cost-effective detection,[37,159] though toxicity remains a concern.[155] Magnetic nanoprobes, valued for operational simplicity and low background noise, are used in magnetic resonance imaging, drug delivery, and bioseparation applications, but they may suffer from magnetic saturation and signal loss in complex biological environments.[276,369] Organic nanoprobes, typically based on fluorophores or organic polymers, allow functionalization for targeted biosensing but may lack photostability under prolonged illumination.[393] Instead, quantum dots are semiconductor nanocrystals with high fluorescence brightness and stability, tunable light emission, and multiplexing capability.[100,434] Despite these valuable properties, they are usually expensive to produce and often contain toxic heavy metals, which may limit their use to selected biological applications.[228]

In this review, we focus on fluorescent nanoprobes, which enable real-time, multiplexed, and photostable monitoring of cellular and molecular processes.[206] Functionalization with biochemical elements, such as antibodies,[88,225] allows precise targeting of cells, tissues, or ECM components.[113] Integrated with fluorescence microscopy, these probes facilitate studies of drug uptake,[112,328] biomarker dynamics,[77,143] and intra- and extracellular interactions at high resolution.[368] They also permit dynamic monitoring of cell migration,[222,314] proliferation,[6] and apoptosis.[292,416] When incorporated into microfluidic chips, fluorescent nanoprobes provide high sensitivity at low volumes and multiplex detection within a single device.[193,408] For example, multiple mRNA transcripts can be detected in individual cells and sorted by fluorescence, enabling non-destructive analysis of cell differentiation at both single-cell and population levels.[193]

Despite their versatility, fluorescent nanoprobes face challenges including cytotoxicity,[31] signal instability, and photobleaching (Sec. II A 2). Their biological impact depends strongly on composition and surface chemistry, which may interfere with cellular activity.[355,365] For example, quantum dots and other heavy-metal probes can release toxic ions or generate reactive oxygen species, impairing cell function in microfluidic OoC systems.[173,228] In perspective, the application of fluorescent nanoprobes in JoC platforms is promising for gene studies, inflammation detection, and ECM degradation monitoring. Probes targeting mRNA (e.g., Runx2, Sox9),[193] cytokines (e.g., TNF-α, IL-6),[195,402] or ECM components (collagen, proteoglycans, metalloproteinases)[192,311] could visualize cartilage degradation and therapeutic responses at single-cell resolution.

Regarding joint applications, Li *et al.*[193] employed fluorescent probes targeting Runx2 and Sox9 mRNA to monitor gene expression in individual cells, providing insights into cartilage homeostasis and OA progression. Gold nanoparticles were functionalized with capture oligonucleotides specific to Runx2 or Sox9 genes, and a fluorescently labeled short peptide. Those probes, directly added into the medium (either growth or osteogenic medium), were taken up by live cells [human bone marrow-derived mesenchymal stem cells (MSCs) cultured in a monolayer] via endocytosis during an overnight incubation. Fluorescence intensity correlated with RT-PCR results and was quantifiable by flow cytometry. MSCs could take up both Runx2 and Sox9 probes: 81% and 87% uptake for Runx2 and 95% and 97% uptake for Sox9 in growth and osteogenic medium, respectively (cf. Table VI). Nonetheless, challenges remain regarding the relatively long incubation time ($\sim$16 h) and the potential variability in probe uptake by endocytosis due to the influence of the probe and the medium. While fluorescent RNA-based nanoparticle probes allow live-cell mRNA detection, variability in probe uptake and intracellular processing via endocytosis can impact fluorescence intensity and measurement accuracy. These limitations, described in critical analyses of SmartFlare probes,[67] caution that intracellular trafficking and probe release dynamics should be considered when interpreting probe-based fluorescence signals, making fluorescence intensity a semi-quantitative rather than absolute measure of mRNA expression.

Although fluorescent nanoprobes have not yet been integrated into JoC platforms, their feasibility has been demonstrated in other OoC systems, where they have enhanced disease modeling and therapeutic testing. For example, a liver-on-chip model of non-alcoholic fatty liver disease (NAFLD) employed fluorescent nanoprobes to track lipid accumulation and metabolic changes.[120] HepG2 hepatoma cells were cultured under free fatty acid supplementation in a microfluidic device mimicking the endothelial–parenchymal interface of liver sinusoids, supporting nutrient diffusion and waste removal. Fluorescent probes (carboxy-H2DCFDA), located in the cell culture compartment, quantified intracellular reactive oxygen species levels, while additional fluorescence-based assays quantified triglyceride accumulation and cell viability. Compared with 2D cultures, the perfused chip showed milder triglyceride accumulation and higher viability, more closely reflecting the gradual progression of chronic steatosis *in vivo*. Hence, the NAFLD-on-a-chip system replicates better than the 2D culture the gradual progression and cellular characteristics of chronic steatosis observed *in vivo*. The authors noted, however, that further work is needed to quantify oxidative stress biomarkers under varied fatty acid conditions and to incorporate co-cultures for improved architectural fidelity.

Fluorescent nanoprobes have also been integrated into microfluidic tumor models to monitor cancer stem cell metabolism in real-time. Lin *et al.*[206] developed an ATP-responsive mitochondrial probe within a 3D glioma-on-chip platform consisting of three parallel channels separated by micropillars. The central channel mimics the ECM and is flanked by a glioma stem cell culture chamber, on one side, and a stimulation chamber, on the other, where biochemical factors can be introduced. The probe combined an ATP aptamer functionalized with a quencher, a complementary peptide nucleic acid labeled with a fluorophore, and a triphenylphosphonium ligand for mitochondrial targeting. In the presence of ATP, the aptamer strand of the probe binds to the ATP, thus disrupting its duplex structure. Then, the mitochondria are targeted by the triphenylphosphonium-conjugated peptide nucleic acid sequence of the probe with the recovery of fluorescence. The probe showed high sensitivity, specificity, and biocompatibility. Functionally, TGF-β stimulation induced invasive migration of glioma stem cells, accompanied by elongated or spindle-shaped mesenchymal morphology and elevated ATP-dependent fluorescence. Instead, acidic stress suppressed ATP production and signal intensity, consistent with low-energy tumor microenvironments. This platform thus enabled dynamic investigation of cancer stem cell metabolism and invasion. A similar strategy could be adapted to OA/RA JoC studies, where altered

ATP synthesis by chondrocytes[63] and extracellular ATP contribute to inflammation and pain.[181,377] Translation would require optimization of ECM composition to joint-specific matrices, validation in relevant cell types (e.g., chondrocytes, synoviocytes), and incorporation of inflammatory stimuli such as TNF-α and IL-6, alongside addressing challenges of long-term culture stability and complex tissue microenvironments.

B. Electrical sensing techniques

Electrical sensing techniques are among the most commonly used in OoC applications, possibly due to the simplicity of integrating miniaturized electrodes that enables the continuous assessment of the cellular behavior. These integrated sensing techniques offer high temporal resolution measurements to monitor dynamic processes,[69] including cell proliferation,[14,105,358] barrier function integrity,[136,154,438] electrophysiological activity,[109,372,382] and response to pharmacological treatments.[264,275,383] The label-free detection approach of electrical sensing techniques eliminates the need for fluorescent markers, overcoming a limitation of the optical sensing techniques. Conventional electrical sensing techniques are typically limited to measuring only one property of electrical response at a time. Efforts have been made recently to integrate multiple sensors in the same platform to achieve multiplexed sensing capabilities,[12,26,151,426] although this poses challenges in signal acquisition (e.g., interference) and scalability. In fact, the multiplexed-sensor approach inherently increases spatial footprint, thereby limiting spatial resolution and complicating cell-level recordings. The spatial difference that may arise from recording multiple signal simultaneously can also compromise the accuracy when studying correlated tissue responses.[109] As a result, this added complexity may elevate the invasiveness of the system, potentially affecting tissue integrity and biological compatibility.

The efficacy of the electrical sensing techniques strongly depends on the choice of microelectrode material and design, which are dictated by the sensor operation mode (as further discussed for each specific technique). Multiple materials have been proposed for manufacturing microelectrodes. Gold and platinum are used due to their biocompatibility, chemical stability, and conductivity, though they suffer from contact impedance that limits low-frequency signal detection.[92,158] Increasing the electrode footprint or the surface area is a successful strategy to overcome this issue, which can be achieved by coating the electrode surface with a thin-film of porous materials, like the platinum-black.[237,412] Silver/silver chloride (Ag/AgCl) electrodes are not polarizable and feature low contact impedance,[376] which make them suitable as reference electrodes for measurements at low frequency in a biological environment. If electrical and optical sensing analyses must be combined, indium tin oxide (ITO) electrodes are particularly interesting thanks to their transparency,[239] though their brittleness restricts their use in flexible devices. Electrodes coated with poly(3,4-ethylenedioxythiophene):polystyrenesulfonate (PEDOT:PSS) represent a major advancement, reducing interfacial impedance up to 40-fold through enhanced charge transfer and capacitive coupling.[200] They are flexible, biocompatible, and suitable for high-resolution recordings, but their performance declines for an electrode diameter smaller than 5 μm due to fabrication limits such as coating inhomogeneities.[387]

In addition to material selection, electrode size and positioning within the OoC platform are other critical manufacturing constraints affecting the electrode sensing performance. As electrode dimensions decrease, impedance increases owing to reduced geometric surface area. In addition to the aforementioned coating strategies, interdigitated geometries may be useful to maximize the effective electrode area[59,411] while preserving optical access for cell imaging. Electrode position and measurement topology further influence the sensor analytical performance: simple two-electrode arrangements are easy to implement and compatible with commercial impedance analyzers but remain susceptible to electrode polarization and non-uniform current density artifacts, whereas tetrapolar configurations separate current injection from voltage sensing to mitigate polarization impedance. 3D electrode arrays[54,161] may also be employed to increase the effective surface area and sensitivity. However, they amplify electric field inhomogeneities and introduce position-dependent sensitivity whereby cells at different locations contribute unequally to the composite impedance signal.[309] In this case, interdigitated electrodes are an option to obtain uniform electric fields. Environmental factors such as temperature fluctuations, culture media, and extra-cellular environment composition introduce additional drift and background noise that should be compensated by performing measurement in a cell-free OoC platform. Environmental factors are also the main cause of long-term stability issues. Electrode degradation due to electrochemical corrosion, biofouling, and mechanical stress limit the operational lifespan of integrated sensors. This is an important design challenge that has to be taken into consideration especially for OoC applications in which the sensors might have an operational use of weeks. All in all, the successful integration of electrical sensing techniques in OoC requires careful balancing of material properties, fabrication constraints, and design requirements. While significant challenges remain in achieving long-term stability and manufacturing scalability, the versatility and high sensitivity of the electrical sensors together with the long-dated experience gained in the field of micro-electro-mechanical systems make this category of sensing techniques appealing for OoC applications. Sections II B 1–II B 4 examine different electrical sensing strategies highlighting, whenever it is possible, examples from JoC within the broader OoC context, while addressing their performance outcomes and the integration complexities they entail.

1. Electric impedance spectroscopy

Electrical impedance spectroscopy (EIS) is a non-destructive and real-time sensing technique that measures how much a material resists or responds to an alternating electrical signal across a spectrum of stimulation frequencies, allowing for insights into the material structure. The perturbation of the electrical system via the application of an AC signal (either current or voltage) over a wide range of frequencies and the measurement of the sinusoidal response (voltage or current, respectively)[186] is performed through pairs of electrodes. For the specific case of OoC applications, EIS is used to derive impedance spectra, which are fitted to an equivalent electric circuit model to extract the specific resistive and capacitive contributions of cell layers and culture medium. In the context of OoC applications, EIS can be used to monitor cellular behavior, barrier function, and tissue development without the need for destructive assays or fluorescent markers.[85] This label-free nature eliminates concerns about cytotoxicity from fluorescent dyes and allows for repeated measurements on the same cell population without interference.

If only the resistive component of the EIS-derived impedance spectra is considered, the transepithelial or transendothelial electrical resistance (TEER) can be computed, which is used as a proxy to characterize the functionality and integrity of biological barriers. In fact, high TEER values are indicative of tight junction formation, which is a measure of the integrity of the barrier itself. Since joints lack an epithelial lining, TEER might potentially only be used to study the integrity of the synovial membrane, which has an inner lining of synoviocytes forming a partially tight membrane, or its pathological progression when subjected to external chemical stimulation with pro-inflammatory mediators. Considering the scope of this review and the fact that, to the best of the author's knowledge, TEER has not yet been applied to JoC applications, readers are referred to dedicated recent reviews for more information.[232,363]

While EIS finds limited applicability in the context of JoC when used as a single sensing method, EIS-based electrochemical sensors hold a bigger potential for joint research because they enable the detection of cytokines and other metabolic molecules in pathological JoC models. As cells deposit ECM components, the electrical properties, such as resistance and capacitance, of the tissue construct progressively change. By monitoring this impedance variation over time, EIS provides quantitative insights into both the amount and quality of matrix deposition. Shabani *et al.*[344] developed a label-free biosensor for the rapid detection of MMP-9, an enzyme particularly expressed during RA that plays a role in joint degradation. The sensor features an MMP-9 mouse monoclonal antibody immobilized on the surface of zinc oxide (ZnO) nanoparticles and gold electrodes. The resistance between the electrodes, computed with EIS and voltammetry (Sec. II B 4), served as an indicator for the MMP-9 concentration. The sensor showed a linear behavior in the range of 1–1000 ng/ml and a limit of detection of 0.15 ng/ml (cf. Table III). In terms of analytical performance, the sensor demonstrated less than 10% difference compared to commercial ELISA for human serum samples while being much more rapid (35 min vs 5 h). Additionally, the sensor showed high-specificity to MMP-9 without being biased by the non-specific adsorption of the other proteins present in the human serum. From a microfabrication perspective, standard manufacturing techniques were employed, namely, e-beam evaporation for metal deposition and hydrothermal method for ZnO growth. The fabrication process resulted suitable for mass production; therefore, no challenges are expected for the integration of this sensor in JoC platforms.

Regarding the topic of this review, EIS has also been used for the detection of specific RA biomarkers in standalone sensors. Various approaches were followed to manufacture sensors for anti-citrullinated peptide antibody (ACPA) detection, including covalent functionalization of interdigitated electrodes with citrullinated peptide antibody (CPP)-coated gold nanoparticles[203,384] or with SAMs.[52] Additionally, label-free methods for detecting RF immunoglobulin M (IgM-RF) and IL-1β have been reported. Chinnadayyala *et al.*[53] proposed a sensor based on an interdigitated wave-type microelectrode array (MEA). Electrodes were functionalized with a thioctic acid SAM for antigen immobilization. Impedimetric analysis performed by EIS with ferro/ferricyanide redox probes revealed clear changes in impedance and charge transfer resistance upon IgM-RF binding. The sensor showed a linear response between 1 and 200 IU/ml, with a detection limit of 0.6 IU/ml in redox probe and 0.22 IU/ml in serum. Aydin *et al.*[13] developed an impedimetric immunosensor for IL-1β detection using semi-conductive poly(2-thiophen-3-yl-malonic acid) (P3-TMA) as immobilization matrix and anti-IL-1β antibodies as biorecognition elements. P3-TMA was covalently attached to transparent ITO thin-film electrodes. EIS measurements were proportional to IL-1β concentrations in the range 0.01–3 pg/ml, with a detection limit of 3 fg/ml.

EIS has also been successfully employed for the detection of TNF-α from non-diluted human synovial serum.[178,306] Pui *et al.*[306] proposed an EIS-based sensor to measure TNF-α concentration as part of a platform to detect toxicity induced by inflammatory responses. For AC sweep impedance measurements, a frequency range of 1 Hz–0.5 MHz was used together with an initial potential of 0 V and an amplitude of 25 mV. The biosensor was microfabricated on a silicon substrate with an array of 24 circular gold electrodes. A titanium/gold layer (Ti/Au, 0.1 μm/1.0 μm) was deposited using an electron-beam evaporation. Electrodes were functionalized with a SAM of dithiobis-succinimidyl propionate (DSP) and utilized immediately for immobilization of TNF-α antibodies (anti-TNF-α). The sensor showed higher sensitivity compared to the conventional ELISA method (limit of detection ~57 vs 890 fM), and a proportionally decreasing response while detecting TNF-α (1–100 pg/ml) in culture media (cf. Table III). Exploiting conventional photolithography techniques, this sensor can be readily manufactured during a JoC fabrication process. The biocompatibility was guaranteed by the selection of the electrode material, and an anti-fouling strategy was implemented to prevent the non-specific adsorption of proteins by adding a coating of ethanolamine to the electrodes. Analytically, the sensor demonstrated high-selectivity through competitive assay against IFN-γ, showing minimal non-specific response. In terms of scalability, the electrode array format enabled simultaneous measurements, thus showing potential for high-throughput drug screening applications.

Considering all previous examples, it appears evident how EIS is a sensing technique with clear added value for the detection of OA/RA biomarkers, yet its use in JoC models is still limited, unlike in other OoC applications. For instance, Fernandes *et al.*[97] exploited EIS for the real-time monitoring of epithelial barrier integrity in a microfluidic platform containing both lung- and gut-on-chip models. Over the course of 5 days, growth and polarization of human epithelial cells from the airway or gastrointestinal tract were continuously monitored. Impedance data were used to mathematically derive the resistance and capacitance of the cell layers. As a proof-of-concept for drug testing, the airway epithelial barrier was treated with RNA to mimic viral infection. EIS was able to retrieve a rapid decrease in barrier integrity due to the disruption of tight junctions and the reverse of this effect upon administration of a corticosteroid drug. Interestingly, Marrero *et al.*[239] developed semitransparent organic PEDOT:PSS-coated electrodes to monitor the impedance of cellular barriers in a gut-on-chip model. In addition to being able to monitor the barrier formation and disruption after treatment with a permeability enhancer, the sensor demonstrated good performance under flow conditions, while the transparency ensured optical accessibility to the OoC. Other examples of EIS applications were reported for on-chip patho-physiological models of lung,[244] gut,[381] and heart.[334,425]

EIS is emerging as a cost-effective and scalable technique for OoC monitoring, offering an accessible alternative to optical methods. However, its successful integration depends on addressing fabrication complexity, material selection, and data interpretation. As we previously discussed, electrodes must remain biocompatible, stable under

TABLE III. List of electrical sensing techniques relevant for application (part I). Matrix metalloproteinase 9 (MMP-9); zinc oxide (ZnO); enzyme-linked immunosorbent assay (ELISA); limit of detection (LOD); limit of quantification (LOQ); tumor necrosis factor alpha (TNF-α); dithiobis-succinimidyl propionate (DSP); self-assembled monolayer (SAM); interferon gamma (IFN $-\gamma$); hydrogen peroxide (H_2O_2); nitric oxide (NO); polydimethylsiloxane (PDMS); nitric oxide synthase (NOS); N(G)-monomethyl L-arginine (L-NMMA).

Sensing technique	Target analyte	Sensing element	OoC integrated?	Sensing performance	Reference
EIS and cyclic voltammetry (CV)	MMP-9	MMP-9 antibody immobilized ZnO nanostructures	No, but applied to joint	Rapid analysis (35 min vs 5 h for ELISA), range: 1–1000 ng/ml, CV sensitivity $= 28\,\mu A/(\text{decade} \times \text{cm}^2)$; EIS sensitivity 2.9 k$\Omega$/decade, LOD = 0.4 and LOQ = 0.92 ng/ml	344
	Challenges	Precise antibody immobilization and surface functionalization is needed; biofouling strategies not implemented but demonstrated high sensitivity without interference from other serum protein; conventional microfabrication techniques allow OoC integration.			
EIS	TNF-α	Anti-TNF-α antibody on a Au microelectrode array functionalized with DSP SAM	No, but applied to joint	Range: 1–100 pg/ml, LOD = 57 fM, sensitivity 0.526 k$\Omega/(\text{g/ml})$, operational time = 48 h	306
	Challenges	Biofouling minimized by ethanol amine blocking of SAM unreacted sites; selectivity demonstrated through competitive assay against IFN-γ; array format allows parallel measurements, potential for high-throughput OoC applications.			
MEAs, EIS, electrochemical voltammetry, and amperometry	Extracellular ionic currents (Na^+andk^+), tissue impedance, epinephrine, H_2O_2	CMOS microelectrode platinum array	Yes, heart-on-chip	Proportional to electrode configuration; action potential: detection range $\sim \mu V_{pp}$, input-referred noise: $4.9 \pm 0.2\,\mu V_{rms}$; tissue impedance: measured for droplet up to $\sim 5\,\mu l$, optimal impedance imaging at 100 kHz; epinephrine: range = 1–200 μM, current noise $\leq 554\,pA_{rms}$, time stability: stable over 3 h washout experiments; H_2O_2: linear range = 1–250 μM, $1.9 \leq \text{LOD} \leq 7.9\,\mu M$	26
	Challenges	Sensing challenges: EIS and electrical voltammetric background noise compensated by measurement in PBS or medium without tissue, non-Faradaic background currents handled digitally, interference due electrode impedance and parasitic capacitance at high frequencies, noninvasive measurements facilitated by direct contact between the analyte and the sensing element, amperometric measurements validated against non-enzymatic H_2O_2 biosensors; fabrication challenges: complex assembly process with 68% success rate due to bonding issues, biocompatibility and long-term stability yet to be demonstrated.			
Electrochemical amperometry	NO	3D stretchable gold nanotubes assembled into porous network	Yes, cartilage-on-chip	Range: 20 nM $-$ 2μM, LOD = 12.3 nM, response time $\leq$2 s, electrochemical stability under	308

TABLE III. (Continued.)

Sensing technique	Target analyte	Sensing element	OoC integrated?	Sensing performance	Reference
		with PDMS as support matrix		dynamic compressions (up to 1500 cycles at 20% and 50% strain).	
	Challenges	Sensor specificity confirmed by control experiments with NOS inhibitor (L-NMMA); demonstrated potential for drug testing via response to Ibuprofen; technological challenges: maintaining sensor performance under cyclic mechanical loading, ensuring stable electrical contacts in a flexible and porous 3D matrix; supported future integration of multi-tissue JoC with multiplexed sensors capability.			

long-term culture conditions, and their placement should be designed to maintain electrical contact with biological samples without obstructing optical access for microscopy. Integrating rigid electrode substrates within flexible microfluidic materials, like PDMS, also presents bonding and sealing difficulties, as fluidic integrity must be preserved alongside reliable electrical connections. Analytical challenges also limit the widespread use of this sensing technique. Measurements at low frequencies are often dominated by electrode polarization effects, while high frequencies may lack sensitivity to subtle biological changes. Moreover, EIS is susceptible to environmental noise (e.g., temperature fluctuations[385]), so signal-processing and calibration strategies are often needed. Among others, these include differential measurement techniques and calibration of the system with media of known electrical properties. Finally, EIS generates frequency-dependent datasets that typically require advanced analysis (e.g., equivalent-circuit fitting[370] or machine learning[406]). With continued improvements in electrode design and data analysis, EIS may be adopted more broadly in the context JoC applications.

2. Electric cell-substrate impedance sensing

Electric cell-substrate impedance sensing (ECIS) is an impedance-based technique to non-destructively monitor the cell behavior in real-time that requires culturing cells directly onto coplanar electrodes integrated on an appropriate substrate. Based on the work of Giaever *et al.*,[117] ECIS measures not only the cell impedance but also the impedance due to the interaction between the cells and the substrate they are grown onto as they attach, spread, and respond to stimuli. In addition to tight junctions, ECIS is used to track changes related to cell adhesion, proliferation, migration, and morphology. In contrast to EIS, ECIS uses a two-electrode configuration with small electrodes embedded at the bottom of the OoC platform, paired with a larger counter electrode. Cells are cultured directly on these electrodes, and the impedance is measured between the cell-covered working electrode and the counter electrode. As the cells grow, the effective electrode surface area is reduced, and an increase in the impedance between the working and the counter electrode can be measured. ECIS differs from EIS/TEER because (i) the measurements are localized and, if an array of electrodes is used, the impedance as a function of the location can be derived;[163] (ii) it does not provide data only on barrier formation, but it measures changes in the cellular adhesion.[396] In the interest of brevity, we only recall here that, given the similar working principle, ECIS shares fabrication and analytical challenges with EIS (Sec. II B 1).

As far as the authors know, ECIS has not yet been used experimentally for JoC applications. Instead, Che *et al.*[47] proposed a numerical workflow that integrates a tissue-specific 3D geometry of cartilaginous cells reconstructed from confocal fluorescence microscopy images to estimate dielectric properties and evaluate their dependence on structural and bioelectric parameters. A realistic ECIS chip geometry was modeled, consisting of interdigitated electrodes embedded within a culture well. Cells, segmented from microscopy images, were arranged to fully cover the electrode surface. The study examined dielectric properties across a broad frequency spectrum (1 kHz–1 THz), focusing on conductivity, relative permittivity, and complex impedance. Multiple cell models were tested, with the most complex being the one incorporating the cell membrane, nucleus, and PCM. At low frequencies, conductivity did not exhibit frequency dependence.

The addition of the PCM resulted in reduced conductivity, whereas including the nucleus increased it. These findings underscore the inadequacy of simplified cell models for cartilage, where layered structures substantially alter dielectric behavior. This approach supports the development of a digital twin framework, integrating numerical models with experimental impedance measurements for real-time monitoring of cartilage impedance.

Because of the implications for musculoskeletal research, we briefly report studies where ECIS has been applied to other OoC platforms that can be translated for the development of mechanically active JoC models. Zhang *et al.*[428] used ECIS to monitor in real-time cell growth and viability under cyclic strain. Bovine aortic endothelial cells (BAECs) were cultured under 8% strain at 1 Hz for 75 h using a novel stretchable ECIS sensor with gold electrodes on a PDMS substrate. The system comprised a circular working electrode (3.14×10^{-4} cm^2) and a semi-circular counter electrode (0.36 cm^2). After calibration (40 Hz–100 kHz), ECIS measurements were performed at 9 kHz. The sensor enabled simultaneous analysis of proliferation, cell density, and mechanical stimulation. A linear correlation was observed between seeding density (30.6×10^3 cells/cm^2, impedance $= 2707 - 2945\,\Omega$) and final density (105.71×10^3 cells/cm^2). Electrodes were seamlessly integrated in microfluidic devices, and PDMS was functionalized with APTES, gelatin, and fibronectin to enhance adhesion. Comparison with fluorescence assays confirmed accuracy, while resistance variations due to stretching ($120 - 200\,\Omega$) were negligible. Such sensors, integrated in JoC models, may allow real-time monitoring of OA/RA progression by detecting altered proliferation, detachment, or inflammatory responses. Considering the 3D nature of OoC platforms, Pan *et al.*[287] developed a 3D-ECMIS method for dynamic, noninvasive monitoring of viability and drug susceptibility. Human hepatoma cells (HepG2) were cultured in Matrigel scaffolds within PET chambers containing vertical Au electrodes. An AC voltage of 30 mV at 10 kHz was applied, with signals recorded from height chambers. A normalized cell index ($\Delta Z/Z_0$) compensated for electrode–electrolyte effects. The system monitored proliferation over 96 h, correlating well with 2D assays. Drug screening with taxol, cisplatin, and sorafenib showed that only 3D-ECMIS captured the correct proportionality between drug efficacy and viability, demonstrating improved accuracy for *in vitro* testing. Finally, Huang *et al.*[144] combined ECIS with microelectrode arrays (MEAs) and perfusion to monitor cortical neuron activity. Sixty Au microelectrodes (50 μm diameter) were fabricated by photolithography. ECIS was performed hourly for 7 days before oxygen glucose deprivation (OGD). Impedance at 1 kHz, sensitive to growth and damage, revealed marked decreases under OGD, with viability dropping to 28% after 30 min. IGF-1 treatment improved adhesion, stabilized impedance, and preserved viability at 49%.

3. Multi-electrode arrays

Multi-electrode arrays (MEAs) are essential microsensors used for real-time, local monitoring of cell electrical activity. They consist of a set of microelectrodes, enabling the simultaneous and noninvasive recording of extracellular activity (e.g., action or field potential) from multiple locations with high spatial resolution. The principle behind MEAs involves measuring the voltage difference between a working electrode, which must be close to the cells, and a reference electrode, which can be placed in a convenient location within the OoC system. MEAs are typically used to quantify extracellular field potential variations resulting from alterations in the cell membrane polarization. Within the OoC environment, cells should be grown directly on the MEA surface to achieve high sensitivity and spatial resolution, as the field potential rapidly diminishes with distance from the source of electrical activity. Being a local sensing technique, MEAs can measure electrical signals from multiple locations even in the presence of cell distribution inhomogeneities. However, traditional MEAs typically have a planar (2D) configuration, and they are manufactured on rigid substrates. This does not mimic the soft material on which cells proliferate *in vivo*. Cells must be cultured directly on top of the MEA for high sensitivity, limiting the ability to capture the 3D nature of complex tissues. Additionally, MEAs often suffer from a low SNR. Although 3D,[424] highly sensitive,[179,291] and soft[2,219,341] have been proposed, many current approaches require cumbersome instrumentation, making direct integration into OoC systems for high-throughput applications challenging.

An important field of application for MEAs is their integration into innervated JoC models to investigate the mechanisms of pain associated with OA and RA. OA is a leading cause of chronic joint pain, yet the mechanisms underlying sensory nerve growth and sprouting remain poorly understood. ECM breakdown and vascular invasion can promote sensory nerve sprouting into articular cartilage,[50] implicating aberrant innervation as a potential driver of pain. A recent work has demonstrated that inflammatory macrophage secretomes can promote neuronal ingrowth via paracrine signaling in a 3D engineered OA cartilage-on-chip model, while miniaturized ELISA-based platforms enabled a quantitative analysis of inflammatory mediators[160] (Sec. II D 1). Moreover, innervated JoC platforms have been developed to directly model pain pathways. Makarczyk *et al.*[231] proposed the so-called NeuSynCar system combining dorsal root ganglion (DRG) innervation with cartilage and synovial constructs in a two-chamber microfluidic device. When the cartilage was inflamed with IL-1β, its conditioned medium induced synovial inflammation, elevated cytokine release (including CCL-2, CXCL-1, IL-6, and IL-8), and robust neuronal activation as measured by calcium imaging. These findings demonstrated that cartilage degradation products can drive synovial inflammation and neuronal sensitization, providing a direct mechanistic link to OA pain. Each component of the joint can release mediators capable of inducing pain, but identifying the key drivers in individual patients remains a major challenge. To address this, Preisegger *et al.*[304] developed innervated synovial-like tissue models, in which human fibroblasts and macrophages are co-cultured and connected to DRG neurons. Exposure of these constructs to conditioned media and IL-1β derived from inflamed chondrocytes triggered macrophage polarization and increased neuronal activity, highlighting their potential to uncover pain-inducing mediators and advance precision medicine approaches for OA pain. Building on this foundation, the same group engineered a multi-component JoC platform to incorporate osteochondral tissue, synovium, adipose tissue, and macrophages,[259] thereby recapitulating the complex tissue interactions of the joint. The system was further advanced by introducing sensory neurons (L4 and L5 DRG) to create the so-called neu-microJoint, enabling direct crosstalk between peripheral nerves and joint tissues. This hybrid PDMS/3D-printed device uses microchannels to permit axonal growth while maintaining compartmentalization. MEAs were integrated into the JoC platform to assess the neural activity together with

real-time calcium imaging. Functional validation demonstrated that human DRG neurons responded to depolarizing stimuli upon administration of increasing concentrations of potassium chloride (KCl, 10, 30, and 50 mM) after 4 days of culture. Little electrical activity was measured under baseline conditions, but starting from a KCl concentration of 30 mM, MEAs were able to detect neuronal spikes. Additionally, rodent and human DRG neurons cultured between 10 and 28 days showed a significant axonal growth through the microchannels, and neurites exhibited calcium responses in the corresponding soma upon electrical stimulation. Importantly, conditioned media from OA-modeled microJoint tissues activated a subset of neurons, suggesting that specific neuronal populations may be potentially responsible for OA pain in the neu-microJoint. All in all, these advances establish innervated JoC systems as versatile platforms for mechanistic studies of arthritis pain and the evaluation of therapeutic strategies. By integrating MEA technology, these models enable dynamic monitoring of neuronal responses in cartilage or bone tissue,[265] offering an additional tool to understand the neuroimmune mechanisms of OA and RA pain.

Although there are currently no other direct applications in the field of JoC research, to the best of the authors' knowledge, we foresee three potential areas where MEAs and, more generally, electrical recording systems could be applied: (i) chondrocyte electrophysiology monitoring, (ii) synovial fibroblast signaling, and (iii) joint multi-tissue interface modeling. In a cartilage-on-chip model, MEAs could be used to monitor the field potential (i.e., streaming potential) generated by the chondrocyte response upon external mechanical loading.[300] In the case of an over-physiological loading, MEAs could spatially map differences in the streaming potentials to identify early-on OA-like degradation zones. MEAs could also be integrated into a synovium-on-chip to investigate the crosstalk between synovial fibroblasts and other co-cultured cells (e.g., macrophages) under inflammatory conditions. In fact, synovial fibroblasts exhibit electrical signaling during cytokine release (e.g., IL-7, IL-1β)[58] and MEAs could monitor field potential changes, thus providing information on the inflammation state and progression toward a pathological phenotype. Finally, MEAs could be integrated into a subchondral unit-on-chip to investigate the cellular response at the bone/cartilage interface driving the pathological degeneration of those tissues during over-physiological mechanical compression. For instance, osteocytes, known as mechanosensors in bone, exhibit changes in ion channel activity and membrane potential during mechanical loading.[307] MEAs could be used to record extracellular electrical signals generated by osteocytes upon mechanical loading. Moreover, MEAs could be used to detect the activation of mechanosensitive ion channels (e.g., Piezo1) and signaling pathways (e.g., Wnt/β-catenin or integrin-mediated pathways) that are triggered by mechanical compression.[307] This is particularly relevant for understanding how mechanical forces drive cellular responses at the bone–cartilage interface during pathological conditions.

In general, despite their limited integration in JoC models, MEAs are used for many other OoC applications. The nervous system is the primary model with electrical activity that can be recapitulated on-chip.[341] MEAs have been used to study neurons at a cellular level[262] as well as at a network level to investigate their long-term connectivity.[87,407] In the context of drug screening, MEAs have also been used as a method to assess drug delivery[352] and neurotoxicity *in vitro*.[72] Interested readers are referred to a recent review dedicated to the engineering of brain-on-chip platforms.[342] Electrical activity associated with muscle contraction, particularly in heart-on-chip models[152,180,214,325] or in neuromuscular junction-on-chip,[82] can also be monitored using MEAs. Here, we briefly report a few examples of technological solutions that have been found to overcome some MEAs limitations, such as the fabrication on soft substrate or the development of 3D MEA configurations. Zhang *et al.*[424] exploited a 3D platform with a cell culture chamber and platinum pillar electrodes for the real-time *in situ* monitoring of 3D cardiac tissues from primary rat cardiomyocytes. The platform was used to record the basal and isoproterenol-elicited local field potential of cardiac tissues for up to 3 weeks. To culture and monitor cardiomyocytes in a more *in vivo*-like microenvironment, Kujala *et al.*[180] developed a heart-on-chip platform featuring MEAs coated with micromolded gelatin. First, the technical feasibility of coating MEAs with gelatin was demonstrated by measuring the spontaneous field potentials in traditional 2D multi-well at rest and upon drug treatment. Then, a 3D heart-on-chip integrated with gelatin-coated MEAs was built. The response of laminar human cardiac tissues from hiPSC-CMs upon isoproterenol was investigated by recording field potentials from multiple sites. The platform proved to be effective in measuring the drug-induced beating frequency increase, thus demonstrating the potential of this sensing technique. Additionally, it is worth mentioning the work by Visone *et al.*[382] who developed a micro-electrode coaxial guide (μECG) to host a pair of electrodes enabling real-time and *in situ* electrophysiology studies on 3D engineered cardiac microtissues. 3D microtissues were generated by combining human iPSC cardiomyocytes and human dermal fibroblasts. The sensing platform allowed to record the spontaneous beating of the cardiac tissues as well as their electrophysiological response to multiple compounds known to induce pro-arrhythmic effects.[382,383] Finally, we report on the recent work by Bounik *et al.*[26] who developed a novel multifunctional CMOS MEA integrated into an open microfluidic system [Fig. 3(a)]. The study aimed to create a versatile platform for real-time monitoring of 3D cardiac tissue models capable of operating in both hanging-drop mode for *in situ* microtissue readouts and standing-drop mode for conventional MEA applications. The electrical activity of cardiac microtissue was evaluated via hanging-drop and standing drop measurements using 64 and 1024 electrodes, respectively. MEAs allowed to measure the baseline electrical activity as well as the cardiomyocytes' response to the administration of epinephrine. Impedance measurements were performed across a frequency range from 1 Hz to 1 MHz using lock-in detection. Results showed a correlation between the impedance magnitude and the microtissue-to-electrode distance, with impedance increasing as droplet height decreased. Electrical measurements also enabled a label-free assessment of the tissue–electrode contact quality, revealing that the spherical microtissue center maintained close electrode contact while peripheral regions showed variable adhesion patterns. Additionally, H_2O_2 measurements were performed using single-potential amperometry at 0.65 V of applied potential (Sec. II B 4). Tested concentrations varied from 0.1to500 μM. A linear detection range extended from 2.7to250 μM and a limit of detection of 1.9 μM was achieved using a 3×3 electrode configuration. As discussed at the beginning of this section, increasing the electrode surface is an effective strategy to improve both detection limits and linear range. In fact, a 4×4 electrode configuration proved useful to achieve optimal performance comparable to state-of-the-art non-enzymatic H_2O_2 biosensors. Despite these capabilities, this

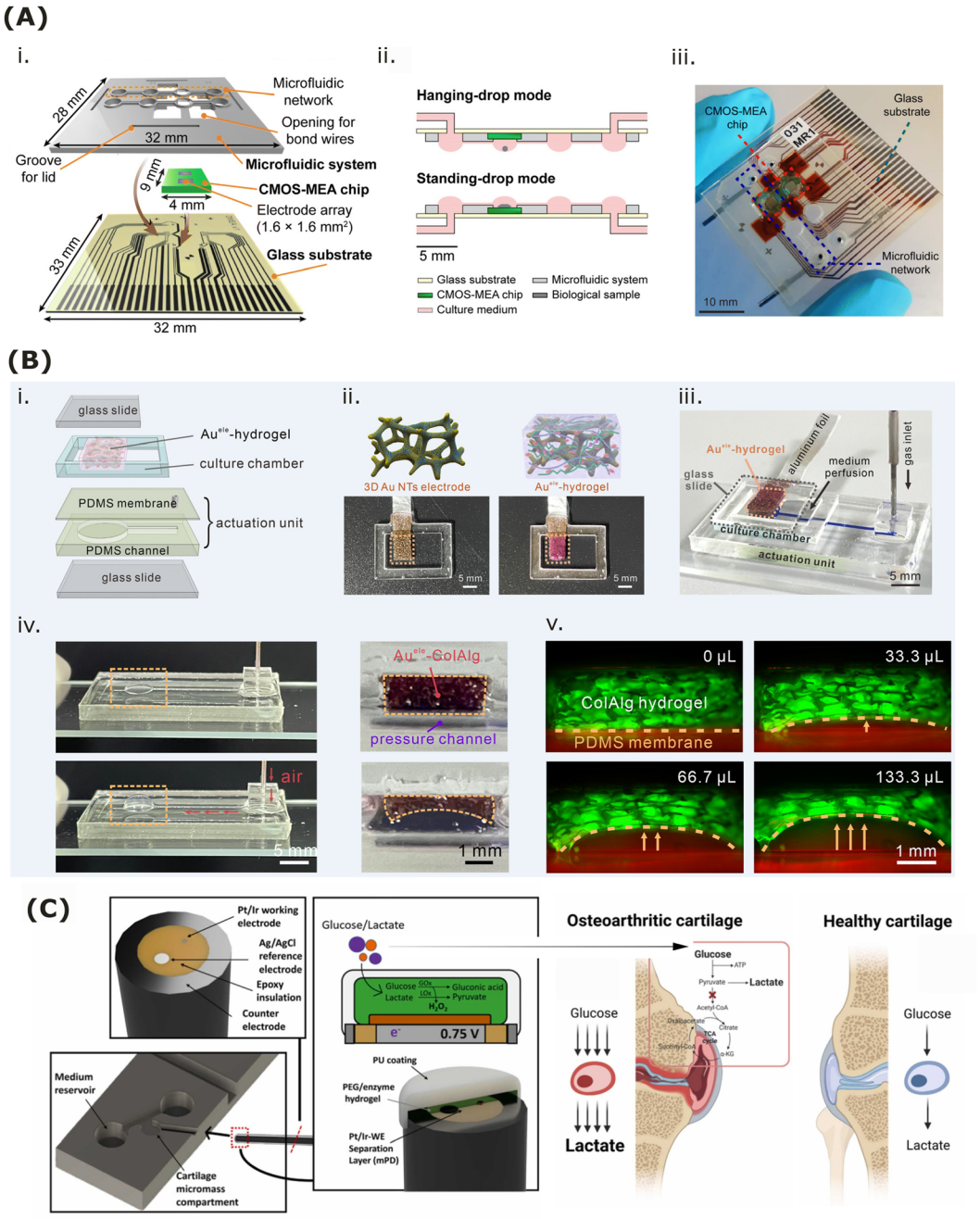

FIG. 3. Examples of electrical sensors. (a) Microfluidic platform integrated with a CMOS-MEA chip. (i) Main structural components of the device. (ii) Side view of the device operated in hanging-drop mode (top) and standing-drop mode (bottom). (iii) Image of the final assembled microdevice. Reproduced with permission from Bounkik *et al.*, Lab Chip **25**, 9 (2025). Copyright 2025 Authors, licensed under a Creative Commons Attribution (CC BY) license. (b) Design of a cartilage-on-a-chip system with integrated 3D electrodes for real-time monitoring of nitric oxide (NO) production under compression loading. (i) Schematic view of the microfluidic device highlighting the cell culture chamber and the actuation unit. (ii) Pictures of the cell culture chamber and the corresponding schematic of the 3D electrodes before and after hydrogel and cell perfusion and (iii) overall assembled device. (iv) Pictures of the device before and after mechanical compression loading by pneumatic gas injection showing the deformation of the cartilage-on-a-chip device. (v) Fluorescence images of the cartilage-on-a-chip device at the maximum compressive strain for different gas volumes. Reproduced with permission from Qin *et al.*, Device **2**, 6 (2025). Copyright 2024 Elsevier Inc. (c) Cartilage-on-a-chip platform with glucose and lactate integrated biosensors, showing a cross-sectional view of the sensor wire and tip coating. Glucose and lactate are oxidized at the sensor tip by GOx and LOx, generating hydrogen peroxide as a by-product. The schematic on the right illustrates the altered glucose metabolism in OA cartilage where increased glycolysis leads to elevated glucose consumption and lactate production. Rothbauer *et al.*, Sens, Actuators, B **427**, 137123 (2025). Copyright 2025 Authors, licensed under a Creative Commons Attribution (CC BY) license.

platform still has some fabrication challenges to address. The assembly success rate is lower than for standard CMOS arrays. To use this platform for high-throughput applications, improvements are needed in layer alignment and wire-bonding procedures, which alone led to 32% of failing devices. However, unlike other single-function microsensor systems, this platform has the merit to combine electrophysiology, impedance spectroscopy, and electrochemical sensing within a single setup, showing a level of integration that is desirable for the next-generation of OoC platforms.

4. Electrochemical sensing

Electrochemical sensors stand out as the most widely used instruments for the continuous and noninvasive monitoring of the extracellular microenvironment. These sensors quantitatively detect the presence of an analyte by converting the result of the electrochemical reaction between the analyte and an electrode into an electrical signal. In amperometry, the current from the working and reference electrodes is measured at a constant applied voltage. The resulting current is proportional to the amount of the electrochemical species undergoing a redox reaction. In case the potential is not held constant but is varied systematically, the sensing technique is named voltammetry. Oxygen, glucose, and lactate levels are typically quantified with this type of electrochemical sensor. In potentiometry, the potential difference between working and reference electrodes is measured.[420] Examples are metal oxide (MOx)-based sensors and ion-sensitive field-effect transistors (ISFET, i.e., a transistor-based sensor where variations in ions concentration change the current through the transistor accordingly). For instance, in ISFET configurations, the transistor gate is functionalized with ion-selective membranes enabling pH sensing.[12]

Electrochemical sensors can also be exploited to perform amperometric measurements of non-electrochemically active analytes by functionalizing the working electrode with a biological recognition element such as enzymes (e.g., glucose or lactate oxidase), antibodies, or DNA aptamers. These elements convert biochemical interactions with the target analyte into measurable electric signals. As an example, glucose oxidase-functionalized electrodes enable glucose detection by catalyzing its oxidation to hydrogen peroxide, which is then electrochemically reduced at the working electrode.[17,251] This approach extends the applicability of electrochemical sensors not only to O_2, H_2O_2, or other reactive oxygen species but also to proteins,[354,417] cytokines (e.g., IL-6[373] or IL-1β[36]), or non-electrochemically active metabolites.[386]

In terms of electrode materials, Ag/AgCl have been traditionally used as reference electrodes for those sensing techniques due to their stable and reliable response during measurements.[420] However, these electrodes are rigid and need bulky electrolyte solutions. To accommodate the needs of miniaturized lab-on-chip (LoC) platforms, solid-state reference electrodes of various materials have been developed including, among others, PEDOT:PPS,[127] polyaniline (PANI),[212] and carbon nanotubes.[66] In the case of amperometry/voltammetry, the working electrode should be made of a chemically stable and conductive material due to redox reaction happening at its surface, such as platinum or gold,[318] whereas zinc,[233] ruthenium,[28] or iridium are used for MOx-based potentiometric sensors.[351] The challenges of integrating electrochemical sensors for long-term monitoring are in many ways consistent with those of electrical sensors that we discussed at the beginning of Sec. II B and are related to the susceptibility to variation of the environmental conditions (e.g., electrochemical interferences), calibration drift, biocompatibility, and protein fouling. In particular, protein adsorption and cellular debris accumulation degrade the sensor performance over time. Strategies to partially mitigate this problem involve regeneration protocols by means of redox cycling or enzymatic cleaning of the electrode surface. While challenges in sensor longevity remain, the high sensitivity and specificity of these sensors make them appealing for in-line and continuous monitoring of the cell metabolic activity.

In the OoC field, electrochemical sensors are often used because they have the advantage of combining the high sensitivity, temporal resolution, and responsiveness typical of electrical sensors with, if needed, the specificity of biological recognition elements. The literature on electrochemical sensors is abundant; the reader is referred to previous reviews for more information on how this type of sensor has been applied to various OoC.[103,169] Specifically regarding the topic of this review, the usage of electrochemical biosensors in cartilage-on-chip models for the in-line monitoring of chondrocytes has been demonstrated only recently. Qin *et al.*[308] presented a novel cartilage-on-a-chip device integrated with a 3D stretchable electrochemical sensor for real-time monitoring of nitric oxide release from chondrocytes under physiological and hyperphysiological mechanical loading, as well as under inflammatory conditions induced by IL-1β. The device mimicked the ECM using a collagen-alginate hydrogel and the mechanical microenvironment of cartilage, exploiting a pneumatic actuation unit to apply controllable mechanical compression to the chondrocyte-laden hydrogel. The sensor was made of a porous gold nanotube/polydimethylsiloxane (Au NTs/PDMS) electrode filled with collagen-alginate hydrogel; platinum and Ag/AgCl wires were used as counter and reference electrodes, respectively. The sensor was integrated into the cartilage-on-a-chip device as part of the cell culture chamber, and the final device was assembled by bonding the culture chamber to the pneumatic actuation unit [Fig. 3(b)]. The sensor could detect NO concentrations ranging from 20nM to 2 μM with a response time of less than 2 s. A limit of detection of 12.3 nM was achieved, corresponding to an SNR = 3 (cf. Table IV). Cyclic voltammetry tests confirmed the long-term stability of the sensor functionality, with peak currents and potential differences remaining stable under static and dynamic compression (up to 1500 cycles at 20% and 50% strain). To account for background noise, the sensor was calibrated with known NO concentrations and control experiments with a NOS inhibitor to confirm the sensor specificity. The study demonstrated that mechanical compression and IL-1β synergistically enhance NO release, which is linked to the nuclear factor kappa B (NF-κB) inflammatory pathway. The device also shows potential for drug screening by analyzing the cartilage tissue response to non-steroidal anti-inflammatory drugs (i.e., ibuprofen), which are the most common treatment for OA pain management. The amperometric measurements indicated that the NO release elicited by mechanical compression and IL-1β decreased after the ibuprofen administration. From a technological perspective, the 3D electrochemical sensor has been successfully integrated on-chip. If an antifouling coating on the electrode surface is added to improve electrode stability, this device may also be used for long-term monitoring. In its current form, this cartilage-on-chip platform has a low throughput; thus, the remaining fabrication challenges are primarily related to industrial-scale production and scale-up processes.

Instead, Rothbauer *et al.*[323] developed glucose and lactate biosensors and integrated them within human cartilage-on-a-chip systems

TABLE IV. List of electrical sensing techniques relevant for application (part II). glucose oxydase (GOx); lactate oxydase (LOx); polyethylene glycol diglycidyl ether (PEGDE); fetal calf serum (FCS); rheumatoid factor (RF); anti citrullinated peptide antibody (ACPA); enzyme-linked immunosorbent assay (ELISA); limit of detection (LOD); signal-to-noise ration (SNR); molybdenum disulfide polyaniline (MoS_2/PANI); bovine serum albumin (BSA); phosphate buffer saline (PBS).

Sensing technique	Target analyte	Sensing element	OoC integrated?	Sensing performance	Reference
Electrochemical amperometry	Glucose and lactate	GOx and LOx immobilized in PEGDE hydrogel	Yes, cartilage-on-chip	Glucose: range = 1.1 − 30 mM, sensitivity = 19.8 $\times 10^3$ nA/(mM · cm^2), LOD = 1.1 mM, 0.05±1.35 mM difference compared to luminescent assay; lactate: range = 0.6 − 25.1 mM, sensitivity = 8.5 $\times 10^3$ nA/(mM · cm^2), LOD = 1.1 mM, 0.01±0.68 mM difference compared to luminescent assay; T90 response time = 0.6±0.2 s; time stability = 7 days; 18%–20% drift over 270 min	323
	Challenges	Biofouling minized by poly-m-phenylenediamine exclusion layer; background noise corrected by performing measurements in cell-free hydrogel controls; demonstrated reversible response to analyte addition/removal; interference challenge: no cross-reactivity between glucose and lactate sensors, limited signal interference due non-specific analytes (i.e., FCS and ascorbic acid), validated against commercial commercial luminescence-based assayssensor integrated directly into the cartilage organoid compartment via needle insertion through electrode inlet; fabrication is time sensitive: electrode insertion before hydrogel polymerization; single organoid per chip demonstrated, potentially scalable.			
Electrochemical amperometry	IgM-RF and ACPA	Screen-printed carbon electrodes with carboxylated magnetic beads for RF and neutravidin-functionalized beads for ACPA	No, but applied to joint	Sample volume 25 μl per assay (4× less ELISA); IgM-RF: range = 3–300 IU/ml, LOD = 0.8 IU/ml, sensitivity = 848±36 nA/decade; ACPA: range = 10–1000 IU/ml, LOD = 2.5 IU/ml, sensitivity = 1409±54 nA/decade; RF SNR ∼50; ACPA SNR ∼15	124
	Challenges	Background electrical noise compensated by measuring blank currents in buffer and in serum; bead bioconjugates stable for more than 20 days at 8 °C, stability at 37 °C yet to be demonstrated; dual-electrode layout designed to minimize signal interference between IgM-RF and ACPA; sensor specificity tested against cytokines and immunoglobulins.			
Electrochemical voltammetry and EIS	ACPA	Anti-ACPA functionalized on MoS_2/PANI-modified screen-printed electrodes	No, but applied to joint	Sample volume 10 μl; assay time ∼2 h, sensitivity 4.4713 μAper log $_{10}$[IU/ml], range = 0.25 − 1500 IU/ml, LOD = 0.16 IU/ml in PBS and 0.22 IU/ml in 10% human serum, time	337

TABLE IV. (Continued.)

Sensing technique	Target analyte	Sensing element	OoC integrated?	Sensing performance	Reference
				stability = 92.3% of initial response retained after 4 weeks at 4 °C; sensor specificity tested against cytokines and immunoglobulins	
	Challenges	Biofouling minimized by 0.5% BSA blocking; background electrical noise compensated with blank voltammetric measurements in PBS and 10% human serum; bead bioconjugates stable for more than 20 days at 4 °C, stability at 37 °C yet to be demonstrated; sensor fabrication is multi-step and complex, implementation in high-throughput OoC to be demonstrated.			

for *in situ* detection of disease-related shifts in chondrocyte metabolism during inflammation. This represents the first reported integration of continuous metabolic biosensing in cartilage-on-chip models. The cartilage-on-a-chip platform was fabricated using standard PDMS soft-lithography. Human primary articular chondrocytes (hAC) were isolated from total knee arthroplasty patients and embedded in a fibrin hydrogel to create 3D organoid structures. An OA phenotype was induced after 3 days of organoid maturation through the addition of IL-1β and TNF-α. The biosensors comprised 50 μm needle-type electrodes made of Ag (reference electrode) and platinum (working electrode) wires. Sensor functionalization involved multiple coating layers: first, poly-m-phenylenediamine (mPD) was electropolymerized to create an interference exclusion barrier. Subsequently, the electrode tip was coated with enzyme-containing polyethylene glycol diglycidyl ether (PEGDE) hydrogels, incorporating either GOx for glucose detection or LOx for lactate detection. Finally, a polyurethane coating was applied to extend the sensor dynamic range [Fig. 3(c)]. The sensing mechanism relied on enzymatic oxidation reactions: glucose and lactate were oxidized at the sensor tip by GOx and LOx, respectively, generating hydrogen peroxide that facilitated electrochemical measurement of analyte concentrations. Electrochemical measurements were performed using amperometric detection at an applied potential of 0.75 V. The biosensors demonstrated robust analytical performance across physiologically relevant concentration ranges. Glucose sensors exhibited a dynamic range from 1.1 to 30 mM, with a sensitivity of 19.8×10^3 nA/(mM cm^2) and a limit of detection of 1.1 mM. Instead, lactate sensors showed a range from 0.6 to 25.1 mM, with a sensitivity of 8.5×10^3 nA/(mM $\times$ cm^2) and an improved limit of detection of 0.6 mM. Both sensors displayed linearity at concentrations below 5 mM and a response time of 0.6 s (cf. Table IV). Additionally, validation against commercial luminescence-based assays revealed strong concordance between electrochemical and optical sensing techniques. Long-term stability tests showed an 18%–20% signal drift over a period of 270 min, consistent with similar biosensors, and stable measurements for up to 7 days.

The integrated biosensors successfully detected metabolic alterations characteristic of OA cartilage. Baseline metabolic activity was demonstrated through reduced glucose sensor responses and elevated lactate levels in cell-laden organoids compared to cell-free controls. Inflammatory stimulation with IL-1β/TNF-α cytokines induced significant metabolic shifts within 5 h, indicating enhanced glucose-to-lactate metabolism in the OA-like model. Long-term monitoring revealed sustained metabolic alterations: 2.2-fold decreased glucose and 8.9-fold increased lactate levels in cell-laden organoids compared to controls. After 2 weeks of culture with pro-inflammatory challenge, supernatant analyses confirmed 1.7-fold decreased glucose and 5.1-fold increased lactate content, with inflamed organoids showing 1.5-fold glucose decrease and 1.9-fold lactate increase compared to untreated controls. Molecular validation through qPCR demonstrated successful induction of the OA phenotype, with significant 183-fold upregulation of pro-inflammatory cytokine IL-6 and a threefold increase in matrix protease MMP-3.

Finally, it is worth mentioning that many standalone electrochemical sensors have been developed for the amperometric detection of RA biomarkers, although they have not yet been implemented in the JoC platform. Guerrero *et al.*[124] presented a dual biosensor for the simultaneous detection of rheumatoid factor (RF) and ACPA. Dual

screen-printed carbon electrodes and carboxyl- or neutravidin-functionalized magnetic beads were used as a substrate to immobilize biorecognition elements specific for RF and ACPA, namely, a Fc fragment of native human IgG protein and a biotinylated CCP peptide, respectively. The sensor demonstrated high selectivity and high sensitivity for both biomarkers, achieving a limit of detection of 0.8 and 2.5 IU/ml for RF and ACPA, respectively (cf. Table III). Additionally, the proposed sensor outperformed the conventional ELISA method in speed and required sample volume. Validated in human serum, this dual biosensor shows clinical utility for RA diagnosis and holds potential as a cost-effective, multiplexed solution in a JoC platform. Instead, Selvam *et al.*[337] developed an electrochemical biosensor to detect ACPA by means of square wave voltammetry. The sensor was microfabricated using molybdenum disulfide PANI as a substrate for screen-printed electrodes, together with an interfacial polymerized PANI-gold nanomatrix to entrap the ACPA antibodies for higher signal amplification. The sensor demonstrated a limit of detection of 0.16 IU/ml in saline solution and 0.22 IU/ml in ACPA-spike human serum as well as high selectivity against competitive interferents and time stability (7.7% signal loss after 4 weeks, cf. Table III), which makes it a promising tool for real-time monitoring in pathological JoC models. Additional studies reported electrochemical biosensors also for many other RA biomarkers, such as the synthetic peptide known as chimeric fibrin/filaggrin citrullinated peptide 1 (CFFCP1),[71] macrophage migration inhibitory factor (MIF),[198] chemokine CXCL7, MMP-3,[123] and the ligand receptor activator nuclear factor-kB (RANKL).[379] From these studies, it is evident that sensing technologies for OA/RA biomarkers have been successfully developed; thus, their integration into JoC platforms remains the critical next step.

C. Mechanical sensing techniques

As outlined in Sec. I, mechanical loading and fluid flow are critical types of stimulation to recapitulate the joint niche *in vitro*. The dynamic environment of the joint is characterized by a complex interplay of mechanical compression, hydrostatic pressure, and shear stress (either mechanical or fluid-dynamical shear stresses) with varying magnitude and direction.[271] These mechanical loadings collectively influence the behavior of joint-resident cells, including progenitors [e.g., mesenchymal stem cells (MSCs)], chondrocytes, and synoviocytes, by shaping their differentiation, proliferation, and responses to external stimuli.[298]

Mechanical readouts, such as forces and deformations experienced by cells, are crucial for understanding how physiological and altered mechanical environments impact the cellular behavior.[253,256] Furthermore, mechanical readouts may help investigate mechanosensation, mechanotransduction, and mechanoresponse pathways, which are essential to maintain tissue homeostasis and understand disease progression.[390,410] A JoC platform embedded with real-time mechanical sensors would provide insights by noninvasively and continuously monitoring the forces applied to joint tissues while simultaneously measuring the resulting strain, stress, and mechanical properties (e.g., elasticity and stiffness).[202,322] Such a system would offer a tool for tracking chondrogenic differentiation of MSCs, tissue maturation, and progressive degradation of the PCM and ECM under both physiological and pathological conditions (e.g., OA and RA).

Despite the growing complexity of OoC platforms, real-time mechanical sensing technologies remain relatively scarce. However, some innovative approaches have emerged, offering promising avenues for their future integration into JoC systems. Shortly, mechanical sensors measure a force or pressure, which is applied to a specific sensing element, using principles such as piezoresistivity or optical deflection.[256] Integrating mechanical sensors into OoC platforms raises several challenges. Miniaturization is required to fit within chips without sacrificing sensitivity or introducing mechanical noise. Integration with actuation systems (internal or external) further complicates device design and can create cross-interference.[60] Additional issues include calibration drift, sensitivity to environmental conditions (e.g., temperature and humidity), and reduced accuracy at the microscale.[256] Another challenge is how sensor signals are interpreted. The constitutive models used to convert measurements into mechanical properties are often oversimplified and may not capture complex tissue mechanics,[256] which impacts the sensor accuracy. As for the previous sensing techniques, the following paragraphs present an overview of diverse mechanical sensing modalities, emphasizing their deployment in OoC platforms with priority given to JoC examples.

1. Microcantilevers

Considering the currently available mechanical sensors, microcantilevers are among the commonly used and effective sensing strategies for measuring cell-generated forces. These deformable beam-like structures, fixed at one end and free at the other, deflect in response to the mechanical forces exerted by the cells during processes such as adhesion, migration, and contraction.[301] The deflection is detected either optically by measuring changes in light reflection or by means of piezoresistive sensing that converts deflection-associated strain into electrical resistance.[16,185] These measurements provide estimates of cell-generated forces, local stress distribution within the ECM, and the mechanical properties of the tissue.[101,133]

Microcantilevers have proven useful in cellular force measurements, yet their application is accompanied by constraints that must be considered when applied to OoC systems. First, their fabrication can be complex, and cantilevers are sensitive to vibrations and noise.[16,185] To reach a high detection sensitivity, the damping effects have to be optimized by the appropriate selection of cantilever material and geometry. Additionally, the measurable force range is limited,[234] multiplexing can be difficult,[16] and maintaining stable electrical connections during long-term culture is still challenging.[185] Finally, improper calibration may lead to drift over time, and careful surface functionalization (i.e., coating with suitable patterning of the molecular recognition element) is necessary to ensure specific and reliable binding in biochemical sensing.[16,60,133]

In the context of JoC, microcantilevers have not been implemented, but label-free microcantilevers could be exploited to monitor cartilage degradation over time by detecting changes in the mechanical properties, such as stiffness and viscoelasticity, which vary during degradation due to changes in cartilage composition and structure (e.g., loss of proteoglycans or collagen disruption). Alternatively, microcantilevers functionalized with specific antibodies or ligands may be used to detect collagen and proteoglycan degradation products.[86] The dual capability of this sensor, coupled with its high sensitivity and compact size, makes it promising to study subtle changes in the behavior of cells affected by OA/RA. For example, a platform integrated with such a microcantilever-based sensor could be exploited to assess the efficacy

of drugs for OA/RA by measuring the restoration of the diseased joint's mechanical properties.

In other OoC, cell behavior has already been monitored with microcantilevers following drug administration. For instance, Lee *et al.*[339] integrated nanotextured polyimide microcantilevers, a material with a high biocompatibility and thermal resistance that is useful for metal deposition and sterilization processes, into a heart-on-chip platform for monitoring the contractile behavior of drug-treated cardiomyocytes. The microcantilevers were subjected to an oxygen–plasma treatment to increase surface hydrophilicity and improve adhesion, ensuring that the subsequent deposition of a metal reflector layer would firmly bond to the surface and enhance its reflectivity for optical sensing measurements. The authors assessed the contractility of the cardiac tissue by detecting with a nanoscale accuracy the bending of the microcantilevers upon contraction/relaxation of the cardiac tissue recorded by a laser vibrometer (i.e., an optical detection system) with different drugs (verapamil and isoproterenol). PDMS and flat polyimide microcantilevers were used as a negative control, and it has been observed that nanotextured polyimide microcantilevers support more mature-like contractile function. Precisely, the cardiomyocytes cultured on the patterned polyimide cantilevers showed much better adhesion and alignment, higher sarcomere length (i.e., over 90% of those of native cardiomyocytes in a living body), faster growth, good contractility and cell junctions, as well as superior characteristics in terms of maturation and contraction force (cf. Table V). Since the continuous long-term use of a laser vibrometer can adversely affect the physiological activity of cardiomyocytes and maintaining long-term stable cell adhesion might be challenging, the study was conducted for 7 days only.[211] This strategy of using nanostructured surfaces to promote cell maturation and functional behavior could further be adapted in JoC with integrated microcantilevers to better mimic the ECM and enhance the mechanosensitivity of joint tissues (that include contractile cells, such as myofibroblasts,[357] which contract to remodel tissue and influence matrix stiffness). Moreover, like the cardiac toxicity screening, where contractility metrics reflect drug effects on cardiac cells, a JoC with microcantilevers could detect biomechanical changes (e.g., stiffness, elasticity) in cartilage or synovial tissues in response to OA/RA drugs.

An interesting initial step toward integrating functionalized microcantilevers into JoC platforms for detecting specific OA/RA biomarkers could be to replicate the work of Ricciardi *et al.*[317] They developed an antibody-coated microcantilever-based LoC system for the detection of angiopoietin-1, a potential marker in tumor progression, within liquid media. Notably, angiopoietin-1 is also upregulated in synovial fibroblasts in response to pro-inflammatory cytokines (e.g., TNF-α) and is expressed in the synovium of both OA and RA patients, with an expression significantly higher and more strongly correlated with inflammation in RA joints.[121] Hence, such a microcantilever-based LoC device could be adapted to investigate synovial fluid in OA/RA. The cantilever chips were fabricated from silicon-on-insulator wafers, with optimization focused on geometry (i.e., aspect ratio) and material.[317] It resulted in a microplate configuration that exhibits higher mass sensitivity in liquids compared to traditional microbeams, as reflected by a higher quality factor. Three materials—SU-8, PDMS, and Pyrex—were tested for microfluidic channel fabrication. The final prototype was built on a Pyrex-silicon chip measuring $200 \times 800 \times 7\,\mu m^2$. Each chip contained two independent cantilevers and corresponding wells on the same platform: one functionalized with anti-angiopoietin-1 monoclonal antibodies for angiopoietin-1 detection, and one for a negative control to assess non-specific adsorption/desorption effects. Detection was performed dynamically by tracking shifts in the microcantilever resonance frequency using piezoelectric actuation combined with optical readout. Frequency shifts upon specific binding were measured by monitoring the vibration of the cantilever, enabling real-time detection of antigen–antibody interactions. The antigen recognition assay involved flowing 30 μl of angiopoietin-1 solution [25 μg/ml in phosphate buffer saline (PBS)] at 0.5 μl/min under controlled temperature ($23 \pm 0.2\,^{\circ}C$). Biologically, the system demonstrated successful detection of Angiopoietin-1, and showed that frequency shifts induced by non-specific interactions (negative control) were approximately one order of magnitude smaller than those resulting from specific protein binding.

Beyond single-organ applications, microcantilever-based sensors have also been adapted for multi-tissue-on-chip systems. Oleaga *et al.*[274] cultured iPSC-derived cardiomyocytes and primary hepatocytes in a single platforms incorporating stainless steel wire electrodes for electrical stimulation of the cardiac tissue, as well as noninvasive sensors (microcantilevers and MEAs) for functional readouts of force and electrical conductivity in case of administration of cardiotoxic compounds [Fig. 4(a)]. The compact optical detection system for force measurements was designed using laser beam deflection from the tip of 32 independent cantilevers fabricated from silicon-on-insulator chips with diethylenetriamine silane coating and fibronectin. The hepatic metabolism was indirectly evaluated by analyzing biochemical markers in the culture medium, specifically albumin and urea production, which reflect liver function and metabolic activity over time (i.e., a sign of hepatic damage is the loss in the hepatocyte ability to produce albumin and urea). The system allowed drug metabolism studies by administering cardiotoxic compounds, such as fexofenadine and terfenadine, whose hepatic metabolism generates toxic metabolites affecting cardiac tissue. Cardiotoxicity was assessed by quantitative changes in cardiomyocyte contractility and electrical signals detected by the microcantilever and electrode sensors. Biologically, the platform supported stable co-culture and functional monitoring of heart and liver tissues for up to 28 days, with clear drug-induced perturbations observable in contractile force and electrical activity after compound administration, demonstrating the system's capability to model multi-organ interactions and drug toxicity. Limitations and challenges include the complexity of maintaining multiple cell types with distinct culture needs within a single microfluidic device, optimization of fluid flows and culture media to support all tissues simultaneously, and especially the indirect nature of linking hepatic metabolism to cardiac responses, which requires comprehensive biochemical and functional integration.

As previously mentioned, the microcantilever deflection is detected either optically or piezoelectrically. An example of the latter is the piezoelectric microelectromechanical system developed by Coln *et al.*,[60] that is capable of both sensing and stimulating cardiac tissues cultured from iPSC-derived cardiomyocytes. Muscle tissue contractions were measured by converting mechanical strain into electrical signals via 16 chemically modified (diethylenetriamine silane treatment) piezoelectric cantilevers (total chip size of $17 \times 14\,mm^2$), each composed of a thin aluminum nitride film placed on its top and sandwiched between two platinum electrodes, while the same tissues were mechanically stimulated to mimic physiological conditions. To validate

TABLE V. List of mechanical sensing techniques relevant for applications. polydimethylsiloxane (PDMS); limit of detection (LOD); poly(3,4-ethylenedioxythiophene):polystyrenesulfonate (PEDOT:PSS); Young's modulus (E); anti citrullinated peptide antibody (ACPA); atomic force microscopy (AFM); extra-cellular matrix (ECM).

Sensing technique	Target analyte	Sensing element	OoC integrated?	Sensing performance	Reference
Microcantilevers	Contractile behavior of drug-treated cardiomyocytes	Nanotextured polyimide, flat polyimide, and PDMS microcantilevers	Yes, heart-on-chip	Polyimide: high biocompatibility and thermal resistance; cardiomyocytes on nanotextured polyimide: better adhesion and alignment, higher sarcomere length (i.e., over 90% of those of native cardiomyocytes in a living body), faster growth, good contractility and cell junctions, superior maturation and contraction force; nanoscale accuracy	339
	Challenges	Oxygen–plasma treatment required to increase surface hydrophilicity and improve adhesion. Short-term study (i.e., 7 days) because the continuous long-term use of a laser vibrometer can adversely affect the physiological activity of cardiomyocytes and maintaining long-term stable cell adhesion might be challenging.			
Strain gauges	PDMS membrane deformation	Metal (Ti) and polymeric (PEDOT:PSS) radial and tangential strain gauges	Yes, heart-on-chip	Metal: gauge factor = 0.8, resistance change ∼0.008% for membrane deformation up to 5% (0–3 kPa pressure range), sensitivity = 4.5 (radial) and 11.6 (tangential) $m\Omega/\mu m$ for strain below 3%; Polymeric: gauge factor = 0.48–17.8, resistance change ∼1.2% for membrane deformation up to 5% (0–3 kPa pressure range), sensitivity = 0.571 (radial) and 62 (tangential) $\Omega/\mu m$ for strain below 3%, E ∼1.2 GPa, transparency ≥90%	310
	Challenges	Metallic and polymeric: minimization of the strain gauges thickness; filtering of the electrical signal with a low cutoff frequency. Polymeric: enablement and optimization of the electrical contact; investigation of the temperature and baking time effects; control of the humidity; minimization of the degradation with stretching and time.			
QCM	ACPA	Quartz crystal microbalance functionalized with single-walled carbon nanotubes (coated with disease-specific cyclic peptides)	No, but applied to joint	LOD = 89 fmol; sensitivity = 71.9%; accuracy = 0.94/1; specificity = 95.8%; reproducibility = high; inter-assay variability ≤14%; intra-assay variability	80

TABLE V. (*Continued.*)

Sensing technique	Target analyte	Sensing element	OoC integrated?	Sensing performance	Reference
				≤15%	
	Challenges	Sensor equilibration in PBS with specific pH before use is required. Effective surface functionalization and selectivity. No drying of the antigen prior to and during QCM analysis.			
AFM	ECM	Custom-built high-bandwidth AFM system: secondary piezo actuator integrated within a commercial AFM platform	No, but applied to joint	Force sensitivity = pN; displacement resolution = nm; frequency bandwidth = 1 Hz–10 kHz	268
	Challenges	Coupling of the commercial AFM with a high-frequency system. Optimization of the plate geometry and material. Maintaining high bandwidth and precise force control during dynamic mechanical testing. Data processing and interpretation (correct mechanical model). Minimization of tissue damage.			

the capability of the microcantilever system to detect alterations in cardiomyocyte function, epinephrine was introduced into the culture medium to elevate the beating frequency. Using this system, more than a two-fold increase in frequency was quantitatively measured. Regarding the actuation capability of the system, the authors mentioned that the actuation characterization showed a filtering effect on input signals, which needs to be considered in controlled mechanical stimulation protocols. Since these piezoelectric cantilevers can provide both mechanical stimulation (actuation) and contractile force measurement (sensing) in a miniaturized format compatible with body-on-a-chip devices, integrating sensory cells onto such cantilevers could allow the investigation of pain pathways, which involve mechanosensitive neurons, which are relevant for more physiologically joint mechanobiology experiments.

2. Strain gauges

Soft strain gauges are flexible, biocompatible sensors made from piezoresistive, highly conductive materials. Materials used for strain gauge manufacturing include, among others, titanium, gold,[208] PEDOT:PSS,[45] PDMS doped with conductive fillers like reduced graphene oxide,[149] or liquid metal such as Galinstan[430] or gallium.[114] Strain gauges are designed to deform elastically in response to an external mechanical load, such as stretching, bending, or pressure. As a result, their deformation induces a proportional change in the electrical resistance of the piezoresistor.[439] The real-time measurement of this deformation provides a noninvasive monitoring of mechanical strain, which could be used to derive mechanical properties of 3D-engineered tissues in OoC platforms such as the stiffness.[213] By capturing subtle mechanical cellular responses related to cell differentiation, proliferation, or function, soft strain gauges can detect early signs of disease or tissue alterations due to external mechanical stimuli.[208,353]

However, even though strain gauge is an appealing technique for the noninvasive continuous monitoring of mechanical strain,[226] with high sensitivity to small strain changes[310] and possible coupling with actuators,[430] that can provide a closed-loop control of mechanical stimuli by continuously measuring and adjusting deformation, several challenges remain regarding their integration into OoC platforms. Producing flexible, biocompatible strain gauges with reproducible and stable electrical resistance under mechanical deformation[131] requires sophisticated microfabrication steps (e.g., injection of liquid metal into microchannels[430] or deposition of metal films by sputtering or evaporation[208]), which increases cost and limits the scalability as they are not directly compatible with standard OoC microfabrication techniques. Sensitivity to environmental conditions, such as humidity and temperature changes,[73,197,310,430] causes measurement drift and reduced sensor stability. Finally, mechanical hysteresis[131] and fatigue should be assessed for reliable long-term use because they may lead to signal drift and reduced sensor lifespan.[430]

While not yet integrated in JoC, strain gauges have already been embedded into other OoC,[209] thus supporting the technical integration feasibility. In JoC, strain gauges could be integrated to get insights on the strain applied to OA cartilage samples by quantifying chondrocytes deformation under joint-like loading conditions, with the possibility of deriving forces if material properties are known or correctly modeled.[90] This assessment of strain applied to damaged cartilage could then be exploited in the study of drug treatments aiming at restoring normal tissue function or alleviating disease symptoms, since healthy

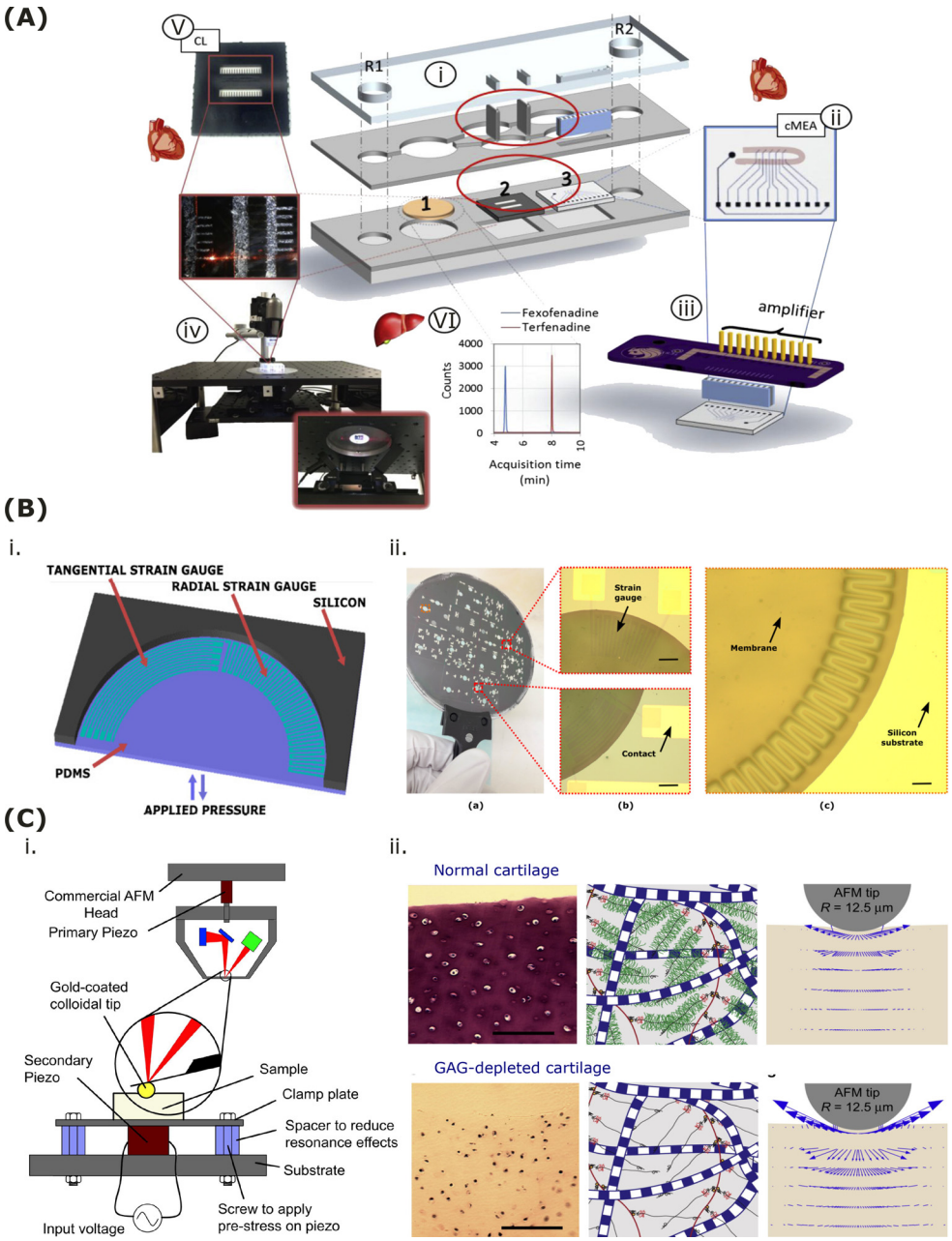

FIG. 4. Examples of mechanical sensors. (a) Schematic of the pumpless microfluidic system for the cardiac and liver co-culture. The microdevice consists of two laser-cut acrylic layers enclosing PDMS gaskets that define the microfluidic pathway and the cell culture compartments (i). Hepatocytes were cultured on a glass coverslip (compartment 1), while cardiomyocytes were cultured on cantilevers (compartment 2) and on MEA chips (compartment 3). Medium exchange was carried out through both reservoirs (R1 and R2), with drug addition via R1. Signals from the MEA chips (ii) were recorded using an amplifier (iii) connected through a printed circuit board. Cardiac contractile function was assessed with a laser-deflection-based apparatus (iv and v). Drug quantification was performed by HPLC-MS (vi). Reproduced with permission from Oleaga *et al.*, Biomaterials **182**, 176–190 (2018). Copyright 2018 Elsevier Inc. (b) PDMS-based organ-on-chip platform with integrated strain gauges for stress sensing. (i) Device design featuring tangential and radial polymeric strain gauges embedded in pneumatically actuated PDMS membranes suspended from a silicon frame to apply controlled stretch to cultured cells. (ii) Wafer containing 36 membranes with integrated strain gauges, with inset showing an enlarged view of the gauge structures (scale bar: 100 μm). Reproduced with permission from Quirós-Solano *et al.*, Micromachines **10**, 8 (2019). Copyright 2019 Authors, licensed under a Creative Commons Attribution (CC BY) license. (c) High-frequency AFM system for probing cartilage mechanics. (i) Commercial AFM coupled with a high-frequency system for dynamic measurements in the rage 1 Hz–10 kHz. (ii) Histological images to visualize GAG distribution and content (scale bars: 100 μm), schematics of molecular structure as well as AFM-based dynamic excitation with intratissue fluid flow velocity indicated by arrows (FEM simulations) for normal (on top) and GAG-depleted bovine cartilage (on the bottom). Reproduced with permission from Nia *et al.*, Biophys. J. **104**, 7 (2013). Copyright 2013 Elsevier Inc.

and damaged cartilage are characterized by different stiffness[168] and exhibit different strain profiles under mechanical loading.[391] In addition, this type of sensor could be used to quantify the deformation of the synovial membrane under both physiological and hyperphysiological loadings by following the approach of Quiros *et al.*[310] In their study, they fabricated radial and tangential polymeric strain gauges (i.e., PEDOT:PSS) to monitor mechanical strain in cardiac models [Fig. 4(b)] and benchmarked their performance against titanium counterparts. The functionality of the sensor was demonstrated in a custom-made setup where the relative resistance change for conventional titanium and PEDOT:PPS strain gauges was measured as a function of the applied pressure when iPSC-derived cardiomyocytes were cultured on the flexible PDMS membrane covering the strain gauges. Relative resistance changes of approximately 0.008% and 1.2% were measured with a linear behavior for pressures up to 3 kPa (pressure at which the pumping system reached the maximum flow capacity) in the titanium and polymeric strain gauges, respectively, which corresponded to a strain up to ∼5%. Such a low level of strain is primarily a material and fabrication limitation. Indeed, metal strain gauges tend to have practical maximum strain limits between 2% and 10%,[177] while polymer-based strain gauges can tolerate larger strains (sometimes exceeding 10%–15%) due to their inherent flexibility but are limited by substrate properties and the integrity of conductive layers.[45] However, regarding the translation to JoC, physiological knee cartilage usually experiences *in vivo* average strains under 10%, and peak strains of 17%.[289] Even though reliable *in vitro* values are not reported yet, extending the strain sensor range with more flexible materials might be required to accurately model the joint in microfluidic platforms. The results also indicated a high level of reproducibility and reliability of the devices. A much lower sensitivity for metallic strain gauges than for polymeric ones was observed: for strain below 3%, the estimated sensitivity for radial and tangential geometries was 4.5 and 11.6 $m\Omega/\mu m$ and 0.571 and 62 $\Omega/\mu m$ for metallic and polymeric devices, respectively (cf. Table V). Nonetheless, this system encountered several technical challenges, such as the thickness of the strain gauges that had to be reduced as much as possible to minimize their effect on the membrane deformation, and the electrical signal that had to be filtered with a cutoff frequency as low as possible to reduce the high-frequency noise after its amplification. Moreover, when employing PEDOT:PSS, the principal challenge was the establishment and optimization of reliable electrical contacts, which required an evaluation of the effects of temperature and baking time. Humidity had also to be controlled for the consistency of the experiment (fabrication and measurements were performed under a relative humidity of ∼48%). Finally, the PEDOT:PSS devices showed significant degradation with stretching and time, suggesting the need for the optimization of its patterning and the proper characterization of the mechanical properties under environmental conditions.

Zhang *et al.*[430] reported a cell-stretching microfluidic platform incorporating an *in situ* flexible strain sensor, offering another technical approach that could be adapted to quantify the deformation of the synovial membrane. To illustrate the working principle of their device, the authors worked with cardiomyocytes, which adhered to a thin, stretchable PDMS membrane and were continuously mechanically stimulated. Cyclic contraction-stretching was driven by compression and expansion of a vacuum chamber located in a layer beneath the membrane. The strain sensor was formed by microchannels embedded within the PDMS membrane and filled with Galinstan, a liquid metal, allowing real-time and quantitative monitoring of mechanical deformation at calibrated strain magnitudes of 5%, 10%, 15%, 20%, and 25%. Cells were seeded on the upper surface of the PDMS membrane, and deformation induced by the underlying vacuum chamber subjected both the membrane and the cells to controlled mechanical strain. Short-term culture (24 h of continuous stimulation) revealed that cell proliferation increased with strain amplitude, while the area of the active sensing region undergoing deformation exhibited only minor changes. A 15% strain more significantly promoted the overall cardiomyocytes alignment, whereas higher mechanical strain levels led to partial cell detachment and decreased viability. These findings were more pronounced during long-term incubation (i.e., 60 h). To achieve a high sensitivity, linear response, and automatic adjustment to temperature changes, the authors used Wheatstone bridge circuits (i.e., four resistors in a diamond shape) with built-in temperature correction to compensate for signal drift. This temperature self-compensation was necessary since liquid metals are sensitive to changes in ambient temperature, impacting the repeatability and stability of the sensor. Further improvements could be done to this device, such as adding uniaxial control in various directions for the vacuum cavity to apply dynamically controllable anisotropic biaxial strain to the cells. This sensor-on-chip could be adapted to study OA/RA by culturing synoviocytes (e.g., fibroblast- and macrophage-like synoviocytes) on the flexible PDMS membrane while applying controlled, quantifiable cyclic tensile strain mimicking the joint mechanical forces. Specifically, by modulating strain profiles and combining the chip with drug treatments, it would be possible to investigate synovial inflammation in response to therapeutics. For an even more advanced modeling of synovial inflammation, this chip could be integrated into a more complex JoC, i.e., in co-culture with endothelial cells to mimic vascularized synovium.

3. Magnetic rheometry

Magnetic rheometry studies the rheological properties of biological tissues by applying a magnetic field to a sample that contains magnetically activated particles. This technique measures the displacement of ferromagnetic or paramagnetic particles embedded in the cell matrix in response to the externally applied magnetic field. The lag between the applied magnetic force and the particle displacement is referred to as the phase shift. The displacement data are then processed offline to yield detailed insights into the viscoelastic properties of the ECM, a major regulator of collective cell dynamics.[64] By quantifying the spatial viscoelasticity differences in the ECM, magnetic rheometry gives estimates of its heterogeneous nature.[190]

The integration of magnetic rheometry into OoC systems remains challenging. Key limitations include the restricted availability of measurement probes and the difficulty of maintaining a sufficiently strong and uniform magnetic field—issues that can be partially addressed through Bayesian multilevel probabilistic modeling.[11,362] Additional concerns involve potential errors in time synchronization arising from phase shifts in sinusoidal fits,[11] the lack of standardized protocols, the tendency of magnetic beads to self-agglomerate,[33] and possible interference with detection methods such as fluorescence due to light scattering.[33] Finally, the magnetic particles themselves must be biocompatible and non-toxic over extended culture periods, with

surface chemistry that does not affect cellular behavior or ECM properties.

In the field of JoC, magnetic rheometry offers a means to probe how pathological mechanical stimulation alters the spatial organization of the ECM (shift in collagen type, i.e., decrease in collagen type II and increased production of collagen type I[221,249]), potentially down to the PCM level given the high achievable resolution. Cartilage ECM mechanical properties are closely linked to alterations in composition and structure[134] and, therefore, vary with pathology. In particular, compared with healthy tissue, human OA cartilage displays increased matrix stiffness[102,171] and reduced viscoelasticity.[76,157] Arasalo *et al.*[11] used this method to quantify the viscoelasticity of 3D cell culture made of breast cancer fibroblasts and collagen type I, which are both components typically present in the tumor ECM. Using a Gaussian process-based spatial inference to analyze the measurements taken over 3 days, the technique allowed to retrieve a spatial mapping of 3D cell cultures at stiffness up to 10 kPa with a 10-μm resolution (resolution governed by the probe diameter), as it is found in breast cancer biopsies. The main advantages of this method are its noninvasiveness and the possibility to measure stiff tissues with a resolution higher than conventional methods (e.g., passive rheometry[11] or optical tweezers[364]). The authors mentioned that the major limiting factor of this technology is the sparsity of the measurement probes, causing some uncertainty in the spatial viscoelasticity maps. There was also a significant mean phase shift uncertainty (higher than the theoretical one), which might be due to spatially varying bulk flow, meaning that the moving magnetic probes themselves can cause local fluid or matrix movement around them, adding variability to the measurements. Finally, the probe concentration has to be optimized to prevent magnetic particles from interacting with each other. In the future, smaller magnetic probes with a higher magnetization could be developed to improve the performance of this technique.

4. Quartz crystal microbalance

Quartz crystal microbalance (QCM) is a real-time, nanogram-accurate technique used to measure mass changes by monitoring the resonant frequency of a quartz crystal, which is a piezoelectric material.[3] This measurement allows the quantification of a target analyte, meaning it can track the analyte production over time, and can also provide kinetic information about the molecular binding occurring at the surface of the crystal sensor itself.[374] The target analyte that will be detected is determined by the antibody coated on the crystal. QCM consists of a thin quartz crystal disk, whose surface is sensitive to applied loads, oscillating at its resonant frequency between two electrodes (typically made of thin layers of gold)[43,48,349,374,392] when an alternating voltage is applied across them. As the mass increases due to intermolecular interactions, the frequency of the alternating voltage decreases.[49] QCM presents several advantages, including the possibility to provide a sensitive biosensor with potential for multiplexing when combined with specialized antibodies.[374] It provides real-time label-free detection of molecular interactions[374] and mass changes on the sensor surface, which enhances its applicability in dynamic biological environments. Additionally, QCM is a cost-effective technology, making it accessible for diverse research and clinical applications.[374] Its nanogram sensitivity and successful integration with small-volume microfluidic systems (e.g., 10–30 μl) have already been demonstrated,[78,273] highlighting its suitability for OoC platforms where volumes are limited. Previous reviews offer a comprehensive outlook on the integration of QCM into OoC.[62,374]

Nonetheless, integrating QCM into OoC comes with difficulties. The quartz crystals within the microfluidic channel should avoid disrupting fluid flow dynamics, shear stress profiles, and cell culture conditions.[422] Sensitivity is influenced by the temperature,[227] as well as the electrode parameters (e.g., shape, diameter, thickness, material),[137,395] but a higher mass sensitivity is at the expense of higher noise levels.[5] Moreover, attention should be addressed to surface functionalization to minimize biofouling[326] and achieve an effective surface covering in terms of the number of recognition elements per surface unit and orientation, which is even more important in the case of small molecule detection.[74] It has also been shown that the surface roughness of the quartz crystal impacts the QCM measurements as it induces an additional shift in the resonance frequency.[312] Finally, QCM sensors have to be equilibrated in PBS with a specific pH before use to ensure sensor stability.[4,80,348]

For the specific case of JoC, QCM sensors have not been integrated yet in microfluidic platforms, but their applicability to joint research has been established. QCM sensors been used to detect OA and RA biomarkers in liquids (e.g., urine and synovial fluid samples), including BMP-2,[246] collagenase, AAT, COMP, and RA autoantibodies.[252] Collagenase is a protease that has been reported to reach elevated levels in synovial fluid and blood serum of OA and RA patients, as well as to cause the first degradation in triple-helical collagen in hyaline cartilage.[4] Ahmad *et al.*[4] used synovial-fluid collagenase detection as a proof-of-concept by depositing thin films of cross-linked four-arm PEG-norbornene on a gold-coated quartz crystal. The gold layer supported strong hydrogel attachment and uniform coverage, enabling QCM monitoring of hydrogel degradation in the presence of collagenase via peptide-cross-link cleavage. The mass loss of the hydrogel coating on the QCM sensor surface caused an increase in resonance frequency, which was detected with a limit of detection of 2 nM in less than 10 min for collagenase concentrations ranging from 2 to 2000 nM. To simultaneously get insights into both the mass and viscoelastic characteristics of the hydrogel during degradation, the authors applied a Butterworth Van Dyke equivalent circuit model. This model fitted the QCM admittance spectra recorded before and after degradation using two parameters: resistance and reflective inductance. Changes in resistance and reflective inductance were reported as a function of time and collagenase concentration, providing information on the hydrogel viscoelasticity and mass loss during degradation, respectively. QCMs have been used for COMP detection in urine samples in several studies,[348,349,392] consistent with elevated urinary AAT and COMP in severe OA. Shen *et al.*[348] developed a QCM-based immunosensor made of quartz crystals sandwiched between gold electrodes, with COMP or AAT monoclonal antibodies immobilized via SAMs. After stabilizing resonance frequency, target-analyte solutions were introduced into a detection chamber containing the QCM. Frequency shifts correlated linearly with antigen concentration for both targets, with more than 80% recovery in repeated measurements and no significant interference vs bovine serum albumin. Simultaneous detection of the two antigens demonstrated high sensitivity, specificity, reliability, and linearity (99%). At 26 °C, the linear detection ranges were 1–10 ng/ml for COMP and 30–3000 ng/ml for AAT.

In another study, RA-specific peptides have been used to detect ACPA in RA serum by immobilizing them onto peptide-functionalized

single-walled carbon nanotubes deposited on a QCM.[80] This antibody binding detected by QCM sensing showed a sensitivity of 71.9%, specificity of 95.8%, and accuracy of 94%, identifying 34.4% more RA patients with ACPA than standard ELISA, with detection limits as low as 89 fmol of antibody (cf. Table V). The sensor selectivity was confirmed by comparing the serum antibody binding in RA patients with controls from healthy individuals and OA patients.

While the use of QCM in traditional biosensing and diagnostic platforms is already established, its direct application in OoC systems is still emerging.[62,374] Since collagenase, COMP, and AAT are all present in the synovial fluid,[135,146,162] QCM sensors could be further integrated into the synovial compartment of JoC platforms to continuously monitor relevant biomarkers of the early-stage OA/RA diagnosis directly in the synovial fluid microenvironment.

5. Atomic force microscopy nanoindentation

Atomic force microscopy (AFM) indentation is a technique for the characterization of surface mechanical properties, including biological membranes,[138] biomolecules, and cells.[46] It estimates the Young's modules across soft-to-stiff materials[130] with nanoscale resolution and pico-Newton force sensitivity.[75,418] AFM uses micrometer-long cantilevers with sharp probes of various geometries (e.g., pyramidal, spherical, or conical[130]). As the probe approaches the sample, surface forces cause cantilever deflection, which is detected by a laser–photodetector system that converts deflection into force measurements exerted by the sample.[130,132] Even though AFM indentation cannot be defined as a sensing technique and will unlikely be exploited for the real-time monitoring of OoC, it is worth mentioning because such a technique is one of the few available options to measure the mechanical properties of tissues at the micro- and nanoscale (even as an end point measurement) already proven compatible with OoC platforms.[270] It enables assessment of cell adhesion forces, topographical imaging, and force mapping, hence offering a multi-modal approach to understanding healthy and pathological tissue behavior.[75,281,401] Force–distance curves measured during tip approach and retraction quantify Young's modulus and adhesion forces, and pixel-wise scanning generates spatial maps of stiffness and adhesion. This provides comprehensive insight into the biomechanical and adhesive properties of biological samples.[156,297]

Despite its advantages—including simultaneous topographical and mechanical mapping, nanostructural resolution, and the ability to probe biomechanical properties of heterogeneous biological samples in air or fluid without sample preparation[130]—AFM nanoindentation presents some limitations for near real-time continuous measurements. The equipment is bulky and costly and, when it is used in contact-mode operation,[153] can damage soft OoC samples. The technique is restricted to surface characterization and cannot probe 3D matrix properties.[183,305] This surface specificity, although it restricts the ability to capture the full mechanical heterogeneity and depth-dependent biomechanical behavior of cartilage, can be advantageous for investigating early pathological processes such as cartilage surface degradation, roughening, and fibrillation, which are hallmarks of joint disease. Indeed, this surface limitation.[148,242] In OoC systems, AFM can be applied before device sealing (once the ECM environment is established[183]) or after fixation, the latter preserving sterility and ECM architecture for detailed mechanical and topographical analysis.

In the future, AFM nanoindentation could be exploited to get new findings of cartilage and meniscus nanomechanics, especially their degradation with age and diseases.[132] This technique has already been applied to cartilage and meniscus, advancing the understanding, detection, and treatment of OA.[130,268] For example, AFM has been employed to quantify age- and disease-related changes in articular cartilage biomechanics in both mice and patients,[79,367] as well as to investigate the mechanical behavior of human meniscal surfaces[260] and the effects of meniscus ageing and pathology.[184] Within the scope of this review, a relevant study is the one of Loparic *et al.*[220] who used AFM with nanometer-sized pyramidal tips to map stiffness distributions of articular cartilage tissue surfaces, derived from animal sources, revealing a characteristic bimodal nanostiffness distribution corresponding to soft proteoglycan gel (∼22 kPa) vs stiffer collagen fibrils (∼384 kPa). Instead, the microstiffness measured with larger micrometer-scale tips was about 1.3 MPa, which reflects a homogenized bulk stiffness of the composite cartilage tissue, integrating mechanical contributions from both proteoglycans and collagen fibrils at the microscale. These results highlight the ability of AFM to detect and quantify cartilage nanomechanical heterogeneity inaccessible by macroscale testing methods. The spatial resolution allowed mapping collagen fibrils spaced ∼187 nm apart with high fidelity. To validate and better interpret their measurements on native cartilage, the authors created a biomimetic gel–microfiber composite consisting of a chondroitin sulfate-containing agarose gel and synthetic fibrillar polymers. This model replicated the bimodal nanostiffness behavior of native cartilage, demonstrating the contribution of soft proteoglycan gel and stiffer fiber components under controlled conditions. Both the native cartilage and the synthetic composite showed similar responses to changes in ionic strength: increasing ionic strength reduced matrix swelling and increased the stiffness of the proteoglycan gel component without affecting collagen fibril stiffness. This demonstrates the sensitivity of this AFM-based nanomechanical method to biochemical cues, such as ionic concentration, that regulate cartilage mechanical properties at the nanoscale.

Nina *et al.*[268] developed a novel high-bandwidth AFM-based rheology system capable of measuring the dynamic nanomechanical behavior of cartilage over a 4-decade frequency range (1 Hz–10 kHz), which simulate the loading rates and encompasses the full spectrum of joint motions (i.e., from normal walking to high-frequency impacts such as jumps) with a pico-Newton force sensitivity [cf. Table V and Fig. 4(c)(i)]. This system integrates a secondary piezo actuator within a commercial AFM to enable nanoscale oscillatory displacements, achieving displacement amplitudes as small as ∼2 nm, whereas standard commercial AFMs are limited to frequencies up to 300 Hz. Applying this method to healthy and GAG-depleted cartilage, which is used as a pathological model of OA at an early stage [Fig. 4(c)(ii)], the authors came to the conclusion that early-stage GAG-depleted OA cartilage tend to be more vulnerable to loading rate rather than load magnitude since the collagen network shows greater sensitivity to high-rate impact loading. A significant drop in dynamic complex indentation modulus, which characterizes the cartilage mechanical response to oscillatory loading, at higher frequencies (1 kHz) for the pathological model, reflecting compromised tissue stiffness during rapid loading. Additionally, the peak frequency of maximal fluid–solid frictional dissipation (i.e., energy loss mechanism arising from the frictional drag between the flowing interstitial fluid and the solid cartilage

matrix during dynamic deformation), increased 15-fold from 55 Hz in healthy cartilage to 800 Hz in degraded tissue. Their fibril-reinforced poroelastic finite-element modeling revealed up to a 25-fold increase in cartilage hydraulic permeability after GAG loss, making permeability a sensitive biomarker for early matrix degradation. The authors noted that optimizing the clamp plate's geometry and material was necessary to minimize mechanical resonances. They also highlighted challenges in integrating the high-frequency system with commercial AFMs and maintaining precise force control, emphasizing the importance of selecting an appropriate mechanical model for accurate data interpretation.[106]

D. Biochemical sensing techniques

Sensors integrated in OoC platforms based on biochemical sensing techniques exploit a biochemical or biological recognition element (like an enzyme or antibody) and a transducer to detect analytes in real-time, converting biological interactions into measurable signals. A selective recognition event—such as antibody–antigen binding, enzyme–substrate conversion, aptamer–target association, or affinity capture on a functionalized surface—occurs at a localized sensing region and produces a measurable change in the sensor microenvironment (e.g., the accumulation of bound mass, changes in local charge distribution, and a redox activity). Biochemical sensing strategies are often implemented alongside optical or electrical readouts to mediate and support continuous measurements in microfluidic cultures. These approaches enable single and multiplexed monitoring under physiologically relevant conditions while using reduced sample and reagent volumes,[206] thereby improving cost-efficiency and throughput while maintaining tight control over the cellular microenvironment.[41,316] Biochemical sensors integrated into OoC platforms provide single and multiplexed real-time detection of multiple analytes ranging from ions and metabolites to signaling molecules in the culture medium or local microenvironment.[126] These biochemical readouts may also be effectively used to assess the inflammation responses (e.g., pro-inflammatory cytokines delivered to the joint cell population to model OA[22]/RA[7]) as well as drug effects on cellular metabolism and tissue function,[324,338] providing a comprehensive view of both cellular health and therapeutic efficacy.[51]

In general, the challenges of integrating biochemical sensors into OoC platforms are similar to those described in Secs. II A–II C, including sensitivity to environmental factors that introduce signal drift and background noise, the need to minimize biofouling, and the requirement for precise antibody immobilization and surface functionalization to ensure consistent long-term sensing performance. The main difficulties for biochemical sensing in OoC lie in sensor functionalization, specificity, and stability. A critical requirement is reproducible immobilization of biorecognition elements (e.g., antibodies, enzymes, aptamers) on the sensor surface.[257] Their orientation matter, especially to ensure high sensitivity in low-volume settings.[40,164] Surface functionalization must support selective target binding while minimizing non-specific adsorption and biofouling.[56] It should also preserve bioreceptor activity and remain stable over long experiments.[119] In fact, achieving a stable and sensitive signal is particularly difficult at low analyte concentrations, where signal drift and background interference caused by non-specific adsorption become pronounced.[223] Sensitivity is further influenced by environmental factors,[346] including temperature, pH, and ionic strength (i.e., ions concentration in solution affecting electrostatic interactions), which affect both the biomolecular recognition and transduction mechanism. Sections II D 1–II D 3 discuss biochemical sensing techniques with particular emphasis on OoC platforms, and JoC applications in particular. Owing to the limited availability of real-time *in situ* biological and biochemical readouts, selected offline sensing approaches relevant to JoC and, more broadly, to OoC platforms are also discussed.

1. Immunoassays

The most widely used biochemical sensors for cytokines and small proteins detection in OoC are based on immunoassays, which leverage antigen–antibody interactions to achieve highly specific and sensitive analyte quantification.[98] Among these immunoassay techniques, the commercial off-chip ELISA remains one of the gold-standard techniques due to its robustness, reproducibility, and ability to provide quantitative biomarker analysis even in complex biological samples.[91] Nevertheless, immunoassays present limitations, including high cost due to the antibodies and reagent, the need for trained operators, and long incubation time.[55] When integrated with microfluidic systems, an additional challenge arises from the small sample volumes typically produced by OoCs, which must be analyzed without diluting the analyte to avoid quantification errors.[116]

Recognizing the need for miniaturized and high-throughput cytokine detection in JoC systems, Kahraman *et al.*[160] developed EliChip™, a microfluidic-based miniaturized ELISA platform designed for high-throughput *in situ* detection of cytokine collected from a JoC system. This portable, automated LoC consists of a disposable microfluidic card and a reader that manages reagent handling and signal acquisition. The system enables quantitative analysis of pro-inflammatory cytokines (IL-6, TNF-α) and neurotrophic growth factors (NGFs) produced in healthy and OA-like cartilage models.

Specifically, the optical module in the reader consists of four white LEDs interfaced with four CMOS minispectrometers featuring eleven reading lines. The disposable card contains 18 reaction chambers arranged across four parallel lines, allowing multiplexed assays. Each functional unit comprises (i) a washing reservoir to remove unbound reagents, (ii) a collection reservoir for effluent, (iii) a 20-μl reaction chamber coated with capture antibodies for antigen binding, and (iv) an inlet for sample introduction [Fig. 5(a)(i)]. Both the reaction chambers and the optical module were fabricated in poly(methyl methacrylate) (PMMA) and thermally bonded. Chamber geometry was optimized to prevent bubble formation and ensure reproducibility. The EliChip™ was then coupled to a JoC comprising two compartments: a nerve unit including dissociated embryonic DRG neurons, and a chondrocyte unit including primary human chondrocytes encapsulated in 5% gelatin methacryloyl (GelMA) hydrogel. Microgrooves were integrated to guide axonal projections from the nerve to the chondrocyte compartment [Fig. 5(a)(ii)]. Specifically, the EliChip™ was used to quantify IL-6, TNF-α, and NGF produced by chondrocytes of healthy cartilage constructs and OA-like models. Performance evaluation demonstrated picogram-range sensitivity with good reproducibility. Notably, EliChip™ outperformed commercial ELISA kits for NGF detection, though its sensitivity for IL-6 and TNF-α was slightly lower (cf. Table VI). By reducing sample requirements by an order of magnitude compared with standard ELISA and shortening assay time, EliChip™ significantly improves the feasibility of cytokine monitoring in dynamic microphysiological environments,

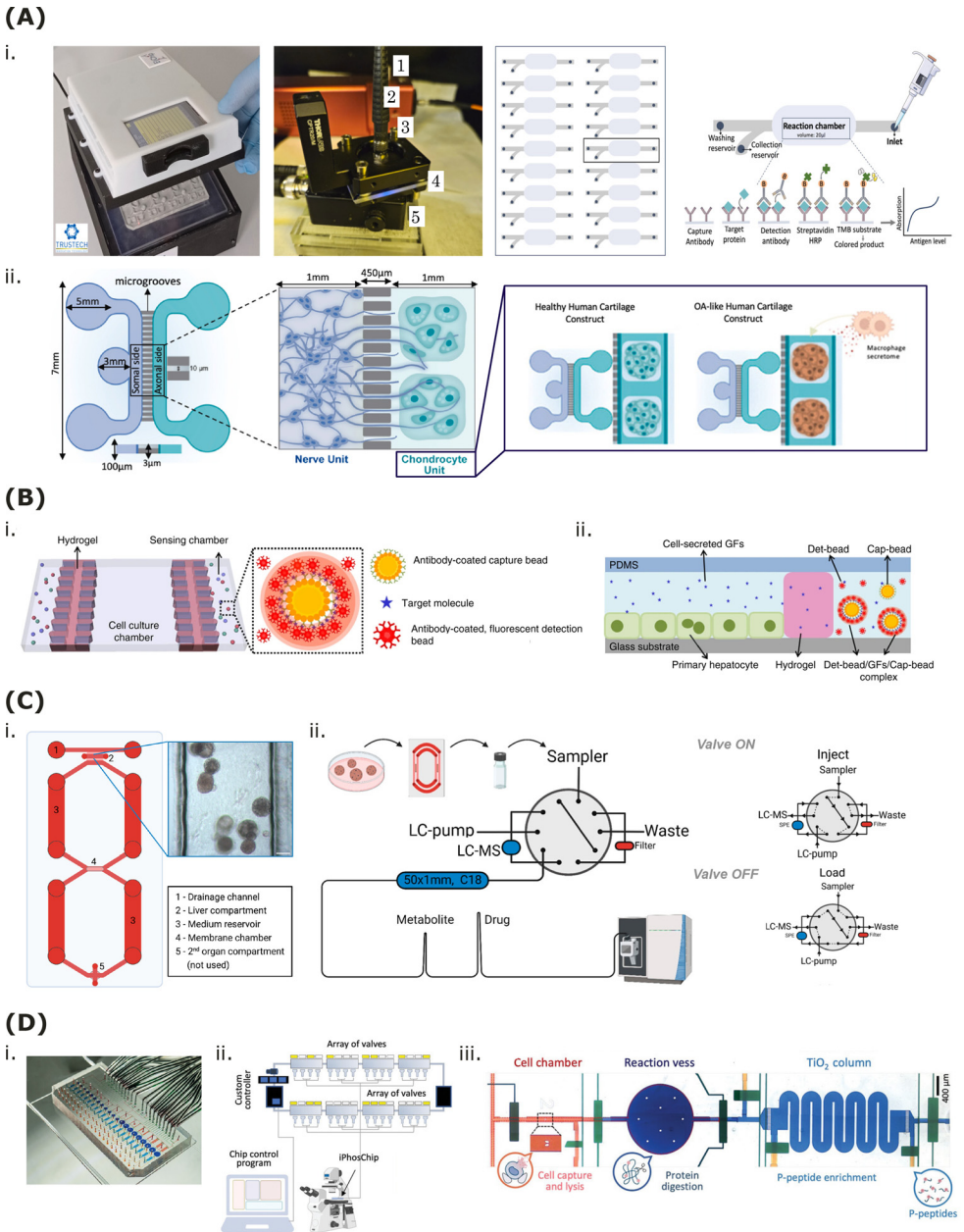

FIG. 5. Examples of biochemical sensors. (a) EliChip™ platform for antibody–antigen detection. (i) EliChip™ reader loaded with a cartridge featuring 18 parallel circuits; antibody–antigen binding occurs in the reaction chamber and is detected through the optical reading module (1: halogen lamp; 2: optical fiber; 3: interface between LoC and the module; 4: LoC; 5: photodiode). (ii) Microfluidic chip layout highlighting the chondrocyte unit. Two compartments—one with dissociated DRG neurons and one with primary human chondrocytes encapsulated in GelMA—enable modeling of healthy or OA-like cartilage under inflammatory stimulation. Reproduced with permission from Kahraman *et al.*, Mater. Today Bio **31**, 101491 (2025). Copyright 2025 Authors, licensed under a Creative Commons Attribution (CC BY) license. (b) Microfluidic device for hepatocyte culture and growth-factor sensing. (i) Hepatocytes are cultured in the main chamber, while secreted growth factors diffuse through a hydrogel barrier into adjacent sensing chambers. (ii) Cross-sectional view showing diffusion-driven aggregation of sensing beads upon growth factor binding. Reproduced with permission from Son *et al.*, Microsys. Nanoeng. **3**, 17025 (2017). Copyright 2024 Authors, licensed under a Creative Commons Attribution (CC BY) license. (c) Organ-on-chip platform for drug-exposure studies with integrated SPE–LC–MS analysis. (i) Representation of the OoC platform and brightfield image of liver organoids cultured on-chip. (ii) Schematic of the automated filtration, solid-phase extraction, and liquid chromatography workflow. In the Load position, samples are filtered and analytes retained on the SPE cartridge; in the Inject position, analytes are eluted to the LC column for MS detection while the filter is back-flushed. Reproduced with permission from Kogler *et al.*, Anal. Chem. **96**, 29 (2024). Copyright 2024 Authors, licensed under a Creative Commons Attribution (CC BY) license. (d) iPhosChip for multiplexed phosphoproteomics on-chip. (i) Bright-field image showing functional modules for cell capture, counting, imaging, and sample processing. (ii) Schematic diagram of the setup of the control system made of an array of pneumatic valves, the iPhosChip mounted on a microscope for real-time monitoring of the entire sample processing workflow, and a chip control program. (iii) Single operation unit made of a cell chamber for cell lysis, a reaction vessel for protein digestion, a TiO_2 column for phosphopeptide enrichment, and control layers (green). Reproduced with permission from Muneer *et al.*, Adv. Sci. **12**, 2402421 (2024). Copyright 2024 Authors, licensed under a Creative Commons Attribution (CC BY) license.

TABLE VI. List of biochemical sensing techniques relevant for joint-on-chip applications. limit of detection (LOD); hepatocyte growth factor (HGF); transforming growth factor beta 1 (TGF-β 1).

Sensing technique	Target analyte	Sensing element	OoC integrated?	Sensing performance	Reference
Immunoassays	IL-6, TNF-α, and NGF	EliChip™ (LoC microfluidic platform based on enzymatic immunoassay)	Yes, portable and off-chip automated LoC applied to JoC	LOD = 11.80 pg/ml (IL-6), 30.03 pg/ml (TNF-α) and 11.20 pg/ml (NGF); maximum concentration = 500 pg/ml (IL-6), 500 pg/ml (TNF-α), and 2000 pg/ml (NGF)	160
	Challenges	Off-chip sensor. Suitably pre-load the reagents necessary for performing the essay. Manual injection of the sample. Opmized design of the chamber to prevent air bubbles to form and provide reproducible results. LOD not always lower than for the standard ELISA.			
Multiplexed bead-based protein-biding assay	Hepatocyte growth factor and TGF-β1	Non-fluorescent capture beads and fluorescent detection beads functionalized with biotinylated anti-HGF or anti-TGF-β1 antibodies	Yes, liver-on-chip	On-chip calibration = 0–40 pM (HGF) and 0–300 pM (TGF-β1); LOD ~6 pM (HGF) and ~21 pM (TGF-β1); culture time = 7 days	356
	Challenges	Fresh beads at each session (avoid saturation and increase lifetime). Correct microbead functionalization and calibration. The thickness of the hydrogel barrier governs the permeation of growth factors. Optimization of the hydrogel formulation (the mesh size of the hydrogel network influences the diffusion coefficient of analytes). Effect of the capturing process of growth factors by microbeads on the autocrine signaling.			
Mass spectrometry-based based sensing for omics	Phosphorylation events	iPhosChip (chemically functionalized integrated MS-phosphoproteomic chip)	Yes, iPhosChip with lung cancel cells	Nanoscale-to-single-cell phosphoproteomic analyses; overall sample processing time = 7 h; high capture efficiency and reproducibility; good enrichment specificity	263
	Challenges	Numerous and complex production steps. Minimization of the specific sample adsorption. Prevention of the competitive binding from acidic peptides.			

offering a promising tool for drug screening and mechanistic studies of joint disease.

2. Multiplexed bead-based protein-binding and DNA-binding assays

Multiplexed bead-based protein-binding and DNA-binding assays are advanced biosensing techniques that utilize functionalized microbeads to selectively capture specific protein or DNA targets, such as hepatocyte growth factor (HGF) and TGF-β1,[356] transferrin and albumin,[316] insulin,[302] and interleukins (e.g., IL-4, IL-6, IL-8, IL-10).[247,279] By enabling the simultaneous detection of multiple biomarkers, these assays are particularly well suited for monitoring complex biological processes in real-time within dynamic microenvironments. This multiplexing capability is especially valuable for tracking disease progression, where rapid and parallel detection of several analytes enhances both diagnostic sensitivity and specificity.[27,39,269] Microbeads are typically fabricated from polymeric materials[371] such as polystyrene[332,340,356,421] or agarose[299] or from magnetic substrates[316,343] and are coated with high-affinity capture molecules (e.g., antibodies or aptamers) to ensure selective binding of target analytes.[116,216,267] Depending on the assay design—including bead material and surface functionalization—detection can be achieved through optical,[356] electrochemical,[316] or magnetic[15] readouts. In terms of analytical performances, achieving ultra-sensitive multiplex detection of low-abundance biomarkers is difficult, and assays are prone to cross-reactivity between capture molecules[118] as well as non-specific adsorption on bead surfaces.[111,217] To address these issues, careful surface passivation using blocking solutions[415] and optimization of capture efficiency are essential, alongside strategies to minimize interference from impurities.[94]

In JoC applications, bead-based sensors could be used to simultaneously monitor multiple cytokines, such as TNF-α and IL-6, MMP, or growth factors such as TGF-β1, which is abundant in OA subchondral bone and synovial fluid. The feasibility of measuring these cytokines has already been demonstrated in other OoC applications. As an example, Son *et al.*[356] incorporated bead-based assays in a liver-on-chip platform to detect HGF and TGF-β1 secreted by primary hepatocytes *in situ*. The microfluidic chip features a central channel for hepatocyte culture. Two lateral sensing channels are separated from the culture chamber by polyethylene glycol diacrylate hydrogel barriers. These barriers prevent the beads from entering the cell chamber while allowing the diffusion of growth factors from the central to the adjacent channels [Fig. 5(b)]. The hydrogel thickness controlled permeation, while the mesh size of the network influenced diffusion coefficients. Non-fluorescent capture beads and fluorescent detection beads (red for HGF and yellow for TGF-β1) conjugated with biotinylated anti-HGF or anti-TGF-β1 antibodies were used. In this design, diffusing growth factors first bound to capture beads, then to detection beads carrying a secondary antibody, forming bead–bead aggregates. Monitoring the fluorescence intensity of capture beads over time allowed quantification of growth factor concentrations in the medium. Compared to the commercial ELISA test, local growth factor measurements obtained with the microbead-based sensing showed an approximately fourfold higher concentration of TGF-β1 and comparable limit of detection for both growth factors ($\sim$6 pM for HGD and $\sim$21 pM for TGF-β1) (cf. Table VI). While the sensors were used over a multi-day culture (days 1, 4, and 7), sensing was accomplished with fresh beads at each session to avoid saturation. Additionally, the extent to which the capturing process of TGF-β1 and HGF by microbeads affected the local growth factor concentration in the cell vicinity was investigated, since a significant decrease in the local growth factor concentration might affect the autocrine signaling. An 11% depletion in the TGF-β1 or HGF local concentration was found, which was considered a negligible decrease without noticeable effects on cell function.

In conclusion, the specificity of this sensing strategy is dictated by the antibodies used for bead functionalization, underscoring its adaptability. By tailoring bead design to relevant targets—such as IL-6, TNF-α, or MMP[243]—this approach holds strong translational potential for JoC applications.

3. Mass spectrometry-based sensing for omics

Mass spectrometry (MS) is an analytical technique to identify, count, and understand the structures of molecules, separating them by their mass and electrical charge. MS measures the mass-to-charge ratio of ionized molecules, enabling their identification and quantification based on mass and fragmentation patterns.[96] This versatile technology can be used in proteomics to analyze the entire proteome,[115,241] metabolomics for small molecule metabolites,[8,205] and phosphoproteomics for phosphorylated proteins.[18,21,25] Typical MS-based omics workflows involve multiple steps. These include sample collection, lysis, and protein or metabolite extraction. In proteomics and phosphoproteomics,[30] proteins are digested into peptides before separation (often by liquid chromatography) and MS analysis. The resulting spectra are then used for compound identification and quantification.[241] Integrating these steps into OoC platforms remains challenging, as it requires seamless coupling of cell input, preparation, detection, and data processing.[115,224]

Technically, a mass spectrometer consists of three main components: an ion source for the sample ionization, a mass analyzer for the ion separation, and a detector.[96] Molecules are ionized, accelerated, and separated by electric and magnetic fields according to their mass-to-charge ratio, then quantified by the detector to generate a mass spectrum.[57] For structural analysis, a tandem MS (MS/MS) approach further isolates parent ions for fragmentation, producing spectra that encode structural fingerprints for compound identification against databases of known molecules.[70,241] This structural resolution is particularly relevant when it comes to probing cellular behaviors and molecular responses to external stimuli.[335,409]

Direct coupling of MS to microfluidic platforms is difficult because samples often require pretreatment before ionization. For example, salts in secretions can cause ion suppression (i.e., matrix effects), which reduces MS signal quality. This sample preparation (e.g., purification, extraction, preconcentration) limits the technique to near-real-time measurements.[128,331] Solid-phase extraction (SPE) is one method that has been integrated on-chip[191,399] and used to monitor non-esterified fatty acids release from adipocytes,[83] vitamin E metabolism by human lung epithelial cells on-chip,[107] and neuronal[236,397,398] or hepatic[108,235,423] activity in OoC systems. However, SPE requires careful flow calibration, is prone to clogging and fouling, consumes large solvent volumes, and is mainly suited for selective purification. To separate a sample into its individual compounds based on their chemical/physical interactions with stationary and mobile phases, liquid chromatography is required.[128] Kogler *et al.*[175] developed a self-cleaning liquid chromatography–MS system to measure

small-molecule drugs and metabolites in the cell medium of OoC systems [Fig. 5(c)]. The device employs automated filtration and backflushing to reduce biofouling, enabling long-term operation. Validated in a liver-on-chip under FDA guidelines, this system could be adapted to other OoC platforms for biomarker identification and disease progression monitoring through ECM and cellular secretions.

Proteomics enables comprehensive profiling of the proteome, revealing signaling pathways, biomarkers, and regulatory networks that govern tissue homeostasis and disease.[115,389,435] It can also be used to understand how proteins respond to different mechanical forces, inflammatory stimuli, and therapeutic agents. Single-cell proteomics extends this by capturing phenotypic heterogeneity and cell-specific functional networks.[115] MS-based proteomic methods provide label-free, broad proteome coverage with sensitivity down to the single-cell level.[29] In the context of JoC systems, single-cell proteomics of chondrocytes under mechanical or biochemical stimulation could uncover pathways regulating proliferation, differentiation, ECM catabolism, and programmed cell death.[166,405,435] Comparative proteomics across patient-derived joint tissue models may further reveal genetic predispositions to joint disorders.[202]

Beyond proteins, MS can profile metabolites and monitor biomolecule release in response to metabolic changes or drug exposure.[8,205] While not yet applied in JoC systems, this approach may have an impact on the research on OA/RA drug metabolism and toxicity. MS has already detected cytokines such as IL-6[65] and TNF-α,[404] demonstrating feasibility for monitoring inflammatory mediators relevant to joint diseases. This would allow to move toward developing personalized interventions for subgroups of OA patients. A first step in this direction could be replicating on a chip the study of Carlson *et al.*,[38] who used liquid chromatography–MS to characterize synovial fluid metabolic phenotypes of cartilage morphological changes associated with OA. Specifically, they worked with human post-mortem synovial fluid samples, spanning from healthy to late OA cases, and identified distinct metabolic pathways associated with OA progression/structural deterioration. To address MS sample-preparation delays, microfluidic bioreactors have been coupled to SPE desalters and MS detectors for near-real-time metabolic analysis of T cells.[238] Adapting this solution to OoC platforms would require addressing several analytical and technological challenges, such as the risk of clogging from large molecules, limited temporal resolution, and a narrow spectrum of detectable analytes.

Phosphoproteomics, a branch of proteomics focused on phosphorylated proteins, provides detailed insights into cellular signaling and disease mechanisms.[272] By quantifying phosphorylation events, phosphoproteomics provides insights into cellular responses, signal transduction, and disease mechanisms. MS-based phosphoproteomics arguably remains one of the best available technologies to comprehensively characterize cellular signaling state.[18,21,25] A notable advance is the integrated phosphoproteomic chip (iPhosChip) clusters[263] [Fig. 5(d)]. With its MS system, iPhosChip facilitates nanoscale-to-single-cell phosphoproteomic analyses, enabling detailed profiling of phosphorylation events with individual cells or small clusters. iPhosChip is an automated, all-in-one platform for phosphoproteomics. It integrates cell capture and imaging, cell lysis, protein digestion, and phosphopeptide enrichment [Fig. 5(d)(iii)]. The total processing time is about 7 h. Tested on patient-derived lung cancer cells, iPhosChip showed high capture efficiency, reproducibility and enrichment specificity, while reducing sample loss and processing time (cf. Table VI). Despite these advantages, fabrication remains complex, requiring minimization of nonspecific adsorption and competitive binding from acidic peptides.

Overall, while integrating MS-based omics into OoC platforms remains technically demanding due to the complexity of sample preparation and analysis, advances such as iPhosChip highlight growing feasibility. By enabling sensitive molecular readouts, MS-based sensing is a technique worth considering for the next generation of OoC platforms.

III. PERSPECTIVE ON SENSING MULTI-SENSING CAPABILITIES INTEGRATION IN JOINT-ON-CHIP PLATFORMS

At the beginning of this review, we presented the JoC as a promising tool to recapitulate the dynamic and multi-faceted joint microenvironment within pathophysiological contexts of use. In our vision, a robust, high-fidelity JoC platform, seeking recognition as a transformative approach in translational musculoskeletal research and drug discovery for the OA/RA treatment, should incorporate the capability of (i) controlling the 3D architecture of joint tissues and allowing multi-tissue interactions (i.e., inter-tissue crosstalk); (ii) recapitulating the complex biochemical and biophysical joint microenvironment; and (iii) integrating multi-sensing strategies for real-time and noninvasive monitoring of tissue behavior under both physiological and pathological conditions. In this section, we start from the latter point summarizing the main challenges related to the integration of multi-sensing strategies within JoC and providing our perspective on possible future directions for the field. Then, we discuss potential additional barriers and considerations toward the widespread adoption of JoC.

A. Multi-tissue integration

As we previously described, the joint is composed of multiple tissues including cartilage, subchondral bone, synovial membrane, meniscus, ligaments, and other auxiliary tissues, and its pathophysiological state heavily depends on inter-tissue communication. Toward the development of a JoC platform recapitulating the interactions among those tissues, attention should be paid to ensure that the model is as simple as possible but as complicated as needed. Although a fully representative system would include all joint structures exposed to *in vivo*-like biochemical and biomechanical cues, only certain tissues or stimuli may be necessary depending on the specific context of use. In this direction, contemporary JoC platforms are transitioning from single-tissue models[188,271,319,320] to multi-compartment systems with the goal of modeling tissue crosstalk.[189,204,207,259,266,286,327] Distinct yet interconnected tissue compartments are incorporated in microfluidic platforms, each maintaining tissue-specific microenvironments while allowing molecular exchange. These systems demonstrated that inter-tissue communication significantly influences the disease progression, as evidenced by inflammatory cascades propagating from synovial compartments to cartilage and subchondral bone regions.[145,400] These multi-tissues systems have been already used in proof-of-concept studies with patient-derived cells, synovial fluid, and tissue samples to create individualized disease models that can potentially predict therapeutics responses at the single patient level.[293] Toward the same line, gender-specific JoC are starting to be considered to enable a better disease stratification (e.g., knowing that OA affects women more

frequently than men) and eventually improve the predictive accuracy of JoC as preclinical models.[61]

B. Immune system integration

In terms of multi-tissue communications, it has also been recognized that the immune system plays a role in the initiation of chronic inflammation to the synovium.[248] The process is the result of the interaction between all joint tissues and immune cells. Therefore, an advancement in the JoC development would be the integration of immune cell populations to model inflammatory process central to OA and RA pathogenesis. Recently published JoC platforms incorporate circulating immune cells,[284] including monocytes[189] and macrophages[250,286] even within perfusable vascular networks that interface with tissue compartments.[255] These models were used to mimic paracrine interactions in healthy and inflammatory joint environments,[250] investigate how the unbalanced communication between cartilage and synovial tissue contributes to the development of OA,[286] and demonstrate that immune cell extravasation and subsequent tissue infiltration create inflammatory microenvironments that more accurately recapitulate pathological states.[255]

C. Multi-sensor integration

Such envisioned combination of multiple immunocompetent tissues within a single JoC platform would make even more relevant the necessity to integrate multiple, possibly tissue-specific, sensing techniques. Multi-sensing strategies have indeed the potential to increase the quality and quantity of data that can be simultaneously obtained from every tissue present in a specific JoC. As noted in Secs. II A–II D, various readouts amenable to OoC technologies could dissect complex biological processes from different angles. By integrating optical, electrical, mechanical, and biochemical sensing modalities into a single JoC platform, a more comprehensive understanding of the cellular behavior, tissue dynamics, and biochemical signaling could be achieved, thus significantly enhancing the relevance of such *in vitro* models of the joint pathophysiology. However, this integration must be balanced against manufacturing feasibility, operational complexity, and clinical validation requirements. Overall, multi-sensing integration should be conceived ensuring that the added complexity does not compromise platform reliability, cost-effectiveness, or usability. Although not yet implemented in JoC platforms, preliminary demonstrations already validated several key technological building blocks within joint-relevant OoC, including optical monitoring in synovium-on-chip,[320] electrochemical sensing integrated in cartilage-on-chip under controlled mechanical loading,[308] and dual continuous metabolic biosensing in cartilage-on-chip.[323] In addition, multi-sensor integration has been demonstrated in other OoC systems, indicating that this strategy is technically realistic. As a final perspective of this review and following its vision, we propose a series of potential combination of integrated biosensors that target specific joint tissues and may be useful to advance our understanding of joint pathophysiology.

Optical and electrochemical sensors. The combination of conventional microscopy with optical and electrochemical sensors could enable real-time imaging of the cell morphology alongside the monitoring of metabolic activity and ion concentration in the ECM. In a JoC featuring synovial and cartilaginous compartments, such sensors could elucidate how synovial inflammation correlates with cartilage microfractures during OA onset. For instance, optical fiber sensors can assess the viability and proliferation of synovial fibroblasts under biochemical stimuli (e.g., pro-inflammatory cytokines) and/or hyperphysiological mechanical loading, while electrochemical sensors could simultaneously measure calcium ion levels associated with fibroblasts signaling pathways.[307] From a practical standpoint, this combination is feasible because both optical and electrochemical sensors have already been applied for cartilage-on-chip[323] and synovium-on-chip optical monitoring.[320]

Optical/electrochemical/biochemical and mechanical sensors. A JoC platform that couples mechanical and optical or electrochemical sensors can capture both morphological and ionic changes in the ECM arising from controlled physiological and pathological mechanical stimulation. This setup could be especially relevant for subchondral bone-on-chip or osteochondral unit-on-chip models, where interactions at the cartilage–bone interface critically influence OA progression. By concurrently measuring mechanical compression and/or shear (e.g., via microcantilevers) and metabolic/inflammatory responses (e.g., using fluorescent nanoprobes or mass spectroscopy), researchers can pinpoint how different levels of mechanical loading activate specific mechanotransduction pathways to drive joint degeneration. This sensor combination is practically achievable in a stepwise manner because mechanical actuation is already compatible with cartilage-on-chip sensing (electrochemical sensing under mechanical loading[308]). A possible implementation pathway would be to start with one chemical modality combined with mechanical readout, and then expand to biochemical assays.

Mechanical and electrical sensors. Integrating mechanical and electrical sensors in a JoC platform offers insights into the biomechanical and electrochemical properties of joint tissues under pathological biochemical or biomechanical stresses. In particular, the delay between a tissue's mechanical reaction and its electrical activity can be quantified, clarifying the relationship between streaming potential and compressive forces within the joint. The streaming potential itself is an electrokinetic phenomenon arising when the synovial fluid, rich in ions, is forced through the cartilage ECM during movement. Notably, the amplitude and timing of this potential depend on the ECM integrity. Early degenerative changes such as proteoglycan loss or collagen disruption alter the fluid flow and thus the electrical signal, making this approach highly relevant for detecting the onset of OA and guiding early intervention strategies.

Multi-modal approach for continuous sensing. A truly multimodal continuous sensing strategy would involve an integrated JoC platform with interconnected joint compartments—e.g., cartilage, subchondral bone, synovium, and ligament—each equipped with dedicated sensors. The design would replicate the functional interdependence found *in vivo* and enable the real-time data acquisition of relevant parameters using tissue-specific sensors: mechanical sensors to capture stress and deformation in tissues like cartilage and ligament, electrical sensors to monitor electrokinetic phenomena (e.g., streaming potential in cartilage and changes in electrical conductivity in bone tissue), and chemical/biochemical sensors to detect inflammatory or degradative markers (e.g., cytokines, MMP in cartilage and

synovium). By feeding real-time data from each sensor into a centralized acquisition system, subtle changes in ECM composition, synovial inflammation, or bone remodeling can be detected at very early stages, providing critical insights into how localized disruptions in one tissue can propagate to others. Such a holistic view is crucial for unraveling joint pathophysiology at a system level. While this represents a longer-term target, it is practically feasible through modular design: individual sensing units can be deployed for each joint compartment and progressively interconnected.

D. Challenges of multi-sensor integration

From this outlook, it appears evident that incorporating multi-sensing capabilities for real-time monitoring would offer several advantages with respect to exclusively performing end point analysis. A JoC platform equipped with integrated sensors not only enables a deeper exploration of biomechanical, electrical, and biochemical factors governing joint health and disease, but also provides a potent testing ground for emerging therapies targeting OA and RA. Continuous monitoring can streamline data collection, facilitate real-time quality control, and significantly boost experimental throughput, potentially outperforming traditional preclinical models in terms of efficiency and predictive power.[42]

Despite these advantages, the integration of multiple sensors into the same platform still remains a non-trivial engineering challenge. As we have specifically discussed in Sec. II, different sensors often demand distinct materials or microfabrication techniques, raising compatibility issues that can undermine the overall performance. Technological strategies should be identified to integrate multiple nearby sensors and maintain sensitivity and accuracy over an extended period of time, while minimizing signal interference that could degrade the data quality.

An additional challenge is the validation of such sensorized JoC models against clinical dataset to demonstrate their predictive accuracy in resembling native joint tissues and/or diseases. While many platforms demonstrated biological plausibility and ability to detect pharmacological responses,[201,207,285,327] their benchmarking against clinical data are still missing. This validation deficit represents a barrier to regulatory acceptance and clinical adoption of JoC technologies as recognized preclinical tools. Establishing clinically relevant validation requires key components, such as identification of biomarkers that correlated between JoC measurements and clinical assessments, the creation of reference datasets from patient populations, and the development of standardized protocols for translating *in vitro* readouts to clinical data.

E. Standardization of JoC platforms

Standardization has also emerged as a critical issue to be addressed to achieve a widespread adoption of OoC technologies, and JoC specifically, for the drug development and potentially in the future clinical applications. The current lack of standardized terminology, protocols, and performance metrics creates hinders the technology transfer, regulatory approval, and commercial adoption of OoC technologies. A recent initiative by European organizations have identified key areas for the OoC widespread adoption including biological, engineering, manufacturing and data collection standardization.[42] Biological standardization represents a particularly complex challenge given the inherent variability in primary cell sources, tissue donors, and culture conditions. Standardized cell characterization protocols, quality control metrics, and acceptance criteria are essential to ensure reproducible results across different laboratories and platforms. Engineering standardization encompasses multiple technical domains including microfluidic interfaces, sensor calibration procedures, and data acquisition protocols. The development of standardized connection interfaces would enable modular integration of different JoC components, facilitating innovation while ensuring compatibility. Standardized calibration procedures for multi-sensor systems are essential for ensuring measurement accuracy and enabling data comparison across different platforms and studies. Manufacturing standardization becomes critical as JoC technologies transition from laboratory prototypes to commercial products. This includes establishing good manufacturing practices guidelines specific to microfluidic devices, quality control procedures for complex multi-component systems, and sterilization protocols compatible with sensitive sensor components. Data standardization represents another critical need, particularly as JoC platforms generate increasingly complex multi-parameter datasets. Standardized data formats, metadata requirements, and sharing protocols are essential for enabling meta-analyses as well as machine learning applications. In fact, collecting large datasets from multiple sensors also adds layers of complexity to data analysis, necessitating sophisticated algorithms and computational tools capable of synchronizing and interpreting real-time signals. Incorporating artificial intelligence tools may help identify patterns, predict disease trajectories and outcomes, and refine interventions.

In summary, while the integration of real-time sensors into JoC poses non-trivial hurdles, it holds promise for advancing our understanding of joint disorders and accelerating the discovery of effective therapies. Continued innovation and interdisciplinary collaboration will be vital to overcome these obstacles, and the potential benefits for studying and treating OA, RA, and other joint-related diseases are unparalleled.

IV. CONCLUSIONS

Multi-tissue dynamic JoC platforms hold the potential to revolutionize the way OA and RA are studied and treated by providing a more precise and comprehensive understanding of these complex diseases already in the preclinical phase. The integration of multi-sensing capabilities will allow the researchers to gain deeper insights into the dynamic changes occurring within the joint microenvironment, leading to more informed decisions in the development and testing of new therapeutics, particularly in the field of precision medicine and personalized drug treatments. Even though some engineering hurdles are yet to be addressed to obtain a standardized and sensorized JoC model, the integration of noninvasive sensors for real-time monitoring ultimately represents a significant leap forward in the development of the next generation of JoC, offering a powerful tool for advancing our knowledge and treatment of joint-related disorders.

ACKNOWLEDGMENTS

This project was funded by European Union (No. GA101077146). Views and opinions expressed are, however, those

of the authors(s) only and do not necessarily reflect those of the European Union. Neither the European Union nor the granting authority can be held responsible for them.

AUTHOR DECLARATIONS

Conflict of Interest

The authors have no conflicts to disclose.

Author Contributions

A. Mantegazza: Conceptualization (equal); Data curation (equal); Formal analysis (equal); Methodology (equal); Visualization (equal); Writing – original draft (equal); Writing – review & editing (equal). **S. Materne:** Data curation (equal); Formal analysis (equal); Methodology (equal); Writing – original draft (equal). **M. Rasponi:** Conceptualization (equal); Writing – review & editing (equal). **P. Occhetta:** Conceptualization (equal); Funding acquisition (lead); Supervision (lead); Writing – review & editing (equal).

DATA AVAILABILITY

Data sharing is not applicable to this article as no new data were created or analyzed in this study.

REFERENCES

[1]Adam, M., Zhuang, H., Ren, X., Zhang, Y., and Zhou, P., "The metabolic characteristics and changes of chondrocytes in vivo and in vitro in osteoarthritis," Front. Endocrinol. **15**, 1393550 (2024).

[2]Adly, N., Weidlich, S., Seyock, S., Brings, F., Yakushenko, A., Offenhäusser, A., and Wolfrum, B., "Printed microelectrode arrays on soft materials: From PDMS to hydrogels," npj Flex. Electron. **2**(1), 15 (2018).

[3]Afzal, A., Mujahid, A., Schirhagl, R., Zafar Bajwa, S., Latif, U., and Feroz, S., "Gravimetric viral diagnostics: QCM based biosensors for early detection of viruses," Chemosensors **5**(1), 7 (2017).

[4]Ahmad, N., Colak, B., Zhang, D.-W., Gibbs, M. J., Watkinson, M., Becer, C. R., Gautrot, J. E., and Krause, S., "Peptide cross-linked poly (ethylene glycol) hydrogel films as biosensor coatings for the detection of collagenase," Sensors **19**(7), 1677 (2019).

[5]Alassi, A., Benammar, M., and Brett, D., "Quartz crystal microbalance electronic interfacing systems: A review," Sensors **17**, 17122799 (2017).

[6]Altea-Manzano, P., Unciti-Broceta, J. D., Cano-Cortes, V., Ruiz-Blas, M., Valero, T., Diaz-Mochon, Juan, and Sánchez-Martín, R., "Tracking cell proliferation using a nanotechnology-based approach," Nanomedicine **12**, 1591 (2017).

[7]Alunno, A., Carubbi, F., Giacomelli, R., and Gerli, R., "Cytokines in the pathogenesis of rheumatoid arthritis: New players and therapeutic targets," BMC Rheumatol. **1**, 11 (2017).

[8]Alvarez-Mamani, E., Buettner, F., Beltran-Castanon, C., and Ibáñez, A., "Exploratory analysis of metabolic changes using mass spectrometry data and graph embeddings," Sci. Rep. **14**, 11 (2024).

[9]Ando, Y., Ta, H. P., Yen, D. P., Lee, S.-S., Raola, S., and Shen, K., "A microdevice platform recapitulating hypoxic tumor microenvironments," Sci. Rep. **7**(1), 15233 (2017).

[10]Antonelli, G., Mencattini, A., Massimiani, M., Lacconi, V., Filippi, J., Losardo, M., D'Orazio, M., Casti, P., Bragaglia, M., Curci, G., Nanni, F., Campagnolo, L., and Martinelli, E., "Development of integrated optical biosensors based on low-cost stereolithography fabrication and multispectral signature for lab-on-chip applications," Sens. Actuators, B **401**, 135009 (2024).

[11]Arasalo, O., Lehtonen, A. J., Kielosto, M., Heinonen, M., and Pokki, J., "Probabilistic analysis of spatial viscoelastic cues in 3D cell culture using magnetic microrheometry," Biophys. J. **124**(2), 351–362 (2025).

[12]Aydogmus, H., Hu, M., Ivancevic, L., Frimat, J.-P., Maagdenberg, A., Sarro, P. M., and Mastrangeli, M., "An organ-on-chip device with integrated charge sensors and recording microelectrodes," Sci. Rep. **13**, 8062 (2023).

[13]Aydın, E. B., Aydın, M., and Sezgintürk, M. K., "Highly sensitive electrochemical immunosensor based on polythiophene polymer with densely populated carboxyl groups as immobilization matrix for detection of interleukin 1β in human serum and saliva," Sens. Actuators, B **270**, 18–27 (2018).

[14]Bagnaninchi, P. O. and Drummond, N., "Real-time label-free monitoring of adipose-derived stem cell differentiation with electric cell-substrate impedance sensing," Proc. Natl. Acad. Sci. U. S. A. **108**(16), 6462–6467 (2011).

[15]Baselt, D. R., Lee, G. U., Natesan, M., Metzger, S. W., Sheehan, P. E., and Colton, R. J., "A biosensor based on magnetoresistance technology," Biosens. Bioelectron. **13**(7), 731–739 (1998).

[16]Basu, A. K., Basu, A., and Bhattacharya, S., "Micro/nano fabricated cantilever based biosensor platform: A review and recent progress," Enzyme Microb. Technol. **139**, 109558 (2020).

[17]Bavli, D., Prill, S., Ezra, E., Levy, G., Cohen, M., Vinken, M., Vanfleteren, J., Jaeger, M., and Nahmias, Y., "Real-time monitoring of metabolic function in liver-on-chip microdevices tracks the dynamics of mitochondrial dysfunction," Proc. Natl. Acad. Sci. U. S. A. **113**(16), E2231–E2240 (2016).

[18]Bekker-Jensen, D., Bernhardt, O., Hogrebe, A., Martinez del Val, A., Verbeke, L., Gandhi, T., Kelstrup, C., Reiter, L., and Olsen, J., "Rapid and site-specific deep phosphoproteome profiling by data-independent acquisition without the need for spectral libraries," Nat. Commun. **11**, 787 (2020).

[19]Belcastro, L., Antonacci, P., Rocchitta, G., Sprecher, C. M., Vernengo, A. J., Serra, P. A., Arduini, F., Grad, S., and Basoli, V., "Real-time nitric oxide and inflammation sensing in 2D osteoarthritis models: Microsensor design and application," Sens. Actuators, B **430**, 137147 (2025).

[20]Bencic-Nagale, S. and Walt, D. R., "Extending the longevity of fluorescence-based sensor arrays using adaptive exposure," Anal. Chem. **77**(19), 6155–6162 (2005).

[21]Bentum, M., Klinger, B., Sieber, A., Zauber, H., Lehmann, N., Haji, M., Niquet, S., Mertins, P., Blüthgen, N., and Selbach, M., "Spike-in enhanced phosphoproteomics uncovers synergistic signaling responses to mek inhibition in colon cancer cells," Nat. Commun. **16**, 4884 (2025).

[22]Berrios, I., Salter, S., Hirday, R., Rabolli, C., Tan, A., Hung, C., Schloss, R., and Yarmush, M., "In vitro inflammatory multi-cellular model of osteoarthritis," Osteoarthritis Cartilage Open **6**, 100432 (2024).

[23]Bock, S., Choi, Y.-S., Kim, M., Yun, Y., Pham, X.-H., Kim, J., Seong, B., Kim, W., Jo, A., Ham, K.-M., Lee, S. G., Lee, S. H., Kang, H., Choi, H., Jeong, D., Chang, H., Kim, D.-E., and Jun, B.-H., "Highly sensitive near-infrared SERS nanoprobes for in vivo imaging using gold-assembled silica nanoparticles with controllable nanogaps," J. Nanobiotechnol. **20**, 130 (2022).

[24]Borisov, S. M. and Wolfbeis, O. S., "Optical biosensors," Chem. Rev. **108**(2), 423–461 (2008).

[25]Bortel, P., Piga, I., Koenig, C., Gerner, C., Val, A., and Olsen, J., "Systematic optimization of automated phosphopeptide enrichment for high-sensitivity phosphoproteomics," Mol. Cell. Proteomics **23**(5), 100754 (2024).

[26]Bounik, R., Landolt, A. E., Lee, J., Viswam, V., Cardes, F., Modena, M. M., and Hierlemann, A., "Seamless integration of CMOS microsensors into open microfluidic systems," Lab Chip **25**, 2205–2221 (2025).

[27]Brand, R. E., Nolen, B. M., Zeh, H. J., Allen, P. J., Eloubeidi, M. A., Goldberg, M., Elton, E., Arnoletti, J. P., Christein, J. D., Vickers, S. M., Langmead, C. J., Landsittel, D. P., Whitcomb, D. C., Grizzle, W. E., and Lokshin, A. E., "Serum biomarker panels for the detection of pancreatic cancer," Clin. Cancer Res. **17**(4), 805–816 (2011).

[28]Brischwein, M., Grothe, H., Wiest, J., Zottmann, M., Ressler, J., and Wolf, B., "Planar ruthenium oxide sensors for cell-on-a-chip metabolic studies," Chem. Anal. **54**(6), 1193–1201 (2009).

[29]Brunner, A.-D., Thielert, M., Vasilopoulou, C., Ammar, C., Coscia, F., Mund, A., Horning, O., Bache, N., Apalategui, A., Lubeck, M., Raether, O., Park, M., Richter, S., Fischer, D., Theis, F., Meier, F., and Mann, M., "Ultra-high sensitivity mass spectrometry quantifies single-cell proteome changes upon perturbation," Mol. Syst. Biol. **18**(3), e10798 (2022).

[30]Bubis, J. A., Gorshkov, V., Gorshkov, M. V., and Kjeldsen, F., "Phosphoshield: Improving trypsin digestion of phosphoproteins by shielding the negatively

charged phosphate moiety," J. Am. Soc. Mass Spectrom. **31**(10), 2053–2060 (2020).
[31]Buchanan, B. C. and Yoon, J.-Y., "Microscopic imaging methods for organ-on-a-chip platforms," Micromachines **13**(2), 328 (2022).
[32]Bussooa, A., Tubbs, E., Revol-Cavalier, F., Chmayssem, A., Alessio, M., Cosnier, M.-L., and Verplanck, N., "Real-time monitoring of oxygen levels within thermoplastic organ-on-chip devices," Biosens. Bioelectron. **11**, 100198 (2022).
[33]Cai, G., Yang, Z., Chen, Y.-C., Huang, Y., Liang, L., Feng, S., and Zhao, J., "Magnetic bead manipulation in microfluidic chips for biological application," Cyborg Bionic Syst. **4**, 0023 (2023).
[34]Calogiuri, A., Bellisario, D., Sciurti, E., Blasi, L., Esposito, V., Casino, F., Siciliano, P., and Francioso, L., "Non-invasive real-time investigation of colorectal cells tight junctions by Raman microspectroscopy analysis combined with machine learning algorithms for organ-on-chip applications," Front. Bioeng. Biotechnol. **12**, 1458404 (2024).
[35]Cao, Y., Tang, S., and Ding, C., "Inflammatory phenotype of osteoarthritis and its potential therapies," Rheumatol. Autoimmunity **1**, 92 (2021).
[36]Cardoso, A. R., de Sá, M. H., and Sales, M. G. F., "An impedimetric molecularly-imprinted biosensor for interleukin-1β determination, prepared by in-situ electropolymerization on carbon screen-printed electrodes," Bioelectrochemistry **130**, 107287 (2019).
[37]Carlos, F. F., Flores, O., Doria, G., and Baptista, P. V., "Characterization of genomic single nucleotide polymorphism via colorimetric detection using a single gold nanoprobe," Anal. Biochem. **465**, 1–5 (2014).
[38]Carlson, A., Rawle, R., Wallace, C., Brooks, E., Adams, E., Greenwood, M., Olmer, M., Lotz, M., Bothner, B., and June, R., "Characterization of synovial fluid metabolomic phenotypes of cartilage morphological changes associated with osteoarthritis," Osteoarthritis Cartilage **27**(8), 1174–1184 (2019).
[39]Carlsson, A., Wingren, C., Kristensson, M., Rose, C., Fernö, M., Olsson, H., Jernström, H., Ek, S., Gustavsson, E., Ingvar, C., Ohlsson, M., Peterson, C., and Borrebaeck, C., "Molecular serum portraits in patients with primary breast cancer predict the development of distant metastases," Proc. Natl. Acad. Sci. U. S. A. **108**, 14252–14257 (2011).
[40]Caroselli, R., Castelló, J., Escorihuela, J., Bañuls, M., Maquieira, A., and García-Rupérez, J., "Experimental study of the oriented immobilization of antibodies on photonic sensing structures by using protein a as an intermediate layer," Sensors **18**, 1012 (2018).
[41]Cedillo-Alcantar, D. F., Rodriguez-Moncayo, R., Maravillas-Montero, J. L., and Garcia-Cordero, J. L., "On-chip analysis of protein secretion from single cells using microbead biosensors," ACS Sens. **8**(2), 655–664 (2023).
[42]CEN/CENELEC FGOoC, *Focus Group Organ-on-Chip Standardization Roadmap* (CEN-CENELEC Focus Group, 2024).
[43]Cennamo, N., Piccirillo, A., Bencivenga, D., Arcadio, F., Annunziata, M., Della Ragione, F., Guida, L., Zeni, L., and Borriello, A., "Towards a point-of-care test to cover atto-femto and pico-nano molar concentration ranges in interleukin 6 detection exploiting PMMA-based plasmonic biosensor chips," Talanta **256**, 124284 (2023).
[44]Cennamo, N., Bencivenga, D., Annunziata, M., Arcadio, F., Stampone, E., Piccirillo, A., Della Ragione, F., Zeni, L., Guida, L., and Borriello, A., "Plasmon resonance biosensor for interleukin-1β point-of-care determination: A tool for early periodontitis diagnosis," iScience **27**(1), 108741 (2024).
[45]Ling Chang, C., Fix, K., and Wang, W.-C., "Reliability of PEDOT-PSS strain gauge on foam structure," Proc. SPIE **7646**, 764616 (2010).
[46]Charras, G. T. and Horton, M. A., "Single cell mechanotransduction and its modulation analyzed by atomic force microscope indentation," Biophys. J. **82**(6), 2970–2981 (2002).
[47]Che, V. L., Zimmermann, J., Zhou, Y., Lu, X. L., and Van Rienen, U., "Deriving models of cartilaginous cells from confocal fluorescence microscopy images to estimate dielectric properties," IEEE Trans. Magn **60**(3), 1 (2024).
[48]Chen, W., Yi, P., Zhang, Y., Zhang, L., Deng, Z., and Zhang, Z., "Composites of aminodextran-coated Fe_3O_4 nanoparticles and graphene oxide for cellular magnetic resonance imaging," ACS Appl. Mater. Interfaces **3**(10), 4085–4091 (2011).
[49]Chen, Y., Qian, C., Liu, C., Shen, H., Wang, Z., Ping, J., Wu, J., and Chen, H., "Nucleic acid amplification free biosensors for pathogen detection," Biosens. Bioelectron. **153**, 112049 (2020).
[50]Chen, Y., Zhao, B., Zhu, Y., Zhao, H., and Ma, C., "HIF-1-VEGF-Notch mediates angiogenesis in temporomandibular joint osteoarthritis," Am. J. Transl. Res. **11**(5), 2969–2982 (2019).
[51]Chimenti, M. S., Triggianese, P., Conigliaro, P., Candi, E., Melino, G., and Perricone, R., "The interplay between inflammation and metabolism in rheumatoid arthritis," Cell Death Dis. **6**, e1887 (2015).
[52]Chinnadayyala, S. R. and Cho, S., "Electrochemical immunosensor for the early detection of rheumatoid arthritis biomarker: Anti-cyclic citrullinated peptide antibody in human serum based on avidin-biotin system," Sensors **21**(1), 124 (2021).
[53]Chinnadayyala, S. R., Park, J., Abbasi, M. A., and Cho, S., "Label-free electrochemical impedimetric immunosensor for sensitive detection of IgM rheumatoid factor in human serum," Biosens. Bioelectron. **143**, 111642 (2019).
[54]Cho, Y. H., Park, Y.-G., Kim, S., and Park, J.-U., "3D electrodes for bioelectronics," Adv. Mater. **33**(47), 2005805 (2021).
[55]Choi, G., Mangadu, B., Light, Y., and Meagher, R., "Portable microfluidic immunoassay platform for the detection of inflammatory protein biomarkers," Sens. Diagn. **3**, 648 (2024).
[56]Choi, S. and Chae, J., "Methods of reducing non-specific adsorption in microfluidic biosensors," J. Micromech. Microeng. **20**, 075015 (2010).
[57]Choo, K. and Tham, W., "Tandem mass spectrometry data quality assessment by self-convolution," BMC Bioinf. **8**, 352 (2007).
[58]Clark, R., Schmidt, T., Sachse, F., Boyle, D., Firestein, G. S., and Giles, W. R., "Cellular electrophysiological principles that modulate secretion from synovial fibroblasts," J. Physiol. **595**, 635–645 (2017).
[59]Cohen, A. E. and Kunz, R. R., "Large-area interdigitated array microelectrodes for electrochemical sensing," Sens. Actuators, B **62**(1), 23–29 (2000).
[60]Coln, E. A., Colón, A., Long, C. J., Sriram, N. N., Esch, M. B., Prot, J., Elbrecht, D., Wang, Y. I., Jackson, M., Hickman, J. J., and Shuler, M. L., "Piezoelectric biomems cantilever for measurement of muscle contraction and for actuation of mechanosensitive cells," MRS Commun. **9**, 1186–1192 (2019).
[61]Conceição, F., Meneses, J., Lebre, F., Becker, M., Araújo-Gomes, N., Vos, R., Ribeiro, A. R., Alfaro-Moreno, E., Leijten, J., and Teixeira, L. M., "Sex-stratified osteochondral organ-on-chip model reveals sex-specific responses to inflammatory stimulation," Mater. Today Bio **32**, 101728 (2025).
[62]Conklin, G., Ngourn, S. C., and Gerdon, A. E., "Quartz crystal microbalance with microfluidic multi-stream solution control for mineralization kinetic analysis," Sens. Actuators, B **214**, 174–180 (2015).
[63]Corciulo, C., Lendhey, M., Wilder, T., Schoen, H., Cornelissen, A., Chang, G., and Kennedy, O., "Endogenous adenosine maintains cartilage homeostasis and exogenous adenosine inhibits osteoarthritis progression," Nat. Commun. **8**, 15019 (2017).
[64]Courbot, O. and Elosegui-Artola, A., "The role of extracellular matrix viscoelasticity in development and disease," npj Biol. Phys. Mech. **2**, 10 (2025).
[65]Crake, R., Strother, R., Phillips, E., Doogue, M., Zhang, M., Frampton, C., Robinson, B., and Currie, M., "Influence of serum inflammatory cytokines on cytochrome P450 drug metabolising activity during breast cancer chemotherapy: A patient feasibility study," Sci. Rep. **11**, 5648 (2021).
[66]Cuartero, M., Bishop, J., Walker, R., Acres, R. G., Bakker, E., De Marco, R., and Crespo, G. A., "Evidence of double layer/capacitive charging in carbon nanomaterial-based solid contact polymeric ion-selective electrodes," Chem. Commun. **52**, 9703–9706 (2016).
[67]Czarnek, M. and Bereta, J., "Smartflares fail to reflect their target transcripts levels," Sci. Rep. **7**, 11682 (2017).
[68]Daans, M., Lories, R. J. U., and Luyten, F. P., "Dynamic activation of bone morphogenetic protein signaling in collagen-induced arthritis supports their role in joint homeostasis and disease," Arthritis Res. Ther. **10**, R115 (2008).
[69]Dai, X., Zhou, W., Gao, T., Liu, J., and Lieber, C. M., "Three-dimensional mapping and regulation of action potential propagation in nanoelectronics-innervated tissues," Nat. Nanotechnol. **11**(9), 776–782 (2016).
[70]Dantus, M., "Tracking molecular fragmentation in electron–ionization mass spectrometry with ultrafast time resolution," Acc. Chem. Res. **57**(6), 845–854 (2024).
[71]de Gracia Villa, M., Jiménez-Jorquera, C., Haro, I., Gomara, M. J., Sanmartí, R., Fernández-Sánchez, C., and Mendoza, E., "Carbon nanotube composite

peptide-based biosensors as putative diagnostic tools for rheumatoid arthritis," Biosens. Bioelectron. **27**(1), 113–118 (2011).
[72]Defranchi, E., Novellino, A., Whelan, M., Vogel, S., Ramirez, T., Van Ravenzwaay, B., and Landsiedel, R., "Feasibility assessment of micro-electrode chip assay as a method of detecting neurotoxicity in vitro," Front. Neuroeng. **4**, 6 (2011).
[73]del Moral, B., Baeza, F. J., Navarro, R., Galao, O., Zornoza, E., Vera, J., Farcas, C., and Garcés, P., "Temperature and humidity influence on the strain sensing performance of hybrid carbon nanotubes and graphite cement composites," Constr. Build. Mater. **284**, 122786 (2021).
[74]della ventura, B., Iannaccone, M., Funari, R., Pica Ciamarra, M., Altucci, C., Capparelli, R., Roperto, S., and Velotta, R., "Effective antibodies immobilization and functionalized nanoparticles in a quartz-crystal microbalance-based immunosensor for the detection of parathion," PLoS One **12**, e0171754 (2017).
[75]Desbiolles, B. X. E., Hannebelle, M. T. M., de Coulon, E., Bertsch, A., Rohr, S., Fantner, G. E., and Renaud, P., "Volcano-shaped scanning probe microscopy probe for combined force-electrogram recordings from excitable cells," Nano Lett. **20**, 4520–4529 (2020).
[76]Desrochers, J., Amrein, M., and Matyas, J. R., "Viscoelasticity of the articular cartilage surface in early osteoarthritis," Osteoarthritis Cartilage **20**, 413–421 (2012).
[77]Ding, N., Liu, R., Zhang, B., Yang, N., Qin, M., Zhang, Y., and Wang, Z., "A fluorescent nanoprobe and paper-based nanofiber platform for detection and imaging of Fe^{3+} in actual samples and living cells," Talanta **271**, 125713 (2024).
[78]Doy, N., Mchale, G., Newton, M., Hardacre, C., Ge, R., MacInnes, J., Kuvshinov, D., and Allen, R. W. K., "Small volume laboratory on a chip measurements incorporating the quartz crystal microbalance to measure the viscosity-density product of room temperature ionic liquids," Biomicrofluidics **4**, 14107 (2010).
[79]Doyran, B., Tong, W., Li, Q., Jia, H., Zhang, X., Chen, C., Enomoto-Iwamoto, M., Lu, X. L., Qin, L., and Han, L., "Nanoindentation modulus of murine cartilage: A sensitive indicator of the initiation and progression of post-traumatic osteoarthritis," Osteoarthritis Cartilage **25**(1), 108–117 (2017).
[80]Drouvalakis, K. A., Bangsaruntip, S., Hueber, W., Kozar, L. G., Utz, P. J., and Dai, H., "Peptide-coated nanotube-based biosensor for the detection of disease-specific autoantibodies in human serum," Biosens. Bioelectron. **23**(10), 1413–1421 (2008).
[81]Du, C., Liu, J., Liu, S., Xiao, P., Chen, Z., Chen, H., Huang, W., and Lei, Y., "Bone and joint-on-chip platforms: Construction strategies and applications," Small Methods **8**(12), 2400436 (2024).
[82]Duc, P., Vignes, M., Hugon, G., Sebban, A., Carnac, G., Malyshev, E., Charlot, B., and Rage, F., "Human neuromuscular junction on micro-structured microfluidic devices implemented with a custom micro electrode array (MEA)," Lab Chip **21**(21), 4223–4236 (2021).
[83]Dugan, C. E., Grinias, J. P., Parlee, S. D., El-Azzouny, M., Evans, C. E., and Kennedy, R. T., "Monitoring cell secretions on microfluidic chips using solid-phase extraction with mass spectrometry," Anal. Bioanal. Chem. **409**, 169–178 (2017).
[84]Duval, K., Grover, H., Han, L.-H., Mou, Y., Pegoraro, A. F., Fredberg, J., and Chen, Z., "Modeling physiological events in 2D vs. 3D cell culture," Physiology **32**(4), 266–277 (2017).
[85]Egunov, A. I., Dou, Z., Karnaushenko, D. D., Hebenstreit, F., Kretschmann, N., Akgün, K., Ziemssen, T., Karnaushenko, D., Medina-Sánchez, M., and Schmidt, O. G., "Impedimetric microfluidic sensor-in-a-tube for label-free immune cell analysis," Small **17**(5), 2002549 (2021).
[86]Elsaid, K. A., Jay, G. D., and Chichester, C. O., "Detection of collagen type II and proteoglycans in the synovial fluids of patients diagnosed with non-infectious knee joint synovitis indicates early damage to the articular cartilage matrix," Osteoarthritis Cartilage **11**(9), 673–680 (2003).
[87]Erickson, J., Tooker, A., Tai, Y.-C., and Pine, J., "Caged neuron MEA: A system for long-term investigation of cultured neural network connectivity," J. Neurosci. Methods **175**(1), 1–16 (2008).
[88]Erstling, J., Naguib, N., Hinckley, J., Lee, R., Feuer, G., Tallman, J., Tsaur, L., Tang, D., and Wiesner, U., "Antibody functionalization of ultrasmall fluorescent core–shell aluminosilicate nanoparticle probes for advanced intracellular labeling and optical super resolution microscopy," Chem. Mater. **35**, 1047 (2023).
[89]Eschweiler, J., Horn, N., Rath, B., Betsch, M., Baroncini, A., Tingart, M., and Migliorini, F., "The biomechanics of cartilage—An overview," Life **11**, 302 (2021).
[90]Estabrook, I., Thiam, H., Piel, M., and Hawkins, R., "Calculation of the force field required for nucleus deformation during cell migration through constrictions," PLoS Comput. Biol. **17**(5), e1008592 (2020).
[91]Eteshola, E. and Leckband, D., "Development and characterization of an elisa assay in PDMS microfluidic channels," Sens. Actuators, B **72**, 129–133 (2001).
[92]Fan, B., Robinson, J. T., and Wolfrum, B., "Impedance scaling for gold and platinum microelectrodes," J. Neural Eng. **18**(5), 056025 (2021).
[93]Fan, M., Chen, J., Zheng, X., Xu, L., Ye, J., Lin, X., Kong, K. V., Lin, D., Lu, Y., and Feng, S., "Precise genotyping via surface-enhanced raman spectroscopy-based optical sensing chip for guiding targeted therapy in lung cancer," Laser Photonics Rev. **19**(5), 2401400 (2025).
[94]Fang, X., Yang, Y., Wang, H., and Xu, H., "Bead-based microfluidic platforms for multiplex and ultrasensitive immunoassays in clinical diagnosis and treatment," Mechanobiol. Med. **2**, 100063 (2024).
[95]Farooq, A., Wood, C. D., Ladbury, J. E., and Evans, S. D., "On-chip Raman spectroscopy of live single cells for the staging of oesophageal adenocarcinoma progression," Sci. Rep. **14**(1), 1761 (2024).
[96]Faull, K. F., Dooley, A. N., Halgand, F., Shoemaker, L. D., Norris, A. J., Ryan, C. M., Laganowsky, A., Johnson, J. V., and Katz, J. E., "Chapter 1: An introduction to the basic principles and concepts of mass spectrometry," Compr. Anal. Chem. **52**, 1–46 (2008).
[97]Fernandes, J., Karra, N., Bowring, J., Reale, R., James, J., Blume, C., Pell, T. J., Rowan, W. C., Davies, D. E., Swindle, E. J., and Morgan, H., "Real-time monitoring of epithelial barrier function by impedance spectroscopy in a microfluidic platform," Lab Chip **22**, 2041–2054 (2022).
[98]Ferrari, E., Palma, C., Vesentini, S., Occhetta, P., and Rasponi, M., "Integrating biosensors in organs-on-chip devices: A perspective on current strategies to monitor microphysiological systems," Biosensors **10**(9), 110 (2020).
[99]Finckh, A., Gilbert, B., Hodkinson, B., Bae, S.-C., Thomas, R., Deane, K. D., Alpizar-Rodriguez, D., and Lauper, K., "Global epidemiology of rheumatoid arthritis," Nat. Rev. Rheumatol. **18**(10), 591–602 (2022).
[100]Freitas, M., Neves, M. M., Nouws, H. P. A., and Delerue-Matos, C., "Quantum dots as nanolabels for breast cancer biomarker HER2-ECD analysis in human serum," Talanta **208**, 120430 (2020).
[101]Fritz, J., "Cantilever biosensors," Analyst **133**(7), 855–863 (2008).
[102]Fu, B., Shen, J., Zou, X., Sun, N., Zhang, Z., Liu, Z., Zeng, C., Liu, H., and Huang, W., "Matrix stiffening promotes chondrocyte senescence and the osteoarthritis development through downregulating HDAC3," Bone Res. **12**, 32 (2024).
[103]Fuchs, S., Johansson, S., Tjell, A. Ø., Werr, G., Mayr, T., and Tenje, M., "In-line analysis of organ-on-chip systems with sensors: Integration, fabrication, challenges, and potential," ACS Biomater. Sci. Eng. **7**(7), 2926–2948 (2021).
[104]Fuchs, S., Rieger, V., Tjell, A. Ø., Spitz, S., Brandauer, K., Schaller-Ammann, R., Feiel, J., Ertl, P., Klimant, I., and Mayr, T., "Optical glucose sensor for microfluidic cell culture systems," Biosens. Bioelectron. **237**, 115491 (2023).
[105]Gajasinghe, R., Jones, M., Ince, T. A., and Tigli, O., "Label and immobilization free detection and differentiation of tumor cells," IEEE Sens. J. **18**(9), 3486–3493 (2018).
[106]Galluzzi, M., Tang, G., Biswas, C., Zhao, J., Chen, S., and Stadler, F., "Atomic force microscopy methodology and AFMech Suite software for nanomechanics on heterogeneous soft materials," Nat. Commun. **9**, 3584 (2018).
[107]Gao, D., Wei, H., Guo, G.-S., and Lin, J.-M., "Microfluidic cell culture and metabolism detection with electrospray ionization quadrupole time-of-flight mass spectrometer," Anal. Chem. **82**, 5679–5685 (2010).
[108]Gao, D., Li, H., Wang, N., and Lin, J.-M., "Evaluation of the absorption of methotrexate on cells and its cytotoxicity assay by using an integrated microfluidic device coupled to a mass spectrometer," Anal. Chem. **84**(21), 9230–9237 (2012).
[109]Gao, H., Yang, F., Sattari, K., Du, X., Fu, T., Fu, S., Liu, X., Lin, J., Sun, Y., and Yao, J., "Bioinspired two-in-one nanotransistor sensor for the simultaneous

measurements of electrical and mechanical cellular responses," Sci. Adv. **8**(34), eabn2485 (2022).
[110]Gao, X., Cui, Y., Levenson, R., Chung, L., and Nie, S., "In vivo cancer targeting and imaging with semiconductor quantum dots," Nat. Biotechnol. **22**, 969–976 (2004).
[111]Gao, Y., Huo, W., Zhang, L., Lian, J., Tao, W., Song, C., Tang, J., Shi, S., and Gao, Y., "Multiplex measurement of twelve tumor markers using a GMR multi-biomarker immunoassay biosensor," Biosens. Bioelectron. **123**, 204–210 (2019).
[112]Ge, C., Chen, Z., Sun, H., Sun, P., Zhao, J., Wu, Y., Xu, J., Zhou, M., and Luan, M., "Visually evaluating drug efficacy in living cells using COF-based fluorescent nanoprobe via CHA amplified detection of miRNA and simultaneous apoptosis imaging," Anal. Chim. Acta **1302**, 342502 (2024).
[113]Ge, M., Zou, H., Chen, J., Zhang, Q., Li, C., Yang, J., Wu, J., Xie, X., Liu, J., Lei, L., Peng, S., and Nie, H., "Cellular fibronectin-targeted fluorescent aptamer probes for early detection and staging of liver fibrosis," Acta Biomater. **190**, 579 (2024).
[114]Ge, Z., Wang, C., Tao, Y., Qiu, F., Liu, F., Guo, W., Liu, W., Zhao, M., Yang, R., Zhang, X., Xue, R., Tu, L., Shi, W., Chang, Z., Zhang, H., Wang, G., Yu, G., and Ren, Y., "Dual-layer flexible liquid metal fiber for plantar pressure monitoring and synchronous wound electrotherapy," Adv. Healthcare Mater. **15**(1), e02681 (2026).
[115]Gebreyesus, S., Siyal, A., Kitata, R. B., Chen, E., Enkhbayar, B., Angata, T., Lin, K.-I., Chen, Y.-J., and Tu, H.-L., "Streamlined single-cell proteomics by an integrated microfluidic chip and data-independent acquisition mass spectrometry," Nat. Commun. **13**, 37 (2022).
[116]Ghodbane, M., Kulesa, A., Yu, H. H., Maguire, T. J., Schloss, R. R., Ramachandran, R., Zahn, J. D., and Yarmush, M. L., "Development of a low-volume, highly sensitive microimmunoassay using computational fluid dynamics-driven multiobjective optimization," Microfluid. Nanofluid. **18**, 199–214 (2015).
[117]Giaever, I. and Keese, C. R., "A morphological biosensor for mammalian cells," Nature **366**(6455), 591–592 (1993).
[118]Gilboa, T., Maley, A., Ogata, A., Wu, C., and Walt, D., "Sequential protein capture in multiplex single molecule arrays: A strategy for eliminating assay cross-reactivity," Adv. Healthcare Mater. **10**, e2001111 (2021).
[119]Goddard, J. and Erickson, D., "Bioconjugation techniques for microfluidic biosensors," Anal. Bioanal. Chem. **394**, 469–479 (2009).
[120]Gori, M., Simonelli, M., Giannitelli, S., Businaro, L., Trombetta, M., and Rainer, A., "Investigating nonalcoholic fatty liver disease in a liver-on-a-chip microfluidic device," PLoS One **11**, e0159729 (2016).
[121]Gravallese, E., Pettit, A., Lee, R., Madore, R., Manning, C., Tsay, A., Gaspar, J., Goldring, M., and Oettgen, P., "Angiopoietin-1 is expressed in the synovium of patients with rheumatoid arthritis and is induced by tumour necrosis factor," Ann. Rheumatic Dis. **62**, 100–107 (2003).
[122]Grist, S. M., Chrostowski, L., and Cheung, K. C., "Optical oxygen sensors for applications in microfluidic cell culture," Sensors **10**(10), 9286–9316 (2010).
[123]Guerrero, S., Sánchez-Tirado, E., Agüí, L., González-Cortés, A., Yáñez-Sedeño, P., and Pingarrón, J. M., "Simultaneous determination of CXCL7 chemokine and MMP3 metalloproteinase as biomarkers for rheumatoid arthritis," Talanta **234**, 122705 (2021).
[124]Guerrero, S., Sánchez-Tirado, E., Martínez-García, G., González-Cortés, A., Yáñez Sedeño, P., and Pingarrón, J. M., "Electrochemical biosensor for the simultaneous determination of rheumatoid factor and anti-cyclic citrullinated peptide antibodies in human serum," Analyst **145**, 4680 (2020).
[125]Guilak, F., Nims, R. J., Dicks, A., Wu, C.-L., and Meulenbelt, I., "Osteoarthritis as a disease of the cartilage pericellular matrix," Matrix Biol. **71–72**, 40–50 (2018).
[126]Gutiérrez-Capitán, M., Sanchís, A., Carvalho, E. O., Baldi, A., Vilaplana, L., Cardoso, V. F., Calleja, Á., Wei, M., de la Rica, R., Hoyo, J., Bassegoda, A., Tzanov, T., Marco, M.-P., Lanceros-Méndez, S., and Fernández-Sánchez, C., "Engineering a point-of-care paper-microfluidic electrochemical device applied to the multiplexed quantitative detection of biomarkers in sputum," ACS Sens. **8**(8), 3032–3042 (2023).
[127]Guzinski, M., Jarvis, J. M., Perez, F., Pendley, B. D., Lindner, E., De Marco, R., Crespo, G. A., Acres, R. G., Walker, R., and Bishop, J., "PEDOT(PSS) as solid contact for ion-selective electrodes: The influence of the PEDOT(PSS) film thickness on the equilibration times," Anal. Chem. **89**(6), 3508–3516 (2017).
[128]Hadavi, D., Tosheva, I., Siegel, T. P., Cuypers, E., and Honing, M., "Technological advances for analyzing the content of organ-on-a-chip by mass spectrometry," Front. Bioeng. Biotechnol. **11**, 1197760 (2023).
[129]Hajjar, S. and Zhou, X., "pH sensing at the intersection of tissue homeostasis and inflammation," Trends Immunol. **44**(10), 807–825 (2023).
[130]Han, B., Nia, H., Wang, C., Chandrasekaran, P., Li, Q., Chery, D., Li, H., Grodzinsky, A., and Han, L., "AFM-nanomechanical test: An interdisciplinary tool that links the understanding of cartilage and meniscus biomechanics, osteoarthritis degeneration, and tissue engineering," ACS Biomater. Sci. Eng. **3**, 2033 (2017).
[131]Han, F., Li, M., Ye, H., and Zhang, G., "Materials, electrical performance, mechanisms, applications, and manufacturing approaches for flexible strain sensors," Nanomaterials **11**(5), 1220 (2021).
[132]Han, L., Grodzinsky, A. J., and Ortiz, C., "Nanomechanics of the cartilage extracellular matrix," Annu. Rev. Mater. Res. **41**, 133–168 (2011).
[133]Hansen, K. M. and Thundat, T., "Microcantilever biosensors," Methods **37**(1), 57–64 (2005).
[134]Hao, W., Chang, M., Shi, D., Yun, C., Li, J., Guo, H., and Lin, X., "Therapeutic targets in aging-related osteoarthritis: A focus on the extracellular matrix homeostasis," Life Sci. **368**, 123487 (2025).
[135]Harris, E. D., Jr., DiBona, D. R., and Krane, S. M., "Collagenases in human synovial fluid," J. Clin. Invest. **48**(11), 2104–2113 (1969).
[136]Henry, O. Y. F., Villenave, R., Cronce, M. J., Leineweber, W. D., Benz, M. A., and Ingber, D. E., "Organs-on-chips with integrated electrodes for trans-epithelial electrical resistance (TEER) measurements of human epithelial barrier function," Lab Chip **17**, 2264–2271 (2017).
[137]Hillier, A. C. and Ward, M. D., "Scanning electrochemical mass sensitivity mapping of the quartz crystal microbalance in liquid media," Anal. Chem. **64**, 2539–2554 (1992).
[138]Hoerber, J. and Miles, M., "Scanning probe evolution in biology," Science **302**, 1002–1005 (2003).
[139]Homola, J., "Surface plasmon resonance sensors for detection of chemical and biological species," Chem. Rev. **108**(2), 462–493 (2008).
[140]Homola, J., Yee, S. S., and Gauglitz, G., "Surface plasmon resonance sensors: Review," Sens. Actuators, B **54**(1), 3–15 (1999).
[141]Hossain, Z. S. M., Shinohara, H., Wang, F., and Kitano, H., "Real-time detection of l-glutamate released from C6 glioma cells using a modified enzyme-luminescence method," Anal. Bioanal. Chem. **389**(6), 1961–1966 (2007).
[142]Hsu, H.-C., Tran, T.-B., Nguyen, T. T.-V., Le, H.-D., and Chiang, C.-C., "Integration of a microfluidics system with a U-shaped optical fiber sensor for sensing various concentrations of glucose," IEEE Sens. J. **24**(13), 20617–20628 (2024).
[143]Huang, J., Xian, S., Liu, Y., Chen, X., Pu, K., and Wang, H., "Renal clearable activatable polymeric nanoprobe for early detection of hepatic ischemia-reperfusion injury," Adv. Mater. **34**, 2201357 (2022).
[144]Huang, S.-H., Lin, S.-P., Liang, C.-K., and Chen, J.-J. J., "Impedimetric monitoring of IGF-1 protection of in vitro cortical neurons under ischemic conditions," Biomed. Microdev. **15**, 135–143 (2013).
[145]Hügle, T. and Geurts, J., "What drives osteoarthritis?—Synovial versus subchondral bone pathology," Rheumatology **56**(9), 1461–1471 (2016).
[146]Hummel, K. M., Neidhart, M., Vilim, V., Hauser, N., Aicher, W. K., Gay, R. E., Gay, S., and Häuselmann, H. J., "Analysis of cartilage oligomeric matrix protein (COMP) in synovial fibroblasts and synovial fluids," Br. J. Rheumatol. **37**(7), 721–728 (1998).
[147]Hutter, E. and Fendler, J. H., "Exploitation of localized surface plasmon resonance," Adv. Mater. **16**(19), 1685–1706 (2004).
[148]Ihnatouski, M., Pauk, J., Karev, D., and Karev, B., "AFM-based method for measurement of normal and osteoarthritic human articular cartilage surface roughness," Materials **13**, 2302 (2020).
[149]Iqra, M., Anwar, F., Jan, R., and Mohammad, M., "A flexible piezoresistive strain sensor based on laser scribed graphene oxide on polydimethylsiloxane," Sci. Rep. **12**, 4482 (2022).
[150]Iuliano, A., Haalstra, M., Raghuraman, R., Bielawski, K., Bholasing, A. P., van der Wal, E., de Greef, J. C., and Pim Pijnappel, W. W. M., "Real-time and multichannel measurement of contractility of hiPSC-derived 3D skeletal muscle using fiber optics-based sensing," Adv. Mater. Technol. **8**(22), 2300845 (2023).

[151]Izadifar, Z., Charrez, B., Almeida, M., Robben, S., Pilobello, K., van der Graaf-Mas, J., Marquez, S. L., Ferrante, T. C., Shcherbina, K., Gould, R., LoGrande, N. T., Sesay, A. M., and Ingber, D. E., "Organ chips with integrated multifunctional sensors enable continuous metabolic monitoring at controlled oxygen levels," Biosens. Bioelectron. **265**, 116683 (2024).
[152]Jans, D., Callewaert, G., Krylychkina, O., Hoffman, L., Gullo, F., Prodanov, D., and Braeken, D., "Action potential-based MEA platform for in vitro screening of drug-induced cardiotoxicity using human iPSCs and rat neonatal myocytes," J. Pharmacol. Toxicol. Methods **87**, 48–52 (2017).
[153]Jensen, E., "Types of imaging, part 3: Atomic force microscopy," Anat. Rec. **296**(2), 179–183 (2013).
[154]Jeong, S., Kim, S., Buonocore, J., Park, J., Welsh, C. J., Li, J., and Han, A., "A three-dimensional arrayed microfluidic blood–brain barrier model with integrated electrical sensor array," IEEE Trans. Biomed. Eng. **65**(2), 431–439 (2018).
[155]Jia, Y.-P., Ma, B.-Y., Wei, X.-W., and Qian, Z.-Y., "The *in vitro* and *in vivo* toxicity of gold nanoparticles," Chin. Chem. Lett. **28**, 691 (2017).
[156]Jiang, Y. and Turner, K., "Measurement of the strength and range of adhesion using atomic force microscopy," Extreme Mech. Lett. **9**, 119–126 (2016).
[157]Joukar, A., Creecy, A., Karnik, S., Noori-Dokht, H., Trippel, S. B., Wallace, J. M., and Wagner, D. R., "Correlation analysis of cartilage wear with biochemical composition, viscoelastic properties and friction," J. Mech. Behav. Biomed. Mater. **142**, 105827 (2023).
[158]Jurczakowski, R., Hitz, C., and Lasia, A., "Impedance of porous Au based electrodes," J. Electroanal. Chem. **572**(2), 355–366 (2004).
[159]Kadivarian, S., Kooti, S., Ahmadpour-Yazdi, H., Abiri, R., Rostamian, M., Moradi, J., Varmira, K., and Alvandi, A., "A gold nanoparticle colorimetric probe-based biosensor for rapid detection of VIM-2 and IMP-1 metallo-beta lactamase genes," Sens. Biosens. Res. **42**, 100588 (2023).
[160]Kahraman, E., Vasconcelos, D., Ribeiro, B., Monteiro, A. C., Mastromatteo, E., Bortolin, A., Couto, M., Boschis, L., Lamghari, M., and Neto, E., "Deciphering cartilage neuro-immune interactions and innervation profile through 3D engineered osteoarthritic micropathophysiological system," Mater. Today Bio **31**, 101491 (2025).
[161]Kamath, R. R. and Madou, M. J., "Three-dimensional carbon interdigitated electrode arrays for redox-amplification," Anal. Chem. **86**(6), 2963–2971 (2014).
[162]Kaneva, M., Muley, M., Krustev, E., Reid, A., Souza, P., Dell'Accio, F., McDougall, J., and Perretti, M., "Alpha-1-antitrypsin reduces inflammation and exerts chondroprotection in arthritis," FASEB J. **35**, e21472 (2021).
[163]Kang, Y.-T., Kim, M.-J., and Cho, Y.-H., "A cell impedance measurement device for the cytotoxicity assay dependent on the velocity of supplied toxic fluid," J. Micromech. Microeng. **28**(4), 045012 (2018).
[164]Kanioura, A., Filippidou, M., Tsounidi, D., Petrou, P., Chatzandroulis, S., and Tserepi, A., "An organ-on-a-chip modular platform with integrated immunobiosensors for monitoring the extracellular environment," Micromachines **16**, 740 (2025).
[165]Karki, B., Uniyal, A., Pal, A., and Srivastava, V., "Advances in surface plasmon resonance-based biosensor technologies for cancer cell detection," Int. J. Opt. **2022**(1), 1476254.
[166]Kaur, B., Rana, D., Konar, M., Sharma, R., Chouhan, D., Saini, U., Prakash, M., Arora, A., Dhillon, M., Kaur, J., Verma, I., and Sharma, S., "Comparative proteomic analysis of osteoarthritis and rheumatoid arthritis: Identifying potential biomarkers," J. Orthop. Res. **43**, 1396 (2025).
[167]Kerr, L. T., Byrne, H. J., and Hennelly, B. M., "Optimal choice of sample substrate and laser wavelength for Raman spectroscopic analysis of biological specimen," Anal. Methods **7**, 5041–5052 (2015).
[168]Khajehsaeid, H. and Abdollahpour, Z., "Progressive deformation-induced degradation of knee articular cartilage and osteoarthritis," J. Biomech. **111**, 109995 (2020).
[169]Kilic, T., Navaee, F., Stradolini, F., Renaud, P., and Carrara, S., "Organs-on-chip monitoring: Sensors and other strategies," Microphysiol. Syst. **2**, 1–32 (2018).
[170]Kim, H., Han, Y., Suhito, I. R., Choi, Y., Kwon, M., Son, H., Kim, H.-R., and Kim, T.-H., "Raman spectroscopy-based 3D analysis of odontogenic differentiation of human dental pulp stem cell spheroids," Anal. Chem. **93**(29), 9995–10004 (2021).
[171]Kim, J.-H., Lee, G., Won, Y., Lee, M., Kwak, J.-S., Chun, C.-H., and Chun, J.-S., "Matrix cross-linking–mediated mechanotransduction promotes posttraumatic osteoarthritis," Proc. Natl. Acad. Sci. U. S. A. **112**, 9424 (2015).
[172]Kim, Y., Gonzales, J., and Zheng, Y., "Sensitivity-enhancing strategies in optical biosensing," Small **17**(4), 2004988 (2021).
[173]Kirchner, C., Liedl, T., Kudera, S., Pellegrino, T., Javier, A., Gaub, H., Stölzle, S., Fertig, N., and Parak, W., "Cytotoxicity of colloidal CdSe and CdSe/ZnS nanoparticles," Nano Lett. **5**, 331–338 (2005).
[174]Niels Klement, W. J., Duijnstee, D. R., Telle, V., Staykov, A., Browne, W. R., and Verpoorte, E., "Exploring surface-enhanced raman spectroscopy of pyrazine-2-carbonitrile for indirect label-free albumin quantification in an in vitro endothelium permeability assay," Anal. Chem. **97**(7), 4075–4083 (2025).
[175]Kogler, S., Pedersen, G. M., Martínez-Ramírez, F., Aizenshtadt, A., Busek, M., Krauss, S. J. K., Wilson, S. R., and Røberg-Larsen, H., "An FDA-validated, self-cleaning liquid chromatography–mass spectrometry system for determining small-molecule drugs and metabolites in organoid/organ-on-chip medium," Anal. Chem. **96**(29), 12129–12138 (2024).
[176]Koman, V. B., Santschi, C., and Martin, O. J. F., "Multiscattering-enhanced optical biosensor: Multiplexed, non-invasive and continuous measurements of cellular processes," Biomed. Opt. Express **6**(7), 2353–2365 (2015).
[177]Kondratov, A. P., Yakubov, V., and Volinsky, A. A., "Strain gauges capable of measuring large cyclical deformations printed on elastic polymer films," Measurement **166**, 108107 (2020).
[178]Kongsuphol, P., Ng, H. H., Pursey, J. P., Arya, S. K., Wong, C. C., Stulz, E., and Park, M. K., "EIS-based biosensor for ultra-sensitive detection of TNF-α from non-diluted human serum," Biosens. Bioelectron. **61**, 274–279 (2014).
[179]Koutsouras, D. A., Perrier, R., Villarroel Marquez, A., Pirog, A., Pedraza, E., Cloutet, E., Renaud, S., Raoux, M., Malliaras, G. G., and Lang, J., "Simultaneous monitoring of single cell and of micro-organ activity by pedot: PSS covered multi-electrode arrays," Mater. Sci. Eng., C **81**, 84–89 (2017).
[180]Kujala, V. J., Pasqualini, F. S., Goss, J. A., Nawroth, J. C., and Parker, K. K., "Laminar ventricular myocardium on a microelectrode array-based chip," J. Mater. Chem. B **4**, 3534–3543 (2016).
[181]Kumahashi, N., Naitou, K., Nishi, H., Oae, K., Watanabe, Y., Kuwata, S., Ochi, M., Ikeda, M., and Uchio, Y., "Correlation of changes in pain intensity with synovial fluid adenosine triphosphate levels after treatment of patients with osteoarthritis of the knee with high-molecular-weight hyaluronic acid," Knee **18**, 160–164 (2011).
[182]Kumavat, R., Kumar, V., Malhotra, R., Pandit, H., Jones, E., Ponchel, F., and Biswas, S., "Biomarkers of joint damage in osteoarthritis: Current status and future directions," Mediators Inflammation **2021**(1), 5574582.
[183]Kutluk, H., Bastounis, E., and Constantinou, I., "Integration of extracellular matrices into organ-on-chip systems," Adv. Healthcare Mater. **12**, e2203256 (2023).
[184]Kwok, J., Grogan, S., Meckes, B., Arce, F., Lal, R., and D'Lima, D., "Atomic force microscopy reveals age-dependent changes in nanomechanical properties of the extracellular matrix of native human menisci: Implications for joint degeneration and osteoarthritis," Nanomed. Nanotechnol. Biol. Med. **10**(8), 1777–1785 (2014).
[185]Lavrik, N., Sepaniak, M., and Datskos, P., "Cantilever transducers as a platform for chemical and biological sensors," Rev. Sci. Instrum. **75**, 2229 (2004).
[186]Lazanas, A. C. and Prodromidis, M. I., "Electrochemical impedance spectroscopy—A tutorial," ACS Meas. Sci. Au **3**(3), 162–193 (2023).
[187]Lee, A. S., Ellman, M. B., Yan, D., Kroin, J. S., Cole, B. J., van Wijnen, A. J., and Im, H.-J., "A current review of molecular mechanisms regarding osteoarthritis and pain," Gene **527**(2), 440–447 (2013).
[188]Lee, D., Erickson, A., You, T., Dudley, A. T., and Ryu, S., "Pneumatic microfluidic cell compression device for high-throughput study of chondrocyte mechanobiology," Lab Chip **18**, 2077–2086 (2018).
[189]Lee, M. S., Kim, S., Lee, J., Bae, Y., and Lee, S. K., "Synovium-on-a-chip reveals fibroblast–macrophage crosstalk underpinning joint homeostasis and evaluation of gout therapies," Adv. Healthcare Mater. **14**(18), e2501471 (2025).
[190]Lehtonen, A., Arasalo, O., Srbova, L., Heilala, M., and Pokki, J., "Magnetic microrheometry of tumor-relevant stiffness levels and probabilistic quantification of viscoelasticity differences inside 3D cell culture matrices," PLoS One **18**, e0282511 (2023).

[191]Leipert, J. and Tholey, A., "Miniaturized sample preparation on a digital microfluidics device for sensitive bottom-up microproteomics of mammalian cells using magnetic beads and mass spectrometry-compatible surfactants," Lab Chip **19**, 3490 (2019).
[192]Leong, D., Gu, X., Li, Y., Lee, J., Laudier, D., Majeska, R., Schaffler, M., Cardoso, L., and Sun, H., "Matrix metalloproteinase-3 in articular cartilage is upregulated by joint immobilization and suppressed by passive joint motion," Matrix Biol. **29**, 420–426 (2010).
[193]Li, B., Menzel, U., Loebel, C., Schmal, H., Alini, M., and Stoddart, M., "Monitoring live human mesenchymal stromal cell differentiation and subsequent selection using fluorescent RNA-based probes," Sci. Rep. **6**, 26014 (2016).
[194]Li, C., Liu, Y., Lang, C., Zhang, Y., and Qu, S., "Femtosecond laser direct writing of a 3D microcantilever on the tip of an optical fiber sensor for on-chip optofluidic sensing," Lab Chip **22**, 3734–3743 (2022).
[195]Li, H., Li, X., Chen, L., Li, B., Dong, H., Liu, H., Yang, X., Ueda, H., and Dong, J., "Quench-release-based fluorescent immunosensor for the rapid detection of tumor necrosis factor α," ACS Omega **6**(46), 31009–31016 (2021).
[196]Li, J., Lee, W. Y., Wu, T., Leung, C. W., Xu, J., Wong, D. S., Li, R., Li, G., Tang, B. Z., and Bian, L., "Detection of matrix metallopeptidase 13 for monitoring stem cell differentiation and early diagnosis of osteoarthritis by fluorescent light-up probes with aggregation-induced emission characteristics," Adv. Biosys. **2**(10), 1800010 (2018).
[197]Li, M., Hu, Z., Yan, B., Wang, J., Zhang, H., Ye, F., Sun, B., Liu, J., Li, Y., Ding, G., Zang, F., and Yang, Z., "A flexible resistive strain gauge with reduced temperature effect via thermal expansion anisotropic composite substrate," Microsyst. Nanoeng. **10**, 129 (2024).
[198]Li, S., Zhang, R., Li, P., Yi, W., Zhang, Z., Chen, S., Su, S., Zhao, L., and Hu, C., "Development of a novel method to measure macrophage migration inhibitory factor (MIF) in sera of patients with rheumatoid arthritis by combined electrochemical immunosensor," Int. Immunopharmacol. **8**(6), 859–865 (2008).
[199]Li, X., Soler, M., Özdemir, C. I., Belushkin, A., Yesilköy, F., and Altug, H., "Plasmonic nanohole array biosensor for label-free and real-time analysis of live cell secretion," Lab Chip **17**, 2208–2217 (2017).
[200]Li, Y., Pang, Y., Wang, L., Li, Q., Liu, B., Li, J., Liu, S., and Zhao, Q., "Boosting the performance of pedot: PSS based electronics via ionic liquids," Adv. Mater. **36**(13), 2310973 (2024).
[201]Li, Z., Lin, Z., Liu, S., Yagi, H., Zhang, X., Yocum, L., Romero-Lopez, M., Rhee, C., Makarcyzk, M. J., Yu, I., Li, E. N., Fritch, M. R., Gao, Q., Goh, K. B., O'Donnell, B., Hao, T., Alexander, P. G., Mahadik, B., Fisher, J. P., Goodman, S. B., Bunnell, B. A., Tuan, R. S., and Lin, H., "Human mesenchymal stem cell-derived miniature joint system for disease modeling and drug testing," Adv. Sci. **9**(21), 2105909 (2022).
[202]Li, Z., Sant, S., Cho, S. K., Goodman, S., Bunnell, B., Tuan, R., Gold, M., and Lin, H., "Synovial joint-on-a-chip for modeling arthritis: Progress, pitfalls, and potential," Trends Biotechnol. **41**(4), 511–527 (2023).
[203]Lin, C.-Y., Nguyen, U. T. N., Hsieh, H.-Y., Tahara, H., Chang, Y.-S., Wang, B.-Y., Gu, B.-C., Dai, Y.-H., Wu, C.-C., Tsai, I.-J., and Fan, Y.-J., "Peptide-based electrochemical sensor with nanogold enhancement for detecting rheumatoid arthritis," Talanta **236**, 122886 (2022).
[204]Lin, H., Lozito, T. P., Alexander, P. G., Gottardi, R., and Tuan, R. S., "Stem cell-based microphysiological osteochondral system to model tissue response to interleukin-1β," Mol. Pharm. **11**(7), 2203–2212 (2014).
[205]Lin, I.-S., Chuang, C.-Y., and Shih, C.-L., "Dose-response technique combined with stable isotope tracing for drug metabolite profiling by using high-resolution mass spectrometry," Front. Pharmacol. **14**, 12 (2023).
[206]Lin, L., Yi, L., Zhao, F., Wu, Z., Zheng, Y., Li, N., Lin, J.-M., and Sun, J., "ATP-responsive mitochondrial probes for monitoring metabolic processes of glioma stem cells in a 3D model," Chem. Sci. **11**, 2744 (2020).
[207]Lin, Z., Li, Z., Li, E. N., Li, X., Del Duke, C. J., Shen, H., Hao, T., O'Donnell, B., Bunnell, B. A., Goodman, S. B., Alexander, P. G., Tuan, R. S., and Lin, H., "Osteochondral tissue chip derived from iPSCs: Modeling OA pathologies and testing drugs," Front. Bioeng. Biotechnol. **7**, 411 (2019).
[208]Lind, J., Yadid, M., Perkins, I., O'Connor, B., Eweje, F., Chantre, C., Hemphill, M., Campbell, P., Vlassak, J., and Parker, K., "Cardiac microphysiological devices with flexible thin film sensors for higher-throughput drug screening," Lab Chip **17**, 3692 (2017).
[209]Lind, J. U., Busbee, T. A., Valentine, A. D., Pasqualini, F. S., Yuan, H., Yadid, M., Park, S.-J., Kotikian, A., Nesmith, A. P., Campbell, P. H., Vlassak, J. J., Lewis, J. A., and Parker, K. K., "Instrumented cardiac microphysiological devices via multimaterial three-dimensional printing," Nat. Mater. **16**(3), 303–308 (2017).
[210]Liszka, B. M., Rho, H. S., Yang, Y., Lenferink, A. T. M., Terstappen, L. W. M. M., and Otto, C., "A microfluidic chip for high resolution Raman imaging of biological cells," RSC Adv. **5**, 49350–49355 (2015).
[211]Liu, B., Wang, S., Ma, H., Deng, Y., Du, J., Zhao, Y., and Chen, Y., "Heart-on-a-chip: A revolutionary organ-on-chip platform for cardiovascular disease modeling," J. Transl. Med. **23**, 132 (2025).
[212]Liu, C., Jiang, X., Zhao, Y., Jiang, W., Zhang, Z., and Yu, L., "A solid-contact Pb^{2+}-selective electrode based on electrospun polyaniline microfibers film as ion-to-electron transducer," Electrochim. Acta **231**, 53–60 (2017).
[213]Liu, H., MacQueen, L. A., Usprech, J. F., Maleki, H., Sider, K. L., Doyle, M. G., Sun, Y., and Simmons, C. A., "Microdevice arrays with strain sensors for 3D mechanical stimulation and monitoring of engineered tissues," Biomaterials **172**, 30–40 (2018).
[214]Liu, H., Bolonduro, O. A., Hu, N., Ju, J., Rao, A. A., Duffy, B. M., Huang, Z., Black, L. D., and Timko, B. P., "Heart-on-a-chip model with integrated extra- and intracellular bioelectronics for monitoring cardiac electrophysiology under acute hypoxia," Nano Lett. **20**(4), 2585–2593 (2020).
[215]Liu, H., Wang, Q., Cheng, S.-B., Mao, W., Mao, L., Zhang, X., Wang, S., Huang, W.-H., and Chen, M.-M., "Dual gold nanostructures-based stretchable electrochemiluminescence sensors for hydrogen peroxide monitoring in endothelial mechanotransduction," ACS Sens. **9**(11), 6276–6283 (2024).
[216]Liu, J., Jarzabek, J., Roberts, M., Majonis, D., and Winnik, M., "A silica coating approach to enhance bioconjugation on metal-encoded polystyrene microbeads for bead-based assays in mass cytometry," Langmuir **37**, 8240 (2021).
[217]Liu, J., Allo, B., and Winnik, M., "Development of multiplexed bead-based immunoassays for profiling soluble cytokines and CD163 using mass cytometry," ACS Meas. Sci. Au **2**, 629 (2022).
[218]Liu, L., Luo, P., Yang, M., Wang, J., Hou, W., and Xu, P., "The role of oxidative stress in the development of knee osteoarthritis: A comprehensive research review," Front. Mol. Biosci. **9**, 1001212 (2022).
[219]Liu, Y., McGuire, A. F., Lou, H.-Y., Li, T. L., Tok, J. B. H., Cui, B., and Bao, Z., "Soft conductive micropillar electrode arrays for biologically relevant electrophysiological recording," Proc. Natl. Acad. Sci. U. S. A. **115**(46), 11718–11723 (2018).
[220]Loparic, M., Wirz, D., Daniels, A. U., Raiteri, R., VanLandingham, M. R., Guex, G., Martin, I., Aebi, U., and Stolz, M., "Micro- and nanomechanical analysis of articular cartilage by indentation-type atomic force microscopy: Validation with a gel-microfiber composite," Biophys. J. **98**(11), 2731–2740 (2010).
[221]Lorenz, H. and Richter, W., "Osteoarthritis: Cellular and molecular changes in degenerating cartilage," Prog. Histochem. Cytochem. **40**, 135–163 (2006).
[222]Luan, M., Li, N., Pan, W., Yang, L., Yu, Z., and Tang, B., "Simultaneous detection of multiple targets involved in PI3K/AKT pathway for investigating cellular migration and invasion with a multicolor fluorescence nanoprobe," Chem. Commun. **53**, 356 (2016).
[223]Luchansky, M. and Bailey, R., "Silicon photonic microring resonators for quantitative cytokine detection and T-cell secretion analysis," Anal. Chem. **82**, 1975–1981 (2010).
[224]Luo, Y., Zhao, C., and Chen, F., "Multiomics research: Principles and challenges in integrated analysis," BioDesign Res. **6**, 0059 (2024).
[225]Mac, J., Nuñez, V., Burns, J., Guerrero, Y., Vullev, V., and Anvari, B., "Erythrocyte-derived nano-probes functionalized with antibodies for targeted near infrared fluorescence imaging of cancer cells," Biomed. Opt. Express **7**, 1311–1322 (2016).
[226]Macqueen, L., Chebotarev, O., Simmons, C., and Sun, Y., "Miniaturized platform with on-chip strain sensors for compression testing of arrayed materials," Lab Chip **12**, 4178–4184 (2012).
[227]Magni, M., Scaccabarozzi, D., Palomba, E., Zampetti, E., and Saggin, B., "Characterization of thermal gradient effects on a quartz crystal microbalance," Sensors **22**(19), 7256 (2022).
[228]Mahto, S., Yoon, T. H., and Rhee, S., "Cytotoxic effects of surface-modified quantum dots on neuron-like PC12 cells cultured inside microfluidic devices," Biochip J. **4**, 82–88 (2010).

[229]Mainardi, A., Cambria, E., Occhetta, P., Martin, I., Barbero, A., Schären, S., Mehrkens, A., and Krupkova, O., "Intervertebral disc-on-a-chip as advanced in vitro model for mechanobiology research and drug testing: A review and perspective," Front. Bioeng. Biotechnol. **9**, 826867 (2022).
[230]Mainardi, A., Börsch, A., Occhetta, P., Ivanek, R., Ehrbar, M., Krattiger, L., Oertle, P., Loparic, M., Martin, I., Rasponi, M., and Barbero, A., "An organ-on-chip platform for strain-controlled, tissue-specific compression of cartilage and mineralized osteochondral interface to study mechanical overloading in osteoarthritis," Adv. Healthcare Mater. **14**(23), 2501588 (2025).
[231]Makarczyk, M., Preisegger, M., Gao, Q., Bunnell, B., Goodman, S., Michael, G., and Lin, H., "An innervated synovium-cartilage chip for modeling knee joint inflammation and associated pain," Osteoarthritis Cartilage **33**, S468–S469 (2025).
[232]Malik, M., Steele, S. A., Mitra, D., Long, C. J., and Hickman, J. J., "Trans-epithelial/endothelial electrical resistance (TEER): Current state of integrated TEER measurements in organ-on-a-chip devices," Curr. Opin. Biomed. Eng. **34**, 100588 (2025).
[233]Mani, G. K., Morohoshi, M., Yasoda, Y., Yokoyama, S., Kimura, H., and Tsuchiya, K., "ZnO-based microfluidic pH sensor: A versatile approach for quick recognition of circulating tumor cells in blood," ACS Appl. Mater. Interfaces **9**(6), 5193–5203 (2017).
[234]Manvi, M. and Swamy, K. B., "Microelectronic materials, microfabrication processes, micromechanical structural configuration based stiffness evaluation in MEMs: A review," Microelectron. Eng. **263**, 111854 (2022).
[235]Mao, S., Gao, D., Liu, W., Wei, H., and Lin, J.-M., "Imitation of drug metabolism in human liver and cytotoxicity assay using a microfluidic device coupled to mass spectrometric detection," Lab Chip **12**, 219–226 (2012).
[236]Mao, S., Zhang, J., Li, H., and Lin, J.-M., "Strategy for signaling molecule detection by using an integrated microfluidic device coupled with mass spectrometry to study cell-to-cell communication," Anal. Chem. **85**(2), 868–876 (2013).
[237]Maoz, B. M., Herland, A., Henry, O. Y. F., Leineweber, W. D., Yadid, M., Doyle, J., Mannix, R., Kujala, V. J., FitzGerald, E. A., Parker, K. K., and Ingber, D. E., "Organs-on-chips with combined multi-electrode array and transepithelial electrical resistance measurement capabilities," Lab Chip **17**, 2294–2302 (2017).
[238]Marasco, C. C., Enders, J. R., Seale, K. T., McLean, J. A., and Wikswo, J. P., "Real-time cellular exometabolome analysis with a microfluidic-mass spectrometry platform," PLoS One **10**(2), e0117685 (2015).
[239]Marrero, D., Guimera, A., Maes, L., Villa, R., Alvarez, M., and Illa, X., "Organ-on-a-chip with integrated semitransparent organic electrodes for barrier function monitoring," Lab Chip **23**, 1825–1834 (2023).
[240]Marsano, A., Conficconi, C., Lemme, M., Occhetta, P., Gaudiello, E., Votta, E., Cerino, G., Redaelli, A., and Rasponi, M., "Beating heart on a chip: A novel microfluidic platform to generate functional 3D cardiac microtissues," Lab Chip **16**, 599–610 (2016).
[241]Mcdonald, H., Saraf, A., Sadygov, R., Clark, J., Tasto, J., Gould, K., Wolters, D., Washburn, M., Weiss, A., Clark, J., and Yates, J., "Shotgun identification of protein modifications from protein complexes and lens tissue," Proc. Natl. Acad. Sci. U. S. A. **99**, 7900–7905 (2002).
[242]McLeod, M. A., Wilusz, R. E., and Guilak, F., "Depth-dependent anisotropy of the micromechanical properties of the extracellular and pericellular matrices of articular cartilage evaluated via atomic force microscopy," J. Biomech. **46**(3), 586–592 (2013).
[243]Meehan, R., Regan, E., Hoffman, E., Wolf, M., Gill, M., Crooks, J., Parmar, P., Scheuring, R., Hill, J., Pacheco, K., and Knight, V., "Synovial fluid cytokines, chemokines and MMP levels in osteoarthritis patients with knee pain display a profile similar to many rheumatoid arthritis patients," J. Clin. Med. **10**, 5027 (2021).
[244]Mermoud, Y., Felder, M., Stucki, J., Stucki, A., and Guenat, O., "Microimpedance tomography system to monitor cell activity and membrane movements in a breathing lung-on-chip," Sens. Actuators, B **255**, 3647 (2018).
[245]Miao, X., Yan, L., Wu, Y., and Liu, P. Q., "High-sensitivity nanophotonic sensors with passive trapping of analyte molecules in hot spots," *Light: Sci. Appl.* **10**(1), 5 (2021).
[246]Michalzik, M., Wendler, J., Rabe, J., Büttgenbach, S., and Bilitewski, U., "Development and application of a miniaturised quartz crystal microbalance (QCM) as immunosensor for bone morphogenetic protein-2," Sens. Actuators, B **105**(2), 508–515 (2005).
[247]Gilbert, M., Livingston, R., Felberg, J., and Bishop, J. J., "Multiplex single molecule counting technology used to generate interleukin 4, interleukin 6, and interleukin 10 reference limits," Anal. Biochem. **503**, 11–20 (2016).
[248]Miller, R. J., Malfait, A.-M., and Miller, R. E., "The innate immune response as a mediator of osteoarthritis pain," Osteoarthritis Cartilage **28**(5), 562–571 (2020).
[249]Miosge, N., Hartmann, M., Maelicke, C., and Herken, R., "Expression of collagen type I and type II in consecutive stages of human osteoarthritis," Histochem. Cell Biol. **122**, 229–236 (2004).
[250]Mirazi, H. and Wood, S. T., "Microfluidic chip-based co-culture system for modeling human joint inflammation in osteoarthritis research," Front. Pharmacol. **16**, 1579228 (2025).
[251]Misun, P. M., Rothe, J., Schmid, Y. R. F., Hierlemann, A., and Frey, O., "Multi-analyte biosensor interface for real-time monitoring of 3D microtissue spheroids in hanging-drop networks," Microsyst. Nanoeng. **2**(1), 16022 (2016).
[252]Mobed, A., Dolati, S., Shakouri, S. K., Eftekharsadat, B., and Izadseresht, B., "Recent advances in biosensors for detection of osteoarthritis and rheumatoid arthritis biomarkers," Sens. Actuators, A **331**, 112975 (2021).
[253]Mok, S., Al Habyan, S., Ledoux, C., Lee, W., MacDonald, K., Mccaffrey, L., and Moraes, C., "Mapping cellular-scale internal mechanics in 3D tissues with thermally responsive hydrogel probes," Nat. Commun. **11**, 4757 (2020).
[254]Molnar, V., Matišić, V., Kodvanj, I., Bjelica, R., Jelec, Z., Hudetz, D., Rod, E., Cukelj, F., Vrdoljak, T., Vidović, D., Starešinić, M., Sabalic, S., Dobričić, B., Petrović, T., Antičević, D., Borić, I., Kosir, R., Zmrzljak, U. P., and Primorac, D., "Cytokines and chemokines involved in osteoarthritis pathogenesis," Int. J. Mol. Sci. **22**, 9208 (2021).
[255]Mondadori, C., Palombella, S., Salehi, S., Talò, G., Visone, R., Rasponi, M., Redaelli, A., Sansone, V., Moretti, M., and Lopa, S., "Recapitulating monocyte extravasation to the synovium in an organotypic microfluidic model of the articular joint," Biofabrication **13**(4), 045001 (2021).
[256]Morales, I. A., Boghdady, C.-M., Campbell, B. E., and Moraes, C., "Integrating mechanical sensor readouts into organ-on-a-chip platforms," Front. Bioeng. Biotechnol. **10**, 1060895 (2022).
[257]Morales, M. A. and Halpern, J. M., "Guide to selecting a biorecognition element for biosensors," Bioconjugate Chem. **29**(10), 3231–3239 (2018).
[258]Shaegh, S. A. M., De Ferrari, F., Zhang, Y. S., Nabavinia, M., Mohammad, N., Ryan, J., Pourmand, A., Laukaitis, E., Sadeghian, R. B., Nadhman, A., Shin, S., Nezhad, A., and Dokmeci, M., "A microfluidic optical platform for real-time monitoring of ph and oxygen in microfluidic bioreactors and organ-on-chip devices," Biomicrofluidics **10**, 044111 (2016).
[259]Moy, J., Li, Z., Liu, F.-W., Loeza-Alcocer, E., Hartung, J., Nagarajan, V., Cho, S. K., Bunnell, B., Goodman, S., Weber, D., Lin, H., and Gold, M., "Modeling joint pain on a chip: Integrating sensory neurons in the microjoint to model osteoarthritis," J. Pain **22**(5), 583 (2021).
[260]Moyer, J., Abraham, A., and Donahue, T., "Nanoindentation of human meniscal surfaces," J. Biomech. **45**, 2230–2235 (2012).
[261]Müller, B., Sulzer, P., Walch, M., Zirath, H., Buryška, T., Rothbauer, M., Ertl, P., and Mayr, T., "Measurement of respiration and acidification rates of mammalian cells in thermoplastic microfluidic devices," Sens. Actuators, B **334**, 129664 (2021).
[262]Müller, J., Ballini, M., Livi, P., Chen, Y., Radivojevic, M., Shadmani, A., Viswam, V., Jones, I. L., Fiscella, M., Diggelmann, R., Stettler, A., Frey, U., Bakkum, D. J., and Hierlemann, A., "High-resolution CMOS MEA platform to study neurons at subcellular, cellular, and network levels," Lab Chip **15**(13), 2767–2780 (2015).
[263]Muneer, G., Gebreyesus, S. T., Chen, C.-S., Lee, T.-T., Yu, F., Lin, C.-A., Hsieh, M.-S., Nesvizhskii, A. I., Ho, C.-C., Yu, S.-L., Tu, H.-L., and Chen, Y.-J., "Mapping nanoscale-to-single-cell phosphoproteomic landscape by chip-DIA," Adv. Sci. **12**, 2402421 (2025).
[264]Nabovati, G., Ghafar-Zadeh, E., Letourneau, A., and Sawan, M., "Smart cell culture monitoring and drug test platform using CMOS capacitive sensor array," IEEE Trans. Biomed. Eng. **66**(4), 1094–1104 (2019).
[265]Neto, E., Leitão, L., Mateus, J. C., Sousa, D. M., Alves, C. J., Aroso, M., Monteiro, A. C., Conceição, F., Oreffo, R. O. C., West, J., Aguiar, P., and Lamghari, M., "Osteoclast-derived extracellular vesicles are implicated in

sensory neurons sprouting through the activation of epidermal growth factor signaling," Cell Biosci. **12**(1), 127–144 (2022).
[266]Neto, E., Monteiro, A. C., Leite Pereira, C., Simões, M., Conde, J. P., Chu, V., Sarmento, B., and Lamghari, M., "Micropathological chip modeling the neurovascular unit response to inflammatory bone condition," Adv. Healthcare Mater. **11**(11), 2102305 (2022).
[267]Nguyen, T. H., Pei, R., Stojanovic, M., and Lin, Q., "Demonstration and characterization of biomolecular enrichment on microfluidic aptamer-functionalized surfaces," Sens. Actuators, B **155**(1), 58–66 (2011).
[268]Nia, H. T., Bozchalooi, I. S., Li, Y., Han, L., Hung, H.-H., Frank, E., Youcef-Toumi, K., Ortiz, C., and Grodzinsky, A., "High-bandwidth AFM-based rheology reveals that cartilage is most sensitive to high loading rates at early stages of impairment," Biophys. J. **104**(7), 1529–1537 (2013).
[269]Nordström, M., Wingren, C., Rose, C., Bjartell, A., Becker, C., Lilja, H., and Borrebaeck, C., "Identification of plasma protein profiles associated with risk groups of prostate cancer patients," Proteomics Clin. Appl. **8**, 951 (2014).
[270]Occhetta, P., Isu, G., Lemme, M., Conficconi, C., Oertle, P., Räz, C., Visone, R., Cerino, G., Plodinec, M., Rasponi, M., and Marsano, A., "A three-dimensional in vitro dynamic micro-tissue model of cardiac scar formation," Integr. Biol. **10**, 174–183 (2018).
[271]Occhetta, P., Mainardi, A., Votta, E., Vallmajo-Martin, Q., Ehrbar, M., Martin, I., Barbero, A., and Rasponi, M., "Hyperphysiological compression of articular cartilage induces an osteoarthritic phenotype in a cartilage-on-a-chip model," Nat. Biomed. Eng. **3**(7), 545–557 (2019).
[272]Ochoa, D., Jarnuczak, A., Vieitez, C., Gehre, M., Soucheray, M., Mateus, A., Kleefeldt, A. A., Hill, A., Garcia-Alonso, L., Stein, F., Krogan, N., Savitski, M., Swaney, D., Vizcaino, J., Noh, K.-M., and Beltrao, P., "The functional landscape of the human phosphoproteome," Nat. Biotechnol. **38**, 365–369 (2020).
[273]Ohlsson, G., Axelsson, P., Henry, J., Petronis, S., Svedhem, S., and Kasemo, B., "A miniaturized flow reaction chamber for use in combination with QCM-D sensing," Microfluid. Nanofluid. **9**, 705–716 (2010).
[274]Oleaga, C., Riu, A., Rothemund, S., Lavado, A., McAleer, C. W., Long, C. J., Persaud, K., Narasimhan, N. S., Tran, M., Roles, J., Carmona-Moran, C. A., Sasserath, T., Elbrecht, D. H., Kumanchik, L., Bridges, L. R., Martin, C., Schnepper, M. T., Ekman, G., Jackson, M., Wang, Y. I., Note, R., Langer, J., Teissier, S., and Hickman, J. J., "Investigation of the effect of hepatic metabolism on off-target cardiotoxicity in a multi-organ human-on-a-chip system," Biomaterials **182**, 176–190 (2018).
[275]Ona, T. and Shibata, J., "Advanced dynamic monitoring of cellular status using label-free and non-invasive cell-based sensing technology for the prediction of anticancer drug efficacy," Anal. Bioanal. Chem. **398**(6), 2505–2533 (2010).
[276]Oropesa-Nuñez, R., Zardán Gómez de la Torre, T., Stopfel, H., Svedlindh, P., Strömberg, M., and Gunnarsson, K., "Insights into the formation of DNA–magnetic nanoparticle hybrid structures: Correlations between morphological characterization and output from magnetic biosensor measurements," ACS Sens. **5**(11), 3510–3519 (2020).
[277]Orte, A., Alvarez-Pez, J. M., and Ruedas-Rama, M. J., "Fluorescence lifetime imaging microscopy for the detection of intracellular pH with quantum dot nanosensors," ACS Nano **7**(7), 6387–6395 (2013).
[278]Ortega, M. A., Rodríguez-Comas, J., Yavas, O., Velasco-Mallorquí, F., Balaguer-Trias, J., Parra, V., Novials, A., Servitja, J. M., Quidant, R., and Ramón-Azcón, J., "In situ LSPR sensing of secreted insulin in organ-on-chip," Biosensors **11**(5), 138 (2021).
[279]Otieno, B. A., Krause, C. E., Latus, A., Chikkaveeraiah, B. V., Faria, R. C., and Rusling, J. F., "On-line protein capture on magnetic beads for ultrasensitive microfluidic immunoassays of cancer biomarkers," Biosens. Bioelectron. **53**, 268–274 (2014).
[280]Owens, N. A., Laurentius, L. B., Porter, M. D., Li, Q., Wang, S., and Chatterjee, D., "Handheld Raman spectrometer instrumentation for quantitative tuberculosis biomarker detection: A performance assessment for point-of-need infectious disease diagnostics," Appl. Spectrosc. **72**(7), 1104–1115 (2018).
[281]Oyen, M., "Nanoindentation of biological and biomimetic materials," Exp. Technol. **37**, 73–87 (2013).
[282]Paggi, C. A., Venzac, B., Karperien, M., Leijten, J. C. H., and Le Gac, S., "Monolithic microfluidic platform for exerting gradients of compression on cell-laden hydrogels, and application to a model of the articular cartilage," Sens. Actuators, B **315**, 127917 (2020).
[283]Paggi, C. A., Teixeira, L. M., Le Gac, S., and Karperien, M., "Joint-on-chip platforms: Entering a new era of in vitro models for arthritis," Nat. Rev. Rheumatol. **18**, 217–231 (2022).
[284]Palma, C., Aterini, B., Ferrari, E., Mangione, M., Romeo, M., Nezi, L., Lopa, S., Manzo, T., Occhetta, P., and Rasponi, M., "A compartmentalized microfluidic platform to investigate immune cells cross-talk in rheumatoid arthritis," Biofabrication **17**, 015008 (2025).
[285]Palma, C., Piazza, S., Visone, R., Ringom, R., Björklund, U., Bermejo Gómez, A., Rasponi, M., and Occhetta, P., "An advanced mechanically active osteoarthritis-on-chip model to test injectable therapeutic formulations: The syn321 case study," Adv. Healthcare Mater. **13**(32), 2401187 (2024).
[286]Palma, C., Salehi, S., Polidoro, M. A., Moretti, M., Rasponi, M., Lopa, S., and Occhetta, P., "A compartmentalized joint-on-chip (JOC) model to unravel the contribution of cartilage and synovium to osteoarthritis pathogenesis," Adv. Sci. **12**, e00374 (2025).
[287]Pan, Y., Hu, N., Wei, X., Gong, L., Zhang, B., Wan, H., and Wang, P., "3D cell-based biosensor for cell viability and drug assessment by 3D electric cell/matrigel-substrate impedance sensing," Biosens. Bioelectron. **130**, 344 (2019).
[288]Pappu, M. H., Rahman, A., and Mollah, M. A., "An H-shaped exposed core surface plasmon resonance sensor and detection of cancer cells," Plasmonics **19**(5), 2795–2811 (2024).
[289]Patel, J., Wise, B., Bonnevie, E., and Mauck, R., "A systematic review and guide to mechanical testing for articular cartilage tissue engineering," Tissue Eng., Part C **25**, 593 (2019).
[290]Patel, M. T. and Goldberg Oppenheimer, P. G., "Advancements in cancer diagnostics: Integrating surface-enhanced Raman spectroscopy and microptofluidics for precision and versatility," Appl. Spectrosc. Rev. **60**(6), 511–554 (2025).
[291]Perrier, R., Pirog, A., Jaffredo, M., Gaitan, J., Catargi, B., Renaud, S., Raoux, M., and Lang, J., "Bioelectronic organ-based sensor for microfluidic real-time analysis of the demand in insulin," Biosens. Bioelectron. **117**, 253–259 (2018).
[292]Petrovsky, A., Schellenberger, E., Josephson, L., Weissleder, R., and Bogdanov, A., "Near-infrared fluorescent imaging of tumor apoptosis," Cancer Res. **63**(8), 1936–1942 (2003).
[293]Petta, D., D'Arrigo, D., Salehi, S., Talò, G., Bonetti, L., Vanoni, M., Deabate, L., De Nardo, L., Dubini, G., Candrian, C., Moretti, M., Lopa, S., and Arrigoni, C., "A personalized osteoarthritic joint-on-a-chip as a screening platform for biological treatments," Mater. Today Bio **26**, 101072 (2024).
[294]Pettinato, G., Coughlan, M. F., Zhang, X., Chen, L., Khan, U., Glyavina, M., Sheil, C. J., Upputuri, P. K., Zakharov, Y. N., Vitkin, E., D'Assoro, A. B., Fisher, R. A., Itzkan, I., Zhang, L., Qiu, L., and Perelman, L. T., "Spectroscopic label-free microscopy of changes in live cell chromatin and biochemical composition in transplantable organoids," Sci. Adv. **7**(34), eabj2800 (2021).
[295]Pi, P., Zeng, L., Zeng, Z., Zong, K., Han, B., Bai, X., and Wang, Y., "The role of targeting glucose metabolism in chondrocytes in the pathogenesis and therapeutic mechanisms of osteoarthritis: A narrative review," Front. Endocrinol. **15**, 1319827 (2024).
[296]Picollet-D'hahan, N., Zuchowska, A., Lemeunier, I., and Le Gac, S., "Multiorgan-on-a-chip: A systemic approach to model and decipher inter-organ communication," Trends Biotechnol. **39**(8), 788–810 (2021).
[297]Pierce, M., Stuart, J., Pungor, A., Dryden, P., and Hlady, V., "Adhesion force measurements using an atomic force microscope upgraded with a linear position sensitive detector," Langmuir **10**(9), 3217–3221 (1994).
[298]Piluso, S., Li, Y., Abinzano, F., Levato, R., Moreira Teixeira, L., Karperien, M., Leijten, J., van Weeren, P., and Malda, J., "Mimicking the articular joint with in vitro models," Trends Biotechnol. **37**, 1063 (2019).
[299]Pinto, I., Caneira, C., Soares, R., Madaboosi, N., Aires-Barros, M., Azevedo, A., and Chu, V., "The application of microbeads to microfluidic systems for enhanced detection and purification of biomolecules," Methods **116**, 112 (2017).
[300]Poillot, P., Le Maitre, C. L., and Huyghe, J. M., "The strain-generated electrical potential in cartilaginous tissues: A role for piezoelectricity," Biophys. Rev. **13**, 91–100 (2021).
[301]Polacheck, W. and Chen, C., "Measuring cell-generated forces: A guide to the available tools," Nat. Methods **13**, 415–423 (2016).

[302]Poudineh, M., Maikawa, C., Ma, E. Y., Pan, J., Mamerow, D., Hang, Y., Baker, S., Beirami, A., Yoshikawa, A., Eisenstein, M., Kim, S., Vuckovic, J., Appel, E., and Soh, H., "A fluorescence sandwich immunoassay for the real-time continuous detection of glucose and insulin in live animals," Nat. Biomed. Eng. **5**, 53–11 (2021).
[303]Power, L. J., Fasolato, C., Barbero, A., Wendt, D. J., Wixmerten, A., Martin, I., and Asnaghi, M. A., "Sensing tissue engineered cartilage quality with Raman spectroscopy and statistical learning for the development of advanced characterization assays," Biosens. Bioelectron. **166**, 112467 (2020).
[304]Preisegger, M. A., Makarcyzk, M., Zhou, C., Shemesh, O., Lin, H., and Gold, M., "Modeling osteoarthritis pain with a tissue chip," J. Pain **25**(4 suppl), 17 (2024).
[305]Proestaki, M., Ogren, A., Burkel, B., and Notbohm, J., "Modulus of fibrous collagen at the length scale of a cell," Exp. Mech. **59**(9), 1323–1334 (2019).
[306]Pui, T. S., Kongsuphol, P., Arya, S., and Bansal, T., "Detection of tumor necrosis factor (TNF-α) in cell culture medium with label free electrochemical impedance spectroscopy," Sens. Actuators, B **181**, 494–500 (2013).
[307]Qin, L., Liu, W., Cao, H., and Xiao, G., "Molecular mechanosensors in osteocytes," Bone Res. **8**(1), 23–46 (2020).
[308]Qin, Y., Li, J.-X., Cai, W., Fan, W.-T., Duan, B., Zhao, Y., Huang, G.-Y., Huang, W.-H., and Liu, Y.-L., "A cartilage-on-a-chip for recapitulating cell microenvironment and real-time nitric oxide monitoring," Device **2**(6), 100410 (2024).
[309]Qiu, Y., Liu, X., Zhu, Y., Jiang, D., Li, F., Yu, W., Wan, H., Zhuang, L., Pan, Y., and Wang, P., "Vertical impedance electrode array for spatiotemporal dynamics monitoring of 3D cells under drug diffusion effect," iScience **26**(12), 107962 (2023).
[310]Quirós-Solano, W. F., Gaio, N., Silvestri, C., Pandraud, G., Dekker, R., and Sarro, P. M., "Metal and polymeric strain gauges for Si-based, monolithically fabricated organs-on-chips," Micromachines **10**(8), 536 (2019).
[311]Rainu, S. K. and Singh, N., "Dual-sensitive fluorescent nanoprobes for simultaneously monitoring in situ changes in pH and matrix metalloproteinase expression in stiffness-tunable three-dimensional in vitro scaffolds," ACS Appl. Mater. Interfaces **16**, 12175 (2024).
[312]Rechendorff, K., Hovgaard, M. B., Foss, M., and Besenbacher, F., "Influence of surface roughness on quartz crystal microbalance measurements in liquids," J. Appl. Phys. **101**(11), 114502 (2007).
[313]Rennert, K., Steinborn, S., Gröger, M., Ungerböck, B., Jank, A.-M., Ehgartner, J., Nietzsche, S., Dinger, J., Kiehntopf, M., Funke, H., Peters, F. T., Lupp, A., Gärtner, C., Mayr, T., Bauer, M., Huber, O., and Mosig, A. S., "A microfluidically perfused three dimensional human liver model," Biomaterials **71**, 119–131 (2015).
[314]Reyes-San-Martin, C., Elias, A., Hamoh, T., Sharmin, R., Zhang, Y., Hermann, A., Woudstra, W., Mzyk, A., and Schirhagl, R., "Towards using fluorescent nanodiamonds for studying cell migration," Cancer Nanotechnol. **15**,44 (2024).
[315]Rezapour Sarabi, M., Jiang, N., Ozturk, E., Yetisen, A. K., and Tasoglu, S., "Biomedical optical fibers," Lab Chip **21**, 627–640 (2021).
[316]Riahi, R., Shaegh, S. A. M., Ghaderi, M., Zhang, Y. S., Shin, S., Aleman, J., Massa, S., Kim, D., and Dokmeci, M., "Automated microfluidic platform of bead-based electrochemical immunosensor integrated with bioreactor for continual monitoring of cell secreted biomarkers," Sci. Rep. **6**, 24598 (2016).
[317]Ricciardi, C., Canavese, G., Castagna, R., Ferrante, I., Ricci, A., Marasso, S. L., Napione, L., and Bussolino, F., "Integration of microfluidic and cantilever technology for biosensing application in liquid environment," Biosens. Bioelectron. **26**(4), 1565–1570 (2010).
[318]Ronkainen, N. J., Halsall, H. B., and Heineman, W. R., "Electrochemical biosensors," Chem. Soc. Rev. **39**(5), 1747–1763 (2010).
[319]Rosser, J., Bachmann, B., Jordan, C., Ribitsch, I., Haltmayer, E., Gueltekin, S., Junttila, S., Galik, B., Gyenesei, A., Haddadi, B., Harasek, M., Egerbacher, M., and Ertl, P., "Microfluidic nutrient gradient–based three-dimensional chondrocyte culture-on-a-chip as an in vitro equine arthritis model," Mater. Today Bio **4**, 100023 (2019).
[320]Rothbauer, M., Höll, G., Eilenberger, C., Kratz, S. R. A., Farooq, B., Schuller, P., Olmos Calvo, I., Byrne, R. A., Meyer, B., Niederreiter, B., Küpcü, S., Sevelda, F., Holinka, J., Hayden, O., Tedde, S. F., Kiener, H. P., and Ertl, P., "Monitoring tissue-level remodelling during inflammatory arthritis using a three-dimensional synovium-on-a-chip with non-invasive light scattering biosensing," Lab Chip **20**, 1461–1471 (2020).
[321]Rothbauer, M., Byrne, R. A., Schobesberger, S., Olmos Calvo, I., Fischer, A., Reihs, E. I., Spitz, S., Bachmann, B., Sevelda, F., Holinka, J., Holnthoner, W., Redl, H., Toegel, S., Windhager, R., Kiener, H. P., and Ertl, P., "Establishment of a human three-dimensional chip-based chondro-synovial coculture joint model for reciprocal cross talk studies in arthritis research," Lab Chip **21**, 4128–4143 (2021).
[322]Rothbauer, M., Reihs, E. I., Fischer, A., Windhager, R., Jenner, F., and Toegel, S., "A progress report and roadmap for microphysiological systems and organ-on-a-chip technologies to be more predictive models in human (knee) osteoarthritis," Front. Bioeng. Biotechnol. **10**, 886360 (2022).
[323]Rothbauer, M., Strauss, J., Reihs, E. I., Heidenberger, J., Alphonsus, J., Gowers, S., Chen, Y.-C., McLeod, J., Toegel, S., Ertl, P., Windhager, R., Boutelle, M., and O'Hare, D., "Integration of glucose and lactate biosensors into human cartilage-on-a-chip models for long-term monitoring of metabolic shifts in osteoarthritis," Sens. Actuators, B **427**, 137123 (2025).
[324]Rousseau, J.-C., Chapurlat, R., and Garnero, P., "Soluble biological markers in osteoarthritis," Ther. Adv. Musculoskeletal **13**, 1759720X211040300 (2021).
[325]Sala, L., Ward-van Oostwaard, D., Tertoolen, L. G. J., Mummery, C. L., and Bellin, M., "Electrophysiological analysis of human pluripotent stem cell-derived cardiomyocytes (HPSC-CMS) using multi-electrode arrays (MEAs)," JoVE **123**, e55587 (2017).
[326]Saleh, S., Alkalamouni, H., Antar, K., Rahme, J., Kazan, M., Karam, P., Muthuswamy, J., Zaraket, H., and Khraiche, M. L., "Quartz crystal microbalance-based biosensor for rapid and ultrasensitive SARS-CoV-2 detection," J. Pharm. Biomed. Anal. Open **5**, 100071 (2025).
[327]Salehi, S., Brambilla, S., Rasponi, M., Lopa, S., and Moretti, M., "Development of a microfluidic vascularized osteochondral model as a drug testing platform for osteoarthritis," Adv. Healthcare Mater. **13**(31), 2402350 (2024).
[328]Sandanaraj, B. S., Gremlich, H.-U., Kneuer, R., Dawson, J., and Wacha, S., "Fluorescent nanoprobes as a biomarker for increased vascular permeability: Implications in diagnosis and treatment of cancer and inflammation," Bioconjugate Chem. **21**(1), 93–101 (2010).
[329]Sanna, R., Gary, F. S., and David, B. L., "Measurement of inflammatory biomarkers in synovial tissue extracts by enzyme-linked immunosorbent assay," Clin. Vaccine Immunol. **10**(6), 1002–1010 (2003).
[330]Santangelo, M. F., Libertino, S., Turner, A. P. F., Filippini, D., and Mak, W. C., "Integrating printed microfluidics with silicon photomultipliers for miniaturised and highly sensitive ATP bioluminescence detection," Biosens. Bioelectron. **99**, 464–470 (2018).
[331]Santbergen, M. J. C., van der Zande, M., Bouwmeester, H., and Nielen, M. W. F., "Online and in situ analysis of organs-on-a-chip," TrAC, Trends Anal. Chem. **115**, 138–146 (2019).
[332]Sato, K., Tokeshi, M., Kimura, H., and Kitamori, T., "Determination of carcinoembryonic antigen in human sera by integrated bead-bed immunoassay in a microchip for cancer diagnosis," Anal. Chem. **73**, 1213–1218 (2001).
[333]Schellberg, B. G., Koppes, R. A., and Koppes, A. N., "Recent advances in integrated organ-chip sensing toward robust and user-friendly systems," J. Biomed. Mater. Res. **113**(2), e37876 (2025).
[334]Schmid, Y. R. F., Bürgel, S. C., Misun, P. M., Hierlemann, A., and Frey, O., "Electrical impedance spectroscopy for microtissue spheroid analysis in hanging-drop networks," ACS Sens. **1**(8), 1028–1035 (2016).
[335]Schymanski, E. L., Jeon, J., Gulde, R., Fenner, K., Ruff, M., Singer, H. P., and Hollender, J., "Identifying small molecules via high resolution mass spectrometry: Communicating confidence," Environ. Sci. Technol. **48**(4), 2097–2098 (2014).
[336]Segarra-Queralt, M., Neidlin, M., Tío, L., Monfort, J., Monllau, J., González Ballester, M. Á., Alexopoulos, L., Piella, G., and Noailly, J., "Regulatory network-based model to simulate the biochemical regulation of chondrocytes in healthy and osteoarthritic environments," Sci. Rep. **12**, 3856 (2022).
[337]Selvam, S. P., Chinnadayyala, S. R., and Cho, S., "Electrochemical nanobiosensor for early detection of rheumatoid arthritis biomarker: Anti-cyclic citrullinated peptide antibodies based on polyaniline (PANI)/MoS_2-modified screen-printed electrode with PANI-Au nanomatrix-based signal amplification," Sens. Actuators, B **333**, 129570 (2021).

[338]Seo, J.-W., Jo, S.-H., Kim, S.-H., Choi, B.-H., Cho, H., Yoo, J., and Park, S.-H., "Application of cartilage extracellular matrix to enhance therapeutic efficacy of methotrexate," Tissue Eng. Regen. Med. **21**, 209 (2024).
[339]Lee, S.-Y., Kim, D.-S., Kim, E.-S., and Lee, D.-W., "Nano-textured polyimide cantilever for enhancing the contractile behavior of cardiomyocytes and its application to cardiac toxicity screening," Sens. Actuators, B **301**, 126995 (2019).
[340]Seong, G. H. and Crooks, R. M., "Efficient mixing and reactions within microfluidic channels using microbead-supported catalysts," J. Am. Chem. Soc. **124**(45), 13360–13361 (2002).
[341]Serra, J., Mateus, J. C., Cardoso, S., Ventura, J., Aguiar, P., and Leitao, D. C., "Stress-actuated partially flexible microelectrode arrays for activity recording in 3D neuronal cultures," Lab Chip **25**, 5574 (2025).
[342]Servais, B., Mahmoudi, N., Gautam, V., Tong, W., Ibbotson, M. R., Nisbet, D. R., and Collins, D., "Engineering brain-on-a-chip platforms," Nat. Rev. Bioeng. **2**(8), 691–709 (2024).
[343]Sha, Z., Ling, T., Yang, W., Xie, H., Wang, C., and Sun, S., "Microfluidic synthesis and accurate immobilization of low-density QD-encoded magnetic microbeads for multiplex immunoassay," J. Mater. Chem. B **12**, 11230 (2024).
[344]Shabani, E., Abdekhodaie, M. J., Mousavi, S. A., and Taghipour, F., "ZnO nanoparticle/nanorod-based label-free electrochemical immunoassay for rapid detection of MMP-9 biomarker," Biochem. Eng. J. **164**, 107772 (2020).
[345]Shah, P., Fritz, J. V., Glaab, E., Desai, M. S., Greenhalgh, K., Frachet, A., Niegowska, M., Estes, M., Jäger, C., Seguin-Devaux, C., Zenhausern, F., and Wilmes, P., "A microfluidics-based in vitro model of the gastrointestinal human–microbe interface," Nat. Commun. **7**, 11535 (2016).
[346]Shao, P., Dong, D., Huang, Y., Wang, Y., Pan, L., Zhu, Q., Wu, Z., Jiang, F., and Wei, W., "Aptamer-based functionalized sers biosensor for rapid and ultrasensitive detection of gastric cancer-related biomarkers," Int. J. Nanomed. **18**, 7523–7532 (2023).
[347]Shehab, M., Ebrahim, S., and Soliman, M., "Graphene quantum dots prepared from glucose as optical sensor for glucose," J. Lumin. **184**, 110–116 (2017).
[348]Shen, C.-Y., Chiu, Y.-C., Huang, K.-N., Fu, S.-L., and Hwang, R.-C., "Application of a flow type quartz crystal microbalance immunosensor for detection of cartilage oligomeric matrix protein and α1-antitrypsin," in *2nd International Symposium on Instrumentation and Measurement, Sensor Network and Automation (IMSNA)* (IEEE, 2013), pp. 712–715.
[349]Shen, C.-Y., Wu, C.-L., Lin, Y.-M., and Hwang, R.-C., "Sensitive and label-free detection of cartilage oligomeric matrix protein on quartz crystal microbalance," Int. J. New Technol. Res. **2**(3), 45–58 (2016).
[350]Shevchenko, Y., Camci-Unal, G., Cuttica, D. F., Dokmeci, M. R., Albert, J., and Khademhosseini, A., "Surface plasmon resonance fiber sensor for real-time and label-free monitoring of cellular behavior," Biosens. Bioelectron. **56**, 359–367 (2014).
[351]Shi, J., Tong, L., Tong, W., Chen, H., Lan, M., Sun, X., and Zhu, Y., "Current progress in long-term and continuous cell metabolite detection using microfluidics," TrAC, Trends Anal. Chem. **117**, 263–279 (2019).
[352]Shin, H., Jeong, S., Lee, J.-H., Sun, W., Choi, N., and Cho, I.-J., "3D high-density microelectrode array with optical stimulation and drug delivery for investigating neural circuit dynamics," Nat. Commun. **12**(1), 492 (2021).
[353]Simmons, C., Sim, J. Y., Baechtold, P., Gonzalez, A., Chung, C., Borghi, N., and Pruitt, B., "Integrated strain array for cellular mechanobiology studies," J. Micromech. Microeng. **21**, 054016–054025 (2011).
[354]Sitkov, N., Ryabko, A., Moshnikov, V., Aleshin, A., Kaplun, D., and Zimina, T., "Hybrid impedimetric biosensors for express protein markers detection," Micromachines **15**(2), 181 (2024).
[355]Soenen, S., Demeester, J., De Smedt, S., and Braeckmans, K., "The cytotoxic effects of polymer-coated quantum dots and restrictions for live cell applications," Biomaterials **33**, 4882–4888 (2012).
[356]Son, K. J., Gheibi, P., Stybayeva, G., Rahimian, A., and Revzin, A., "Detecting cell-secreted growth factors in microfluidic devices using bead-based biosensors," Microsyst. Nanoeng. **3**, 17025 (2017).
[357]Song, H., Kim, M., Kim, K., Lee, I., Shin, S. H., Lee, J., and Kim, J., "Synovial fluid of patients with rheumatoid arthritis induces alpha-smooth muscle actin in human adipose tissue-derived mesenchymal stem cells through a TGF-beta1-dependent mechanism," Exp. Mol. Med. **42**, 565–573 (2010).
[358]Song, J. H., Lee, S.-M., and Yoo, K.-H., "Label-free and real-time monitoring of human mesenchymal stem cell differentiation in 2D and 3D cell culture systems using impedance cell sensors," RSC Adv. **8**, 31246–31254 (2018).
[359]Song, S. Y., Han, Y. D., Hong, S. Y., Kim, K., Yang, S. S., Min, B.-H., and Yoon, H. C., "Chip-based cartilage oligomeric matrix protein detection in serum and synovial fluid for osteoarthritis diagnosis," Anal. Biochem. **420**(2), 139–146 (2012).
[360]Sønstevold, L., Czerkies, M., Escobedo-Cousin, E., Blonski, S., and Vereshchagina, E., "Application of polymethylpentene, an oxygen permeable thermoplastic, for long-term on-a-chip cell culture and organ-on-a-chip devices," Micromachines **14**, 532 (2023).
[361]Soundaram Jeevarathinam, A., Saleem, W., Martin, N., Hu, C., and McShane, M. J., "NIR luminescent oxygen-sensing nanoparticles for continuous glucose and lactate monitoring," Biosensors **13**(1), 141 (2023).
[362]Srbova, L., Arasalo, O., Lehtonen, A., and Pokki, J., "Measuring mechanical cues for modeling the stromal matrix in 3 cell cultures," Soft Matter **20**, 3483 (2024).
[363]Srinivasan, B., Kolli, A. R., Esch, M. B., Abaci, H. E., Shuler, M. L., and Hickman, J. J., "TEER measurement techniques for *in vitro* barrier model systems," J. Lab. Autom. **20**(2), 107–126 (2015).
[364]Staunton, J. R., Vieira, W., Fung, K. L., Lake, R., Devine, A., and Tanner, K., "Mechanical properties of the tumor stromal microenvironment probed *in vitro* and *ex vivo* by *in situ*-calibrated optical trap-based active microrheology," Cell. Mol. Bioeng. **9**, 398 (2016).
[365]Stavitskaya, A. V., Novikov, A. A., Kotelev, M. S., Kopitsyn, D. S., Rozhina, E. V., Ishmukhametov, I. R., Fakhrullin, R. F., Ivanov, E. V., Lvov, Y. M., and Vinokurov, V. A., "Fluorescence and cytotoxicity of cadmium sulfide quantum dots stabilized on clay nanotubes," Nanomaterials **8**(6), 391 (2018).
[366]Steinmetz, J., Culbreth, G., Haile, L., Rafferty, Q., Lo, J., Fukutaki, K., Cruz, J., Smith, A., Vollset, S., Brooks, P., Cross, M., Woolf, A., Hagins, H., Abbasi-Kangevari, M., Abedi, A., Ackerman, I., Amu, H., Antony, B., Arabloo, J., and Kopec, J., "Global, regional, and national burden of osteoarthritis, 1990–2020 and projections to 2050: A systematic analysis for the global burden of disease study 2021," Lancet Rheumatol. **5**, e508 (2023).
[367]Stolz, M., Gottardi, R., Raiteri, R., Miot, S., Martin, I., Imer, R., Staufer, U., Raducanu, A., Jakob, M., Baschong, W., Daniels, A. U., Friederich, N., Aszodi, A., and Aebi, U., "Early detection of aging cartilage and osteoarthritis in mice and patient samples using atomic force microscopy," Nat. Nanotechnol. **5**(11), 821 (2010).
[368]Summers, P., Lewis, B., González García, J., Porreca, R., Lim, A., Cadinu, P., Martin-Pintado, N., Mann, D., Edel, J., Vannier, J.-B., Kuimova, M., and Vilar, R., "Visualising G-quadruplex DNA dynamics in live cells by fluorescence lifetime imaging microscopy," Nat. Commun. **12**, 162 (2021).
[369]Sun, C., Lee, J. S. H., and Zhang, M., "Magnetic nanoparticles in MR imaging and drug delivery," Adv. Drug Delivery Rev. **60**(11), 1252–1265 (2008).
[370]Sun, T., Green, N. G., and Morgan, H., "Analytical and numerical modeling methods for impedance analysis of single cells on-chip," Nano **03**(01), 55–63 (2008).
[371]Tangson, J., Du, X., Grogan, J., Schrlau, M., and Bau, H., "Polymeric microbead arrays for microfluidic applications," J. Micromech. Microeng. **20**, 115017 (2010).
[372]Tentellino, C., d'Amora, M., Melikov, R., Iachetta, G., Bruno, G., Tantussi, F., Dipalo, M., and De Angelis, F., "Electrode- and label-free assessment of electrophysiological firing rates through cytochrome C monitoring via Raman spectroscopy," ACS Sens. **10**(2), 1228–1236 (2025).
[373]Tertiș, M., Ciui, B., Suciu, M., Săndulescu, R., and Cristea, C., "Label-free electrochemical aptasensor based on gold and polypyrrole nanoparticles for interleukin 6 detection," Electrochim. Acta **258**, 1208–1218 (2017).
[374]Thies, J.-W., Kuhn, P., Thürmann, B., Dübel, S., and Dietzel, A., "Microfluidic quartz-crystal-microbalance (QCM) sensors with specialized immunoassays for extended measurement range and improved reusability," Microelectron. Eng. **179**, 25 (2017).
[375]Tjell, A. Ø., Jud, B., Schaller-Ammann, R., and Mayr, T., "Optical hydrogen peroxide sensor for measurements in flow," Sens. Actuators, B **400**, 134904 (2024). https://www.sciencedirect.com/science/article/pii/S0925400523016222.
[376]Tjon, K. C. E. and Yuan, J., "Impedance characterization of silver/silver chloride micro-electrodes for bio-sensing applications," Electrochim. Acta

320, 134638 (2019). https://www.sciencedirect.com/science/article/pii/S0013468619314975.
[377]Tripathy, A., Padhan, P., Swain, N., Raghav, S. K., and Gupta, B., "Increased extracellular ATP in plasma of rheumatoid arthritis patients activates CD8+ T cells," Arch. Med. Res. **52**(4), 423–433 (2021).
[378]Vala, M., Robelek, R., Bocková, M., Wegener, J., and Homola, J., "Real-time label-free monitoring of the cellular response to osmotic stress using conventional and long-range surface plasmons," Biosens. Bioelectron. **40**(1), 417–421 (2013).
[379]Valverde, A., Serafín, V., Montero-Calle, A., González-Cortés, A., Barderas, R., Yáñez-Sedeño, P., Campuzano, S., and Pingarrón, J. M., "Carbon/inorganic hybrid nanoarchitectures as carriers for signaling elements in electrochemical immunosensors: First biosensor for the determination of the inflammatory and metastatic processes biomarker rank-ligand," ChemElectroChem **7**(3), 810–820 (2020).
[380]van Aalen, E. A., Rosier, B. J. H. M., Jansen, T., Wouters, S. F. A., Vermathen, R. T., van der Veer, H. J., Yeste Lozano, J., Mughal, S., Fernández-Costa, J. M., Ramón-Azcón, J., den Toonder, J. M. J., and Merkx, M., "Integrated bioluminescent immunoassays for high-throughput sampling and continuous monitoring of cytokines," Anal. Chem. **95**(23), 8922–8931 (2023).
[381]van der Helm, M. W., Henry, O. Y. F., Bein, A., Hamkins-Indik, T., Cronce, M. J., Leineweber, W. D., Odijk, M., van der Meer, A. D., Eijkel, J. C. T., Ingber, D. E., van den Berg, A., and Segerink, L. I., "Non-invasive sensing of transepithelial barrier function and tissue differentiation in organs-on-chips using impedance spectroscopy," Lab Chip **19**, 452–463 (2019).
[382]Visone, R., Ugolini, G. S., Cruz-Moreira, D., Marzorati, S., Piazza, S., Pesenti, E., Redaelli, A., Moretti, M., Occhetta, P., and Rasponi, M., "Micro-electrode channel guide (μECG) technology: An online method for continuous electrical recording in a human beating heart-on-chip," Biofabrication **13**, 035026 (2021).
[383]Visone, R., Lozano-Juan, F., Marzorati, S., Rivolta, M. W., Pesenti, E., Redaelli, A., Sassi, R., Rasponi, M., and Occhetta, P., "Predicting human cardiac QT alterations and pro-arrhythmic effects of compounds with a 3D beating heart-on-chip platform," Toxicol. Sci. **191**, 47–60 (2023).
[384]Vu, T. T., Song, S., Lai, H. D. N., Mai, N. L., Trinh, T. T., Do, H. T., Phu-Huynh, D., and Nguyen, A. H., "Coverage degrees of colloids on electrochemical electrodes and signal amplification for anti-citrullinated peptide antibody detection," Sens. Biosens. Res. **27**, 100322 (2020).
[385]Wade, T. and Kar-Narayan, S., "Temperature-dependent microfluidic impedance spectroscopy for non-invasive biofluid characterization," Biomicrofluidics **19**(3), 034101 (2025).
[386]Walker, N. L. and Dick, J. E., "Versatile potentiometric metabolite sensing without dioxygen interference," Biosens. Bioelectron. **201**, 113888 (2022).
[387]Wang, A., Jung, D., Lee, D., and Wang, H., "Impedance characterization and modeling of subcellular to micro-sized electrodes with varying materials and pedot: PSS coating for bioelectrical interfaces," ACS Appl. Electron. Mater. **3**(12), 5226–5239 (2021).
[388]Wang, H., Li, X., Tse, B. W.-C., Yang, H., Thorling, C. A., Liu, Y., Touraud, M., Chouane, J. B., Liu, X., Roberts, M. S., and Liang, X., "Indocyanine green-incorporating nanoparticles for cancer theranostics," Theranostics **8**(5), 1227–1242 (2018).
[389]Wang, L.-C., Wei, W.-H., Zhang, X.-W., Liu, D., Zeng, K.-W., and Tu, P.-F., "An integrated proteomics and bioinformatics approach reveals the anti-inflammatory mechanism of carnosic acid," Front. Pharmacol. **9**, 370 (2018).
[390]Wang, N., Lu, Y., Rothrauff, B., Zheng, A., Lamb, A., Yan, Y., Lipa, K., Lei, G., and Lin, H., "Mechanotransduction pathways in articular chondrocytes and the emerging role of estrogen receptor-α," Bone Res. **11**, 13 (2023).
[391]Wang, S., Bao, Y., Guan, Y., Zhang, C., Liu, H., Yang, X., Gao, L., Guo, T., and Chen, Q., "Strain distribution of repaired articular cartilage defects by tissue engineering under compression loading," J. Orthop. Surg. Res. **13**, 19 (2018).
[392]Wang, S.-H., Shen, C.-Y., Weng, T.-C., Lin, P.-H., Yang, J.-J., Chen, I.-F., Kuo, S.-M., Chang, S.-J., Tu, Y.-K., Kao, Y.-H., and Hung, C.-H., "Detection of cartilage oligomeric matrix protein using a quartz crystal microbalance," Sensors **10**(12), 11633–11643 (2010).
[393]Wang, Z., Han, D., Wang, H., Zheng, M., Xu, Y., and Zhang, H., "Organic semiconducting nanoparticles for biosensor: A review," Biosensors **13**, 494 (2023).
[394]Wang, Z. and Rothberg, L. J., "Origins of blinking in single-molecule Raman spectroscopy," J. Phys. Chem. B **109**(8), 3387–3391 (2005).
[395]Ward, M. D. and Delawski, E. J., "Radial mass sensitivity of the quartz crystal microbalance in liquid media," Anal. Chem. **63**, 886–890 (1991).
[396]Wegener, J. and Seebach, J., "Experimental tools to monitor the dynamics of endothelial barrier function: A survey of in vitro approaches," Cell Tissue Res. **355**(3), 485–514 (2014).
[397]Wei, H., Li, H., Gao, D., and Lin, J.-M., "Multi-channel microfluidic devices combined with electrospray ionization quadrupole time-of-flight mass spectrometry applied to the monitoring of glutamate release from neuronal cells," Analyst **135**, 2043–2050 (2010).
[398]Wei, H., Li, H., Mao, S., and Lin, J.-M., "Cell signaling analysis by mass spectrometry under coculture conditions on an integrated microfluidic device," Anal. Chem. **83**(24), 9306–9313 (2011).
[399]Wei, X., Hao, Y., Huang, X., Hu, Y., and Xiong, B., "Automated solid phase extraction and electrospray chip based on programmatic pneumatic microvalves," Talanta **198**, 404 (2019).
[400]Wei, Y. and Bai, L., "Recent advances in the understanding of molecular mechanisms of cartilage degeneration, synovitis and subchondral bone changes in osteoarthritis," Connect. Tissue Res. **57**(4), 245–261 (2016).
[401]Wilusz, R. E., Zauscher, S., and Guilak, F., "Micromechanical mapping of early osteoarthritic changes in the pericellular matrix of human articular cartilage," Osteoarthritis Cartilage **21**(12), 1895–1903 (2013).
[402]Wu, Y., Hu, Y., Jiang, N., Georgi, M., Yetisen, A., and Cordeiro, M., "Dual lateral flow assay using quantum nanobeads for quantitative detection of BDNF and TNF-α in tears," Lab Chip **25**, 2291–2303 (2025).
[403]Xie, L., Yan, X., and Du, Y., "An aptamer based wall-less lspr array chip for label-free and high throughput detection of biomolecules," Biosens. Bioelectron. **53**, 58–64 (2014).
[404]Xie, Z., Chen, E., Ouyang, X., Xu, X., Ma, S., Ji, F., Wu, D., Zhang, S., Zhao, Y., and Li, L., "Metabolomics and cytokine analysis for identification of severe drug-induced liver injury," J. Proteome Res. **18**(6), 2514–2524 (2019).
[405]Xu, S., Li, Z., Wang, Z., Zhai, C., Liang, W., Zhu, C., and Fan, W., "Proteomic analysis reveals GRB2 as a key regulator of periodic mechanical stress transduction in chondrocytes," Cell. Physiol. Biochem. **44**, 1509–1525 (2017).
[406]Xu, Y., Li, C., Mei, W., Guo, M., and Yang, Y., "Equivalent circuit models for a biomembrane impedance sensor and analysis of electrochemical impedance spectra based on support vector regression," Med. Biol. Eng. Comput. **57**(7), 1515–1524 (2019).
[407]Yalcin, D., Bastiaens, A. J., Frimat, J.-P., and Luttge, R., "Long-term brain-on-chip: Multielectrode array recordings in 3D neural cell cultures," J. Vac. Sci. Technol. B **39**(6), 064004 (2021).
[408]Yan, J., Hu, M., Li, D., He, Y., Zhao, R., Jiang, X., Song, S., Wang, L., and Fan, C., "A nano- and micro-integrated protein chip based on quantum dot probes and a microfluidic network," Nano Res. **1**, 490–496 (2008).
[409]Yang, Q., Ji, H., Xu, Z., Li, Y., Wang, P., Sun, J., Fan, X., Zhang, H., Lu, H., and Zhang, Z., "Ultra-fast and accurate electron ionization mass spectrum matching for compound identification with million-scale in-silico library," Nat. Commun. **14**(1), 3722 (2023).
[410]Yao, Q., Wu, X., Tao, C., Gong, W., Chen, M., Qu, M., Zhong, Y., He, T., Chen, S., and Xiao, G., "Osteoarthritis: Pathogenic signaling pathways and therapeutic targets," Sig. Transduct. Target. Ther. **8**, 56 (2023).
[411]Yeste, J., Illa, X., Gutiérrez, C., Solé, M., Guimerá, A., and Villa, R., "Geometric correction factor for transepithelial electrical resistance measurements in transwell and microfluidic cell cultures," J. Phys. D **49**(37), 375401 (2016).
[412]Yeste, J., García-Ramírez, M., Illa, X., Guimerà, A., Hernández, C., Simó, R., and Villa, R., "A compartmentalized microfluidic chip with crisscross microgrooves and electrophysiological electrodes for modeling the blood–retinal barrier," Lab Chip **18**, 95–105 (2018).
[413]Yin, M-j, Huang, B., Gao, S., Zhang, A. P., and Ye, X., "Optical fiber LPG biosensor integrated microfluidic chip for ultrasensitive glucose detection," Biomed. Opt. Express **7**(5), 2067–2077 (2016).
[414]Yin, T., Huang, P., Gao, G., Shapter, J., Shen, Y., Sun, R., Yue, C., Zhang, C., Liu, Y., Zhou, S., and Cui, D., "Superparamagnetic Fe_3O_4-PEG_{2K}-FA@Ce6 nanoprobes for in vivo dual-mode imaging and targeted photodynamic therapy," Sci. Rep. **6**, 36187–36111 (2016).

[415]Yu, Z. T. F., Guan, H., Ki Cheung, M., McHugh, W. M., Cornell, T. T., Shanley, T. P., Kurabayashi, K., and Fu, J., "Rapid, automated, parallel quantitative immunoassays using highly integrated microfluidics and AlphaLISA," Sci. Rep. **5**, 11339 (2015).
[416]Yuan, J., Hui, M., Ma, X., Wang, Z., and Ma, X., "SERS-fluorescence nanoprobe for monitoring and imaging mitochondrial ROS during cell apoptosis," Spectrochim. Acta, Part A **332**, 125824 (2025).
[417]Yunus, M. H., Yusof, N. A., Raston, N. H. A., Noor, S. S. M., Sulaiman, Y., and Abdullah, J., "A novel amperometric aptamer–antibody sandwich assay for the detection of tuberculosis with diazonium electrografted enhanced modified electrode," IEEE Sens. J. **21**(20), 22442–22449 (2021).
[418]Zamprogno, P., Thoma, G., Cencen, V., Ferrari, D., Putz, B., Michler, J., Fantner, G. E., and Guenat, O. T., "Mechanical properties of soft biological membranes for organ-on-a-chip assessed by bulge test and AFM," ACS Biomater. Sci. Eng. **7**(7), 2990–2997 (2021).
[419]Zbinden, A., Marzi, J., Schlünder, K., Probst, C., Urbanczyk, M., Black, S., Brauchle, E. M., Layland, S. L., Kraushaar, U., Duffy, G., Schenke-Layland, K., and Loskill, P., "Non-invasive marker-independent high content analysis of a microphysiological human pancreas-on-a-chip model," Matrix Biol. **85–86**, 205–220 (2020).
[420]Zdrachek, E. and Bakker, E., "Potentiometric sensing," Anal. Chem. **91**(1), 2–26 (2019).
[421]Zhang, H., Liu, L., Fu, X., and Zhu, Z., "Microfluidic beads-based immunosensor for sensitive detection of cancer biomarker proteins using multienzyme-nanoparticle amplification and quantum dotslabels," Biosens. Bioelectron. **42**, 23–30 (2013).
[422]Zhang, J., Kim, M.-H., Lee, S., and Park, S., "Integration of nanobiosensors into organ-on-chip systems for monitoring viral infections," Nano Convergence **11**, 11 (2024).
[423]Zhang, J., Wu, J., Li, H., Chen, Q., and Lin, J.-M., "An in vitro liver model on microfluidic device for analysis of capecitabine metabolite using mass spectrometer as detector," Biosens. Bioelectron. **68**, 322–328 (2015).
[424]Zhang, N., Stauffer, F., Simona, B., Zhang, F., Zhang, Z.-M., Huang, N.-P., and Vörös, J., "Multifunctional 3D electrode platform for real-time in situ monitoring and stimulation of cardiac tissues," Biosens. Bioelectron. **112**, 149 (2018).
[425]Zhang, X., Wang, T., Wang, P., and Hu, N., "High-throughput assessment of drug cardiac safety using a high-speed impedance detection technology-based heart-on-a-chip," Micromachines **7**(7), 122 (2016).
[426]Zhang, X., Guo, L., Zeng, H., White, S. L., Furniss, M., Balasubramanian, B., Lis, E., Lagrutta, A., Sannajust, F., Zhao, L. L., Xi, B., Wang, X., Davis, M., and Abassi, Y. A., "Multi-parametric assessment of cardiomyocyte excitation-contraction coupling using impedance and field potential recording: A tool for cardiac safety assessment," J. Pharmacol. Toxicol. Methods **81**, 201–216 (2016).
[427]Zhang, X., Su, R., Wang, H., Wu, R., Fan, Y., Bin, Z., Gao, C., and Wang, C., "The promise of synovial joint-on-a-chip in rheumatoid arthritis," Front. Immunol. **15**, 1408501 (2024).
[428]Zhang, X., Wang, W., Li, F., and Voiculescu, I., "Stretchable impedance sensor for mammalian cell proliferation measurements," Lab Chip **17**, 2054–2066 (2017).
[429]Zhang, Y. S., Aleman, J., Shin, S., Kilic, T., Kim, D., Mousavi Shaegh, S. A., Massa, S., Riahi, R., Chae, S., Hu, N., Avci, H., Zhang, W., Silvestri, A., Nezhad, A., Radmanesh, A., De Ferrari, F., Polini, A., Calzone, G., and Shaikh, N., "Multisensor-integrated organs-on-chips platform for automated and continual in situ monitoring of organoid behaviors," Proc. Natl. Acad. Sci. U. S. A. **114**, 201612906 (2017).
[430]Zhang, Y., Wang, Y., Yin, H., Wang, J., Liu, N., Zhong, S., Li, L., Zhang, Q., and Yue, T., "Strain sensor on a chip for quantifying the magnitudes of tensile stress on cells," Microsyst. Nanoeng. **10**, 88 (2024).
[431]Zhao, C., Wang, Z., Tang, X., Qin, J., and Jiang, Z., "Recent advances in sensor-integrated brain-on-a-chip devices for real-time brain monitoring," Colloids Surf., B **229**, 113431 (2023).
[432]Zhong, H., Zhu, W., Yan, Z., Xu, C., Wei, B., and Wang, H., "A quantum dot-based fluorescence sensing platform for the efficient and sensitive monitoring of collagen self-assembly," N. J. Chem. **44**, 11304–11309 (2020).
[433]Zhu, J., He, J., Verano, M., Brimmo, A. T., Glia, A., Qasaimeh, M. A., Chen, P., Aleman, J. O., and Chen, W., "An integrated adipose-tissue-on-chip nanoplasmonic biosensing platform for investigating obesity-associated inflammation," Lab Chip **18**, 3550–3560 (2018).
[434]Zhu, Y., Hong, H., Xu, Z., Li, Z., and Cai, W., "Quantum dot-based nanoprobes for *in vivo* targeted imaging," Curr. Mol. Med. **13**, 1549 (2013).
[435]Zignego, D., Hilmer, J., Bothner, B., Schell, W., and June, R., "Primary human chondrocytes respond to compression with phosphoproteomic signatures that include microtubule activation," J. Biomech. **97**, 109367 (2019).
[436]Zirath, H., Rothbauer, M., Spitz, S., Bachmann, B., Jordan, C., Müller, B., Ehgartner, J., Priglinger, E., Mühleder, S., Redl, H., Holnthoner, W., Harasek, M., Mayr, T., and Ertl, P., "Every breath you take: Non-invasive real-time oxygen biosensing in two- and three-dimensional microfluidic cell models," Front. Physiol. **9**, 815 (2018).
[437]Zirath, H., Spitz, S., Roth, D., Schellhorn, T., Rothbauer, M., Müller, B., Walch, M., Kaur, J., Wörle, A., Kohl, Y., Mayr, T., and Ertl, P., "Bridging the academic–industrial gap: Application of an oxygen and pH sensor-integrated lab-on-a-chip in nanotoxicology," Lab Chip **21**, 4237–4248 (2021).
[438]Zoio, P., Lopes-Ventura, S., and Oliva, A., "Barrier-on-a-chip with a modular architecture and integrated sensors for real-time measurement of biological barrier function," Micromachines **12**(7), 816 (2021).
[439]Ştefănescu, D., "Strain gauges and wheatstone bridges—Basic instrumentation and new applications for electrical measurement of non-electrical quantities," in *International Multi-Conference on Systems, Signals and Devices (SSD'11)* (IEEE, 2011).